INFORMATION TO USERS

This material was produced from a microfilm copy of the original document. While the most advanced technological means to photograph and reproduce this document have been used, the quality is heavily dependent upon the quality of the original submitted.

The following explanation of techniques is provided to help you understand markings or patterns which may appear on this reproduction.

1. The sign or "target" for pages apparently lacking from the document photographed is "Missing Page(s)". If it was possible to obtain the missing page(s) or section, they are spliced into the film along with adjacent pages. This may have necessitated cutting thru an image and duplicating adjacent pages to insure you complete continuity.

2. When an image on the film is obliterated with a large round black mark, it is an indication that the photographer suspected that the copy may have moved during exposure and thus cause a blurred image. You will find a good image of the page in the adjacent frame.

3. When a map, drawing or chart, etc., was part of the material being photographed the photographer followed a definite method in "sectioning" the material. It is customary to begin photoing at the upper left hand corner of a large sheet and to continue photoing from left to right in equal sections with a small overlap. If necessary, sectioning is continued again — beginning below the first row and continuing on until complete.

4. The majority of users indicate that the textual content is of greatest value, however, a somewhat higher quality reproduction could be made from "photographs" if essential to the understanding of the dissertation. Silver prints of "photographs" may be ordered at additional charge by writing the Order Department, giving the catalog number, title, author and specific pages you wish reproduced.

5. PLEASE NOTE: Some pages may have indistinct print. Filmed as received.

Xerox University Microfilms
300 North Zeeb Road
Ann Arbor, Michigan 48106

Downloaded from SHAREOK. Persistent Handle URL: https://hdl.handle.net/11244/4169

77-1819

DOSWELL, Charles Arthur, III, 1945-
THE USE OF FILTERED SURFACE DATA TO REVEAL SUBSYNOPTIC SCALE DYNAMICS.

The University of Oklahoma, Ph.D., 1976
Physics, atmospheric science

Xerox University Microfilms, Ann Arbor, Michigan 48106

THE UNIVERSITY OF OKLAHOMA

GRADUATE COLLEGE

THE USE OF FILTERED SURFACE DATA TO REVEAL SUBSYNOPTIC SCALE DYNAMICS

A DISSERTATION

SUBMITTED TO THE GRADUATE FACULTY

in partial fulfillment of the requirements for the degree of

DOCTOR OF PHILOSOPHY

BY

CHARLES A. DOSWELL III

Norman, Oklahoma

1976

THE USE OF FILTERED SURFACE DATA

TO REVEAL SUBSYNOPTIC SCALE DYNAMICS

APPROVED BY

Robert K. Smith

Maurice Rasmussen

Stanley B. Elias

Duane Rapp

Eugene M. Wilkins

DISSERTATION COMMITTEE

ABSTRACT

A band-pass filtering technique, based on an exponential weight function interpolation method, is presented. The technique filters both spatially and temporally and the center of the band can be positioned in the spectral domain to suit the needs of the user. Test data to which the filter is applied are conventional surface meteorological observations for three severe thunderstorm days in Oklahoma.

By combining results of the filtering with available numerical studies, a scale analysis for subsynoptic systems is developed. Surface subsynoptic systems are shown to be well correlated with severe weather events. Three fundamental findings about these systems are developed: first, the data support the hypothesis that the circulations derive their energy from baroclinic sources; second, anisentropic processes of eddy mixing and latent heat release are apparently vital to the subsynoptic flow; and third, evidence supports the existence of a balance between pressure forces and vertical circulations. These findings are in basic agreement with previous medium-scale dynamical theory and

experiment, but the lack of information about vertical structure precludes a definitive description of subsynoptic circulations.

ACKNOWLEDGEMENTS

As is normally the case, many people have made essential contributions to the success of this effort. I feel it is worth the effort to thank many of them by name.

First, the cooperation and service provided by the Environmental Data Service of the National Climatic Center made the acquisition of complete data sets possible.

Second, many members of staff of the National Severe Storms Laboratory, directed by Dr. Edwin Kessler, helped make this work both possible and enjoyable. Drs. Joseph T. Schaefer and Robert P. Davies-Jones were always ready to listen to my ideas and participate in fruitful discussions about them. Dr. Dusan Zrnic and Mr. Rodger A. Brown made important contributions by pointing out specific problem areas and helping to iron them out. The whole Computer Data Processing section, directed by Mrs. Kathryn C. Gray, provided able support throughout the effort. Messrs. Mike Weible, Ed Helm, Bill Bumgarner, and Leroy Fortner were essential in developing the computer programming. Ms. Rhonda Wood did an outstanding keypunching job, and those unsung heroes, computer operators

Hadley Bowman, Tully Davis, and Lucreta Butcher, put in long hours of sincerely appreciated effort. Mr. Conrad Ziegler helped prepare comparison analyses and Mr. Ed Brandes made other comparison analyses available, as well as many useful discussions. Mr. Charles Clark helped with the figures. Also, I am grateful for the help of Ms. Carol Cunningham, who typed the manuscript.

Third, my advisor, Dr. Yoshi K. Sasaki, has been a source of inspiration, a patient counselor, a personal friend, and an outstanding teacher -- in short, all that an advisor can and should be. Without his help and support, I could not possibly be where I am today, and this effort simply would not have been. A portion of this research was supported under NSF Grant No. GA 30976.

Finally, my wife Vickie has made an important contribution through her loving support and patience. My son, Chad, contributed by being -- a living source of joy for Vickie and me. This work is as dependent on all these people (and others) as my infant son is dependent on my wife and me. I owe all of you a lot. Thank you very sincerely!

TABLE OF CONTENTS

		Page
ACKNOWLEDGEMENTS		v
TABLE I		viii
LIST OF FIGURES		xi
Chapter		
I.	INTRODUCTION	1
II	FILTERING TECHNIQUES	8
	The Barnes Interpolation Scheme	8
	Band-Pass Filter Design	10
	The Data and the Analysis Grid	19
III.	RESULTS OF FILTERING - JUNE 18, 1973	22
IV.	SCALE ANALYSIS OF SUBSYNOPTIC SYSTEMS	28
V.	SUBSYNOPTIC SCALE DYNAMICS	39
VI.	SUMMARY AND RECOMMENDATIONS	48
REFERENCES		53
APPENDIX A		58
APPENDIX B		68
APPENDIX C		72

TABLE I

NOMENCLATURE

Note: Except where otherwise noted, an asterisk (*) denotes the dimensional form of a variable.

ROMAN SYMBOLS

C	condensation rate
c_p	specific heat at constant pressure
D	spatial weight function parameter; characteristic depth scale
$\hat{e}$	unit vector
f	general function; Coriolis parameter
$\vec{F}$	frictional force vector
f_o	characteristic Coriolis parameter
Fr	Froude number
g	acceleration of gravity
H	scale height of the atmosphere; heat flux
k^*,k	wavenumber
$\hat{k}$	unit vector in the vertical
L^*,L	wavelength, characteristic horizontal length scale
N	temporal weight function parameter
N_1^*,N_2^*	pseudo-random numbers (asterisk convention does not apply)
p	pressure
p^*	period
p_Δ	minimum resolvable period
Q	diabatic heating rate
r	response function; mixing ratio

R^*, R	radius from observation point to grid point
Ri	Richardson number
Ro	Rossby number
T^*, T	time separation of observation from grid point; temperature
u	eastward wind component
v	northward wind component
V	characteristic horizontal velocity amplitude
$\vec{V}$	horizontal wind vector
w	weight function
W	characteristic vertical velocity amplitude
$\vec{x}$	position vector
$\vec{X}$	weighted position vector
x_o, y_o	coordinates of uniformly distributed grid points
x_r, y_r	coordinates of pseudo-randomly distributed grid points

GREEK SYMBOLS

α	ratio of radius to spatial grid interval; specific volume
β	ratio of time separation to temporal grid interval
γ	β/T
δ	difference in low-pass responses at center of band; horizontal divergence
$\delta( )$	a finite difference operator
Δ	grid interval-general
Δs	Spatial grid interval
Δt	temporal grid interval

ζ	vertical component of vorticity
η	temporal weight function parameter-dimensional
θ	potential temperature
κ	spatial weight function parameter-dimensional
λ	ratio of wavelength to spatial grid interval
ν^*, ν	frequency
ρ	α/R
σ	image scale factor
σ_s	standard atmosphere lapse rate parameter
τ	ratio of period to temporal grid interval; characteristic time scale
ϕ	general variable
ϕ_{ijk}	filtered value of ϕ at the grid point $x=x_o+i\Delta s$, $y=y_o+j\Delta s$, $t=t_o+k\Delta t$
Φ	characteristic value for ϕ

SPECIAL SYMBOLS

∇	horizontal gradient operator
$( )_a$	low-pass value from filter with least response
$( )_b$	low-pass value from filter with most response
$( )_L$	large scale component
$( )_M$	medium scale component
$( )_S$	small scale component
$( )'$	perturbation quantity

Where a variable name has more than one definition, the second is separated from the first by a semicolon. The meaning should be clear from the context.

LIST OF FIGURES

FIGURE		PAGE
1	Schematic illustration of development of band-pass filter as difference between two low-pass filters	78
2	Spatial response function with band-pass peak centered at $12\Delta s$.	79
3	Temporal response function with band-pass peak centered at $6\Delta t$	79
4	Spatial weight functions for low-pass filters shown in Fig. 2.	80
5	Temporal weight functions for low-pass filters shown in Fig. 3.	80
6	Map showing analysis grid, map coordinate system, and spatial distribution of data points (black circles) used for interpolation.	81
7	Smoothed terrain analysis based on station heights, in meters	82
8	Hourly values of u-component (to the nearest m sec^{-1}) for low-pass data (open circles) and band-pass data (dark circles). The curves show an approximate continuous interpolation .	83
9a	Low-pass results for June 18, 1973 at 1200 CST. Vorticity and divergence are multiplied by 10^5 and units are sec^{-1}	84
9b	Altimeter setting in mb, mixing ratio in g kg^{-1}, moisture divergence is multiplied by 10^4 and has units of g kg^{-1} sec^{-1}, temperature in deg k	85
9c	Ageostrophic speed in m sec^{-1}, isobaric crossing angle in degrees with positive angles toward low pressure, geostrophic isotachs in m sec^{-1}.	86

FIGURE		PAGE
10a	Band-pass results for June 8, 1974 at 1200 CST. Vorticity and divergence are multiplied by 10^4 and units are sec^{-1}.	87
10b	Same as Fig. 8, except for band-pass results and moisture divergence is multiplied by 10^3.	88
11	Satellite photo at 1221 CST on June 18, 1974.	89
12	Satellite photo at 1642 CST on June 18, 1974.	89
A1(a)	Hypothetical uniform grid with roughly the same average spacing as real data..	90
A1(b)	Hypothetical uniform grid with dense and coarse distribution of stations..	90
A2(a)	Same as Fig. A1(a), except for pseudo-random distribution of data.	91
A2(b)	Same as Fig. A1(b), except for pseudo-random distribution of data.	91
A3(a)	Low-pass results for regular data mesh with influence radius of $18\Delta s$.	92
A3(b)	Same as Fig. A3(a), except for band-pass results..	93
A4(a)	Same as Fig. A3(a), except for random data mesh.	94
A4(b)	Same as Fig. A4(a), except for band-pass results..	95
A5(a)	Same as Fig. A3(a), except uses grid one inch (on map-4 grid points) smaller on all sides. Includes data outside grid.	96
A5(b)	Same as Fig. A5(a), except for band-pass results..	96
A6(a)	Same as Fig. A5(a), except excludes data from outside grid.	97
A6(b)	Same as Fig. A5(b), except excludes data from outside grid.	97

FIGURE		PAGE
A7(a)	Low-pass results, using data grid shown in Fig. A1(b)	98
A7(b)	Same as Fig. A7(a), except for band-pass results.	99
A8(a)	Same as Fig. A7(a), except for grid shown in Fig. A2(b)..	100
A8(b)	Same as Fig. A8(a), except for band-pass results.	101
A9(a)	Same as Fig. A3(a), except for influence radius of 6Δs.	102
A9(b)	Same as Fig. A9(a), except for band-pass results.	103
A10(a)	Same as Fig. A3(a), except for influence radius of 11Δs..	104
A10(b)	Same as Fig. A10(a), except for band-pass results.	105
A11(a)	Same as Fig. A3(a), except for input with no y-dependence.	106
A11(b)	Same as Fig. A11(a), except for band-pass results.	107
B1(a)	Same as Fig. 9a, except for 1200 CST on June 8, 1974..	108
B1(b)	Same as Fig. 9b, except for 1200 CST on June 8, 1974..	109
B1(c)	Same as Fig. 9c, except for 1200 CST on June 8, 1974..	110
B2(a)	Same as Fig. 10a, except for 1200 CST on June 8, 1974..	111
B2(b)	Same as Fig. 10b, except for 1200 CST on June 8, 1974..	112
B3	Satellite photo at 1452 CST on June 8, 1974.	113
B4(a)	Same as Fig. 9a, except for 1200 CST on May 24, 1973..	114

FIGURE		PAGE
B4(b)	Same as Fig. 9b, except for 1200 CST on May 24, 1973	115
B4(c)	Same as Fig. 9c, except for 1200 CST on May 24, 1973	116
B5(a)	Same as Fig. 10a, except for 1200 CST on May 24, 1973	117
B5(b)	Same as Fig. 10b, except for 1200 CST on May 24, 1973	118
B6	NSSL WSR-57 radar photograph at 1518 CST on May 24, 1973. Range marks at 40 km intervals.	119
C1(a)	Analysis using NSSL package at 1200 CST on June 8, 1974. Temperature in deg C, "PO" denotes pressure anomaly (from 1000 mb), in mb .	120
C1(b)	Dewpoint in deg C, divergence and vorticity times 10^6 with units of sec^{-1}, moisture divergence times 10^4 with units of g kg^{-1} sec^{-1}.	121
C2(a)	Same as Fig. C1(a), except for 1600 CST, May 24, 1973	122
C2(b)	Same as Fig. C1(b), except for 1600 CST, May 24, 1973 and mixing ratio in g kg^{-1}. . . .	123
C3	Vorticity times 10^6 (sec^{-1}) for 1500 CST, May 24, 1973	124
C4(a)	Successive corrections analysis (plus smoothing) for 1200 CST, May 24, 1973. Temperature in deg C; altimeter setting used for surface pressure, in mb.	125
C4(b)	Potential wet-bulb temperature in deg C, vorticity and divergence times 10^5 (sec^{-1}), moisture divergence times 10^4 (g kg^{-1} sec^{-1}) -- note that moisture divergence is mislabelled "MCON"	126

THE USE OF FILTERED SURFACE DATA TO REVEAL SUBSYNOPTIC SCALE DYNAMICS

CHAPTER I

INTRODUCTION

Observation of a phenomenon and analysis of the observations are the first steps in the development of most meteorological concepts. Unlike modern physics, where theory frequently precedes observation,[1] meteorological concepts have typically developed after a long series of observations of a phenomenon, followed by the abstraction of the relevant physical concept. Recent meteorological theory consistently emphasizes the concept of the scale of the phenomenon of interest (e.g., Palmén and Newton, 1969) in an effort to separate the meaningful phenomena from the "noise". An unfortunate problem is that there is no general agreement on the definition of those scales. Meteorological phenomena generally operate over

[1] As an example, the prediction of the existence of sub-nuclear particles based on theoretical evidence has typically preceded actual observation of the particles.

a range of values for the scaling parameters. As a result, a particular phenomenon may occur in that part of the range overlapped by another phenomenon. When arbitrary scale limits lie in this overlap region, neither phenomenon has an unambiguous scale with which it can be associated. For example, most internal gravity waves may be regarded as "noise" when we wish to consider the planetary circulation. On the other hand, an extensive thunderstorm squall line may have space and time scales large enough to be within the same order of magnitude as the extratropical cyclone (ETC) scale. It is not clear that the squall line is "noise" in such a case. Experience indicates that the phenomena are different, even if a singular example of a squall line is of scale comparable to the ETC. In summary, we generally assign arbitrary limits to small (micro), medium (meso), and large (macro) scales, but these are only rough guidelines in description of the phenomena. A purpose for doing so is elimination of those events which have relatively insignificant effects on the phenomenon of interest.

Definition of scales of motion is complicated by the lack of an information theory for meteorological observations such as exists for pure time series observations (see Blackman and Tukey, 1958). Meteorological data involve both spatial and temporal sampling. Since meteorological waves travel and evolve in space and time, further complications are introduced. If the waves were steady-state and all had the same constant

phase speed, we could use time-to-space conversion techniques to decrease the effective data separation in space, and actually improve the resolving power of our fixed observation network. However, meteorological waves have phase velocities that depend on the phenomenon generating them, as well as being dispersive (i.e., dependent on the wavelength). It seems clear that by using the time series observations available at the fixed locations of our network, we should be capable of improving our analysis. However, it is not clear how this is to be accomplished most effectively. Such a problem can be resolved by a study of the theoretical information content of meteorological observations in general. This is beyond the scope of the present study.

Much of meteorological data analysis is empirical or heuristic. In fact, the subject of objective analysis is largely concerned with interpolation and the methods used can be only subjectively justified. In simple terms, since we don't know what the "true" fields are, the quality of interpolation/analysis is a matter of definition. Gandin's work (1963) is an attempt to clarify the effects of interpolation errors, based on correlation functions developed for ensembles of data. The variational methods of Sasaki, (1958, 1970) may be thought of as a filtering technique based in part on the constraining physics of the phenomena of interest. Stephens (1971) has pointed out that physical constraints involving observed derivatives can actually

reduce aliasing by effectively decreasing the Nyquist interval. Methods based on physics hold great promise for extending the utility of meteorological analysis. But no synthesis of information theory with the physics has been accomplished and, additionally, one must have some prior knowledge of the physics to apply such constraints.

One scale of meteorological phenomena which remains poorly observed and, hence, poorly understood is the so-called mesoscale. For our purposes, mesoscale motions encompass phenomena whose spatial dimensions are 10^1 to 10^3 km, and whose temporal dimensions range from 10^0 hr to 10^1 hr. Sampling theory suggests the upper limits of the mesoscale range are sampled more or less adequately by the surface station network of reporting stations run operationally by the National Weather Service (in cooperation with the Federal Aviation Administration). It is within the mesoscale range that there exists a so-called "spectral gap" (see Lumley and Panofsky, 1964). That is, the time averaged power in that part of the spectrum is generally much less than at larger and smaller scales. However, it is also within this range that the relatively rare (but exceedingly important) severe local storm phenomenon occurs.

Individual severe storms and their attendant effects are at the lower mesoscale range and thus are not adequately sampled by the operational network. But these storms tend to occur in ways which indicate organization on a larger

scale (Tegtmeier, 1974 or McFarland, 1975) and yet this larger scale is not as large as the extratropical cyclone scale (the so-called synoptic scale). The question is thereby raised whether there exist physical systems whose scales allow the operational data network to resolve them. Provided that such "subsynoptic" systems exist, we must observe them enough times to be able to abstract the relevant physical concepts -- i.e., their dynamics.

It is with these considerations in mind that this study has been undertaken. In order to isolate phenomena of the scale considered, a band-pass filtering technique is proposed. By band-pass filter, we mean one which reduces amplitudes at scales below and above the one of interest. Variational band-pass filters have been developed by Hylton (1972) and Sheets (1972). The band-pass filter of Hylton is only designed to limit the derivatives of the analyzed fields and so contains little physics concerning the scale of motion being considered. The work of Sheets treats the tropical cyclone and incorporates the same sort of derivative filters plus a simple model applicable to tropical cyclones.

The state of knowledge concerning the subsynoptic scale is sketchy, at best. Tegtmeier (1974) has indicated, via subjective analysis, some of the types of subsynoptic systems that occur in the Great Plains. Matsumoto, Ninomiya, and Akayama (1967) present a case study of a subsynoptic system and Matsumoto and Ninomiya (1969) propose one

Theoretical model that may be applicable. Sasaki (1973) presents some provocative results concerning momentum fluxes based on variational analysis of surface data for a case study in Oklahoma. Nevertheless, there is not enough observational knowledge of the four-dimensional structure of these systems to allow any clear-cut model to emerge as the basic physical mechanism.

As a consequence of this lack of knowledge, the author deems it inadvisable to incorporate any preconceived physical picture into the analysis at this time. It is likely that such a model will be difficult to develop, owing to the apparently large variety of subsynoptic scale mechanisms that may play a role. McGinley and Sasaki (1975) have proposed that symmetric baroclinic instabilities may be present in severe storm generating systems. The model of Matsumoto and Ninomiya (op. cit.) proposes an interaction between gravitational modes and "synoptic" modes. There have been proposals (Maddox and Gray, 1973), that CISK (forced Ekman boundary layer pumping, described by Charney and Eliassen, 1964) may have some crucial role.

In spite of our lack of prior understanding of events on the subsynoptic scale, we can pose some problems we can expect to resolve by the technique of band-pass filtering. We can design the filter to isolate subsynoptic scale features, so we should be able to estimate characteristic values for the variables of interest. When these values are more or

less firmly established, we can perform a scale analysis appropriate to the subsynoptic range. This scale analysis is tentative, owing to the lack of information about the vertical structure on this scale. However, we can use the results of numerical simulations and theoretical studies of subsynoptic scale motions to help supplement our surface observations. By this means, we should be able to develop insights into the dynamics of these systems and the role they play in severe convective storms.

CHAPTER II

FILTERING TECHNIQUE

The Barnes Interpolation Scheme

The basic tool used throughout this analysis is the interpolation scheme developed by Barnes (1964, 1973). Any interpolation scheme could be used to develop a band-pass filter, but Barnes' method is particularly convenient, owing to the simple functional form of the weight function. This method is the weighted-average type, with the weight function given by

$$w(\vec{x}) = \exp\ [-\vec{X} \cdot \vec{X}],$$

where $\vec{x}$ is the position vector given by

$$\vec{x} = (x_1\hat{e}_1 + x_2\hat{e}_2 + \ldots + x_n\hat{e}_n),$$

and $\vec{X}$ is the weighted position vector

$$\vec{X} = \left[\frac{x_1}{2(\kappa_1)^{1/2}}\,\hat{e}_1 + \frac{x_2}{2(\kappa_2)^{1/2}}\,\hat{e}_2 + \ldots + \frac{x_n}{2(\kappa_n)^{1/2}}\,\hat{e}_n\right],$$

and the $\hat{e}_i$ are the n unit vectors in the n-dimensional space over which the analysis is being applied. For our purposes, we are concerned with a weight function which is isotropic and homogeneous in x-y space, so that the spatial coordinate is simply the distance from the grid point to the data point in question. We will consider the second coordinate to be the temporal separation. Thus, we have

$$w(R^*,T^*;\ \kappa,\eta) = \exp\left[-\frac{R^{*2}}{4\kappa} - \frac{T^{*2}}{4\eta}\right],$$

where R* and T* are the dimensional distance and time separation, and κ and η are the distance and time parameters at our disposal, for specification of the weighting.

Barnes has shown that his interpolation scheme acts as a low-pass filter with a particularly simple response function:

$$r(k^*,\nu^*;\ \kappa,\eta) = \exp\left[-\kappa k^{*2} - \eta\nu^{*2}\right],$$

where k* and ν* are the dimensional wavenumber and frequency. To within a constant, the above weight function and response function comprise a Fourier transform pair. The spectral characteristics of the low-pass filter are well-documented in Barnes (op. cit.). It may be emphasized here that, owing to the smooth nature of the weight function, the response is also smooth and problems associated with side lobes (Sasaki, 1960) are thereby avoided.

In what follows, the desired application of this interpolation method is, in fact, as a filter. Thus, it is not desirable to reproduce accurately the input observations at all points in space and time. Results will be expected to violate the observations, especially in areas affected by thunderstorm-induced flows. If such storm-generated patterns are large enough and last long enough, they will be retained, of course. But a measure of goodness of fit, such as an RMS error, is not useful in determining the quality of the analysis from this viewpoint. Thus, only one pass through the data (Barnes, 1973) is made to produce a low-pass filtered field.

Band-Pass Filter Design

Consider non-dimensionalizing wavenumber (k*) and frequency (ν^*) -- we have grid intervals of Δs in space and Δt in time; consider a wave whose wavelength is L* (or whose period is p*). By definition

$$k^* = \frac{2\pi}{L^*} \text{ and let } \lambda = \frac{L^*}{\Delta s} .$$

Now define $L_\Delta \doteq 2\Delta s$ (the minimum resolvable wavelength). Thus, on our grid, we can non-dimensionalize k* by letting the non-dimensional wavenumber k be defined by

$$k = \frac{L_\Delta}{2\pi} k^* = \frac{2\Delta s}{2\pi} \cdot \frac{2\pi}{\lambda \Delta s} = \frac{2}{\lambda} .$$

Similarly, for the frequency,

$$\nu^* = \frac{2\pi}{p^*} \quad \text{and let} \quad \tau = \frac{p^*}{\Delta t} .$$

If we define $p_\Delta = 2\Delta t$, then the non-dimensional frequency ν is given by

$$\nu = \frac{p_\Delta}{2\pi} \nu^* = \frac{2\Delta t}{2\pi} \frac{2\pi}{\tau \Delta t} = \frac{2}{\tau} .$$

In the k (ν) system, rather than the k* (ν*) system, we design our response with respect to the grid, not with respect to space. This means that k (or ν) runs from 0 -- at the spatial (temporal) mean, to 1 -- at the spatial (temporal) Nyquist wavenumber (frequency).

Let us consider the Barnes exponential weight function: in space and time

$$\begin{aligned} w\ (R^*,T^*;\ \kappa,\eta) &= \exp\ [-(R^{*2}/4\kappa + T^{*2}/4\eta)] \ , \\ &= e^{-R^{*2}/4\kappa}\ e^{-T^{*2}/4\eta} \ , \\ &\equiv w_s(R^*;\kappa)\ w_t(T^*;\eta) \ , \end{aligned}$$

where R* and T* are the respective distances in space and time from the grid point to the data point. In his paper, Barnes showed that the response functions (i.e., the amplitude ratio of input to output) were

$$r_s\ (k^*, \kappa) = e^{-\kappa k^{*2}} ,$$

$$r_t\ (k^*, \eta) = e^{-\eta \nu^{*2}} ,$$

to within a constant. Now, let us consider these in our non-dimensional form: if we let $R^* \equiv \alpha \Delta s$ where the non-dimensional radius R is given by

$$R = \frac{R^*}{\rho \Delta S} \Rightarrow \rho R = \frac{R^*}{\Delta S} = \alpha ,$$

and let $\kappa = D^2 \Delta s^2$, recalling that $k^* = \frac{\pi}{\Delta S}\ k$, then

$$\kappa k^{*2} = (D^2 \Delta S^2)\ \frac{\pi^2}{\Delta S^2}\ k^2 = \pi^2 D^2 k^2 ,$$

and

$$\frac{R^{*2}}{4\kappa} = \frac{(\rho R \Delta S)^2}{4(D^2 \Delta S^2)} = \frac{(\rho R)^2}{4D^2} .$$

Similarily we define $T^* \equiv \beta \Delta t$, $T = \frac{T^*}{\gamma \Delta t}$, $\eta = N^2\ \Delta t^2$; so that

$$\eta \nu^{*2} = \pi^2 N^2 \nu^2 \quad \text{and} \quad \frac{T^{*2}}{4\eta} = \frac{(\gamma T)^2}{4N^2} .$$

Now the response function/weight function pairs in space are

$$r_s(k;D) = \exp\ [-(\pi Dk)^2],$$

$$w_s(R;D) = \exp\ [-(\frac{\rho R}{2D})^2].$$

For time, we have

$$r_t(\nu;N) = \exp\ [-(\pi N\nu)^2]\ ,$$

$$w_t(T;N) = \exp\ [-(\frac{\gamma T}{2N})^2]\ .$$

Let us now consider the problem of using these to develop a band-pass filter. To do so, we define

$$\Delta r_{ij}^{(m)} = r_s(k_i;D_m) - r_s(k_j;D_m)\ .$$

In particular, we wish to define three wavenumbers ($k_1 < k_2 < k_3$) such that k_2 is the wavenumber at which the band-pass response is a maximum, with k_1 and k_3 being the high and low wavenumber "limits". These are not limits in the sense of response cut-off values -- however, we will achieve peak response at k_2 if we simultaneously maximize

$$\Delta r_{12}^{(a)} = r_s(k_1;D_a) - r_s(k_2;D_a)\ ,$$

and

$$\Delta r_{23}^{(b)} = r(k_2;D_b) - r_s(k_3;D_b) \ ,$$

subject to the constraint that

$$\Delta r_{12}^{(a)} = \Delta r_{23}^{(b)} \tag{1}$$

This is illustrated schematically in Fig. 1. We maximize by differentiating with respect to the parameter of the response, D_m. Thus

$$\frac{\partial}{\partial D_a}\left[\Delta r_{12}^{(a)}\right] = \frac{\partial}{\partial D_a}\left[e^{-(\pi D_a k_1)^2} - e^{-(\pi D_a k_2)^2}\right] \overset{\text{set}}{=} 0 \ ,$$

$$= -e^{-(\pi D_2 k_1)^2} \frac{\partial}{\partial D_a}\left[(\pi D_a k_1)^2\right] -$$

$$-e^{-(\pi D_a k_2)^2} \frac{\partial}{\partial D_a}\left[(\pi D_a k_2)^2\right] \ .$$

Thus, we have

$$e^{-(\pi D_a k_1)^2}\left[2\pi^2 D_a k_1^2\right] = e^{-(\pi D_a k_2)^2}\left[2\pi^2 D_a k_2^2\right] \ ,$$

or, after simplifying and rearrangement,

$$\frac{k_1^2}{k_2^2} = e^{-\left[(\pi D_a k_2)^2 - (\pi D_a k_1)^2\right]} ,$$

or, by taking the natural logarithm

$$2 \ln\left(\frac{k_1}{k_2}\right) = -\pi^2 D_a^2 \left(k_2^2 - k_1^2\right) .$$

Thus, we find an expression for D_a in terms of k_1 and k_2:

$$D_a^2 = \frac{2 \ln\left(\frac{k_1}{k_2}\right)}{\pi^2\left(k_1^2 - k_2^2\right)} . \qquad (2)$$

Similarly, by differentiating $\Delta r_{23}^{(b)}$ with respect to D_b, we find an expression for D_b in terms of k_2 and k_3:

$$D_b^2 = \frac{2 \ln\left(\frac{k_2}{k_3}\right)}{\pi^2\left(k_2^2 - k_3^2\right)} . \qquad (3)$$

The constraint given in (1) implies

$$e^{-(\pi D_a k_1)^2} - e^{-(\pi D_a k_2)^2} = e^{-(\pi D_b k_2)^2} - e^{-(\pi D_b k_3)^2} ,$$

so that

$$e^{-(\pi D_a k_1)^2} = e^{-(\pi D_a k_2)^2} + e^{-(\pi D_b k_2)^2} - e^{-(\pi D_b k_3)^2} ,$$

or, by taking the natural logarithm

$$- \pi^2 D_a^2 k_1^2 = \ln \left[e^{-(\pi D_a k_2)^2} + e^{-(\pi D_b k_2)^2} - e^{-(\pi D_b k_3)^2} \right] .$$

Consequently, we have an expression for k_1:

$$k_1 = \frac{1}{\pi D_a} \sqrt{- \ln [\ ]} ,$$

where the contents in brackets come from the expression above. If we choose k_2 and k_3, we can immediately calculate D_b from (3). On a desk calculator, we can iterate on k_1 and D_a until both (2) and (4) are satisfied -- in practice, the process converges very quickly.

As may be seen in Figs. 2 and 3, we have normalized the band-pass response so that the band-pass peak response is always unity. If the response difference at k_2 is given by

$$r_s^{(b)}(k_2;\kappa) - r_s^{(a)}(k_2;\kappa) = \delta r_s ,$$

then the normalized band-pass filter has response

$$r_{bs} = \frac{1}{\delta r_s} \left[r_s^{(b)} - r_s^{(a)} \right] .$$

A completely analogous argument holds for the temporal response.

The process of band-pass filtering is as follows: The data are interpolated to grid points using weight function w_a, where

$$w_a(R,T) = \exp\left[- \frac{(\rho R)^2}{4D_a^2} - \frac{(\gamma T)^2}{4N_a^2} \right] ,$$

and again using w_b, where

$$w_b(R,T) = \exp\left[- \frac{(\rho R)^2}{4D_b^2} - \frac{(\gamma T)^2}{4N_a^2} \right] .$$

These result in grid-point values for the analyzed field of $\phi_{ijk}^{(a)}$ and $\phi_{ijk}^{(b)}$. The band-pass field at the grid point is then given by

$$\phi_{ijk} = \frac{1}{\delta} \left(\phi_{ijk}^{(b)} - \phi_{ijk}^{(a)} \right) ,$$

where

$$\delta = e^{-[(\pi D_b k_2)^2 + (\pi N_b \nu_2)^2]} - e^{-[(\pi D_a k_2)^2 + (\pi N_a \nu_2)]^2} .$$

If we know precisely the scale of the phenomenon for which we search, then it is possible via the method just described to place the center of our band-pass filter at exactly that scale. In general, of course, we want to look at a range of scales, albeit a narrow one. The aim of this research is, in part, to examine events at the limits of resolution of the operational surface data network.[1] Accordingly, it is deemed appropriate to place the center of the band at that limit, or nearly so. If the limit is placed at or near the Nyquist frequency/wavenumber for the data, then it is clear (as shown in Appendix A) that truncation error is a serious problem. There is no clear-cut lower limit to the frequency of sampling for a wave of given frequency to avoid truncation problems. However, a rule of thumb is that we should sample roughly six to eight times to be reasonably sure of the results if we plan on examining fields of derivatives of that wave.

The filter used, therefore, centers on waves that the data mesh samples at about three times the Nyquist. The response functions in space and time are shown in Figs. 2 and 3, while the corresponding weight functions are seen in Figs. 4 and 5. It may be observed that k_2 and k_3 (ν_2 and ν_3) determine a unique band-pass filter centered at k_2. The value of k_1 is determined in the process of solving Eqs. (1) and (2), simultantously.

---

[1] That is, the subsynoptic scales of length and time fall at or near the resolution limits for that data.

The Data And The Analysis Grid

Data used for this study are the standard surface observations obtained from the original WBAN-10 (or equivalent) forms. By using these data, all the "special" and "local" observations which are frequently not transmitted over the teletype can be included as well as the hourly "record" observations. The information from the forms, (including wind speed, wind direction, time of the observation, altimeter setting, temperature, and dewpoint) is put on cards and thence to magnetic tape, after being subjected to a "pre-filtering". All observations between 0515 CST and 1845 CST are used.

The pre-filtering is designed to remove only gross errors (such as would be introduced by keypunch mistakes) and obviously unrepresentative observations. An observation is considered unrepresentative when its second time derivative exceeds some threshold value. This threshold is set high enough so that about 40 or fewer observations are rejected out of about 1800 (per data set). When an observation is rejected, the four surrounding "good" data are used to fit a cubic polynomial and a smoothed observation is put in place of the rejected one.

Altimeter setting (which has been reduced to sea level) is used in place of the so-called sea-level pressure (SLP) for two basic reasons: one is that more stations record altimeter setting, more frequently than SLP, and the

second is that the means of reduction of altimeter setting is the same at all stations, independent of the temperature history. This introduces a diurnal trend in the altimeter setting, but the standard SLP also contains some diurnal trend and diurnal influences may be physically meaningful to severe weather activity.

The wind speed used, in the event of gusts, is the arithmetic mean of the "sustained" wind and the gust, rounded to the next highest knot, if necessary. It is felt that both extremes would be unrepresentative of advective wind speeds.

Cases were chosen by several criteria. First, the author has been a resident in Oklahoma since 1972 and is generally familiar with the severe storm events considered. Second, of course, severe weather of some type has to be present in a case. An exhaustive test of the technique must include a variety of non-storm cases so that a comparison of magnitudes for the variables to storm cases can be made, but a technique has to function properly during storm events before even being considered for general use. Finally, since various analysis methods are being compared, a severe storm case must have been analyzed previously by another analysis method. With these criteria in mind, the following three days were chosen: May 24, 1973; June 8, 1974; and June 18, 1973. The latter case is the primary testbed for the analysis.

Interpolation is accomplished on a grid of 25 x 19 points superimposed on a polar stereographic map (true at

60°N latitude with a map scale factor of $1:10^7$). The map coordinates, the grid, and the stations used in the analyses are shown in Fig. 6. Maps of the quantities analyzed are produced at hourly intervals from 0600 CST to 1800 CST. There are about 125 stations used in the analysis, including those within roughly two grid lengths of the borders of the grid, as shown. Not all stations report hourly, especially in the western part of the grid. A terrain analysis based on the low-pass filtered station heights is shown in Fig. 7. On the grid, the x-axis runs roughly east-west and the y-axis runs roughly north-south. Map coordinates shown are based on map inches from the north pole and 100°W longitude for the y- and x-directions, respectively. The 0.25 inch grid spacing corresponds to 63.5 km.

CHAPTER III

RESULTS OF FILTERING - JUNE 18, 1973

In this chapter, we describe the results of applying the band-pass filter to surface data for a case of relatively isolated severe weather events. Available upper air data at 0600 CST indicate a strong trough along the northern border of the United States, centered in Montana. There are two minor short waves imbedded in this trough -- one extending into western Kansas and another into central Arizona. We have 500 mb winds in the base of the trough of the order of 10 m sec^{-1} from Arizona into Illinois. Isotherms at 500 mb show no indications of cold air advection that might be affecting Oklahoma. At 700 mb, a weak thermal ridge is centered along a line from the Big Bend area in Texas, through the Texas and Oklahoma Panhandles into west central Kansas, with moderate cold air advection behind it in the base of the trough. Analysis at 850 mb shows a broad band of moisture from southern Texas through Oklahoma and extreme eastern Kansas into Iowa, ahead of a well-defined trough axis. A wedge of dry, warm air separates this moist air from a strong

850 mb cold front in central Kansas through the extreme western Oklahoma panhandle into Northern New Mexico. Winds at 850 mb in the moist air are southwesterly at speeds of 15 to 25 m sec^{-1}, and northwesterly at about 20 m sec^{-1} in the cold air to the north.

To summarize the synoptic pattern for this case, the upper-air pattern is relatively weak with an apparent strengthening of the system as one approaches the surface. The moist air mass ahead of the front is quite unstable, and many of the 700 mb and 850 mb parameters mentioned by Miller (1972) are moderate to strong, while the 500 mb parameters are weak or nonexistent. In total, this situation is not typical of a classic outbreak of severe weather, but it is typical of many severe weather situations in the Great Plains during the late spring, when the polar jet stream is usually well north of Oklahoma.

In turning our attention to our analyzed fields of surface data, let us examine the temporal continuity of the filtered results. We can assume that the "u-component" of the wind field (basically, the eastward component, on this analysis grid) is most likely to exhibit rapid temporal fluctuations in the center of the grid. This is a reasonable assumption since wind components are the noisiest data with which we deal, and we know a posteriori that rapid changes do in fact occur in the approximate center of our analysis grid. By showing satisfactorily continuous results for the

u-component, we can infer that the rest of our analyzed fields show good time continuity. Figure 8 shows the hourly values of the u-component at a centrally located grid point. As may be seen, the temporal behavior is, indeed, quite smooth. An examination of the time evolution of the spatial patterns has confirmed this conclusion.

We can comment on the spatial continuity by examination of the output at 1200 CST shown in Figs. 9 and 10. In general, the patterns are free of erratic spatial behavior. The low-pass streamline/isotach pattern reveals the dominant frontal convergence zone across Oklahoma from southwest to northeast. This convergence zone is associated, but not coincident, with a trough of low pressure (altimeter setting) and and is characterized by cyclonic vorticity, as might be expected (Saucier, 1955). The mixing ratio field shows a distinctive pattern, curving southward in western Oklahoma where the surface dryline intersects the surface cold front. It may be observed that the moisture convergence zone is more or less coincident with the dryline, while the kinematic convergence lags somewhat behind the dryline. This agrees with the findings of Schaefer (1974) for quiescent dryline situations.

We note that the dryline is not clearly depicted in the low-pass streamline field, but it shows clearly as the trailing edge of a band of high isobaric crossing angles that extends into southwest central Oklahoma. The wind speeds are basically subgeostrophic everywhere (as might well

be anticipated at the surface), with ageostrophic speed maxima associated with low crossing angles in the moist air and high crossing angles in the dry air. An ageostrophic speed minimum lies in the pressure trough. We see that the crossing angle is relatively low both in the cold air and in the moist air.

Before we examine the band-pass results, we should comment on these low-pass patterns. With only minor changes, these configurations remain nearly fixed throughout the 12-hour analysis period. This is, in part, a result of the filtering, of course. Nevertheless, the remarkable consistency of the crossing angle pattern suggests that this large scale flow is being influenced by a systematic, relatively time-independent process which causes a characteristic departure from geostrophic balance. The pattern is not suggestive of frictional effects. This subject is examined further in a later chapter.

It is in the band-pass fields that we see more temporal and spatial detail, naturally. The most striking feature in the streamline/isotach fields at 1200 CST is the cyclonic circulation in southwest Oklahoma. In general, we can see the frontal zone and the dryline in greater detail and this cyclone is associated with the dryline/front intersection. The center of circulation has moved out of the central Texas Panhandle area since 0600 CST and is now (at 1200 CST) almost coincident with the nearly stationary band-pass pressure

minimum. There are several features of note in the derived properties of this flow field. We see that significant cyclonic vorticity extends westward from the circulation center, which is interpreted as the westward extension of the cold front. The large kinematic convergence maximum (still to the rear of the dryline) south of the circulation has developed rapidly since 0900 CST, coincident with an increase in the westerly component in the dry air. This has been associated with a rapid temperature rise and a sharp decrease of moisture, which suggests the convergence has arisen from eddy momentum transport via dry convection. The three moisture convergence maxima seen at 1200 CST have evolved as a result of the continuing presence and very gradual decline since 0600 CST of the maximum northeast of the circulation, the rapid increase in kinematic convergence near the dryline we have just discussed, and the persistence of the frontal moisture convergence maximum in extreme northeastern Oklahoma.

If we compare our 1200 CST moisture convergence field with Fig. 11, the satellite photo valid at about the same time, we can find only that a band of towering cumulus lies along the front and that the cumulus apparently terminate near the center of circulation. However, the picture taken several hours later, seen in Fig. 12, shows that active severe thunderstorms coincide remarkably well with the three moisture convergence centers. The time history of the storms indicates that the storms develop only after several hours of

pre-existing moisture convergence -- the activity in Texas, south of the Red River in the convergence zone associated with the dryline, is only beginning to develop by the time of the picture, whereas the storms in Oklahoma are already producing tornadoes at picture time.

The success of band-pass moisture convergence in delineating preferred areas of storm development several hours before storm initiation is, perhaps, the most convincing demonstration of the utility of band-pass filtering. We should emphasize that this case is an exceptionally good one, especially in this regard. This is not to say that other cases we have studied do not fit the overall pattern shown here, however. In Appendix B, we examine two other case studies that suggest the dominance of both larger and smaller scales of motion in severe weather events. Thus, on any given severe weather day, we may find that the dynamics that organize the thunderstorms can operate over a relatively wide range of scales. There is a substantial number of events in the southern Great Plains whose organizing dynamics seems to fall in the range we have called subsynoptic and which we have emphasized with the band-pass filter.

CHAPTER IV

SCALE ANALYSIS OF SUBSYNOPTIC SYSTEMS

Despite the scarcity of definitive upper air observations on the subsynoptic scale, we can proceed with a formal scale analysis, using surface data when available. Estimates for the vertical variations can be derived in part from numerical simulations and in part from inference from the surface data. The scaling follows the procedures outlined in Haltiner (1971).

We shall first specify characteristic values used in that which follows. In doing so, we will provide a more specific definition of the term "subsynoptic". As in Haltiner, our physical scales in space and time are

L = characteristic horizontal scale (about a quarter wavelength),

D = characteristic depth scale (also a quarter wavelength),

H = scale height of the atmosphere,

V, W = characteristic horizontal and vertical velocity amplitudes,

τ = characteristic period (advective period).

The notation here and in what follows will be similar to that used by Haltiner. However, the values will reflect the difference in scales. Here, we use

$$V = 20 \text{ m sec}^{-1}, \; L = 2 \times 10^5 \text{ m}, \; D = 2.5 \times 10^3 \text{ m} ,$$

which implies $\tau = 10^4$ sec. The magnitude of W is to be developed.

Before we proceed into the analysis, we must make one point clear. This development is concerned only with the medium scale flow and does not include the so-called synoptic scale terms and their interactions on this scale. To be more precise, if we suppose that any general physical variable ϕ is the sum of three basic components -- i.e., a large scale, a medium scale, and a small scale -- so that

$$\phi = \phi_L + \phi_M + \phi_S ,$$

then the band-pass results we are discussing are

$$\phi_b - \phi_a = \phi_M ,$$

where we have defined the meanings of the subscripts a and b in the preceding chapter about the design of the band-pass filter. For linear terms like

$$\frac{\partial \phi_M}{\partial t} = \frac{\partial \phi_b}{\partial t} - \frac{\partial \phi_a}{\partial t} ,$$

we have no difficulty in separating the two scales. However, nonlinear terms are not as simple. For example, consider

$$u\frac{\partial \phi}{\partial x} = (u_L+u_M+u_S)\ \frac{\partial}{\partial x}\ (\phi_L+\phi_M+\phi_S).$$

When we low-pass filter the products

$$u\frac{\partial \phi}{\partial x})_b = (u_L+u_M)\ \frac{\partial}{\partial x}\ (\phi_L+\phi_M)\ ,$$

and

$$u\ \frac{\partial \phi}{\partial x})_a = u_L\ \frac{\partial \phi_L}{\partial x}\ ,$$

so that when we take the difference, we find

$$u\frac{\partial \phi}{\partial x})_b - u\frac{\partial \phi}{\partial x})_a = u_M\ \frac{\partial \phi_L}{\partial x} + u_L\ \frac{\partial \phi_M}{\partial x} + u_M\ \frac{\partial \phi_M}{\partial x}\ .$$

However, if we take the product of the differences, we have

$$(u_b-u_a)\ \frac{\partial}{\partial x}\ (\phi_b-\phi_a) = u_M\ \frac{\partial u_M}{\partial x}\ .$$

Now our characteristic values of u and ϕ may be different between the scales -- e.g., if ϕ is temperature,

$$V_L \sim 10 \text{ m sec}^{-1},\ V_M \sim 20 \text{ m sec}^{-1},\ L_L \sim 10^6 \text{ m},$$

$$\phi_L \sim \Phi\ ^\circ\text{K}\ ,\ \phi_M \sim 2\Phi\ ^\circ\text{K}\ ,\ L_M \sim 2 \times 10^5 \text{ m}.$$

so that

$$u_M \frac{\partial \phi_L}{\partial x} \sim \frac{V_M \Phi}{L_L} \sim 2\Phi \times 10^{-5} \ ^\circ K \ sec^{-1} ,$$

$$u_L \frac{\partial \phi_M}{\partial x} \sim \frac{2V_L \Phi}{L_M} \sim \Phi \times 10^{-4} \ ^\circ K \ sec^{-1} ,$$

$$u_M \frac{\partial \phi_M}{\partial x} \sim \frac{4V_M \Phi}{L_M} \sim 2\Phi \times 10^{-4} \ ^\circ K \ sec^{-1} .$$

In the scale analyses to follow, we consider only the last such term. This ignores any interaction terms, as they are likely to be of the same order or smaller than the terms we include. This is particularly significant when we examine the pressure terms, as we shall see.

Let us define the Rossby number, Ro, by

$$Ro \equiv \frac{V}{f_o L} ,$$

where f_o is the characteristic value of the Coriolis parameter ($f_o \sim 10^{-4}$ sec^{-1}). By the above, Ro ~ 1. Furthermore, we shall assert that the Richardson number, Ri, defined by

$$Ri \equiv \frac{g \frac{\partial (\ln \theta)}{\partial z}}{\left(\frac{\partial V}{\partial z}\right)^2}$$

is also of order unity. This assertion is examined below. Finally, if the Froude number, Fr, is given by

$$Fr \equiv \frac{V^2}{gD}$$

we find that $Fr \sim 10^{-2}$. We use a scale height of the atmosphere of 10 km or 10^4 m. We can now use the relation (Haltiner, op. cit.) that

$$W \sim \frac{D}{RiRo} \frac{V}{L}$$

to find that $W \sim 2.5 \times 10^{-1}$ m sec^{-1} or about 25 cm sec^{-1}. This value is of the same order as the numerical results of Tokioka (1972) or Nitta and Ogura (1972), differing only by being a factor of about three larger than their numerical simulations on this scale of flow.

If we follow Haltiner's discussion of the pressure terms, we can determine their order by using the relation that

$$\delta_p' \sim \frac{DF}{HRo} \sim 4 \times 10^{-3}$$

This implies a dimensional pressure perturbation of the order of 8 mb, which is again in agreement with the numerical simulations.

We are now prepared to analyze the horizontal equations of motion which are, in vector form,

$$\frac{\partial \vec{V}}{\partial t} + \vec{V}\cdot\nabla\vec{V} + w\frac{\partial \vec{V}}{\partial z} = -\alpha\nabla p + f\hat{k} \times \vec{V} + \vec{F},$$

where $\vec{F}$ is the friction term. If we follow Lewis (1971) and replace this term by $\kappa\vec{V}$, and use a value for $\kappa = 8\times10^{-5}$ sec^{-1} (Haurwitz, 1947), then we find that all terms in this equation are of the order of 10^{-3} m sec^{-2}. This implies that there are no a priori simplifications that we can apply to the horizontal equations of motion for subsynoptic motion scales.

As shown in numerous texts, including Haltiner's, we need only to show that the characteristic depth is sufficiently small compared to the characteristic length to verify the hydrostatic assumption. In this case,

$$\frac{D^2}{L^2} \sim 10^{-4} << 1,$$

so we can legitimately assume hydrostatic equilibrium on this scale.

For the conservation of energy (First Law of Thermodynamics), we again call on Haltiner's discussion as our framework. In his notation,

$$\left(\frac{\partial}{\partial t} + \vec{V}\cdot\nabla\right) \ln\theta \sim \frac{V}{L}\ \frac{Fr}{Ro} \sim 10^{-6},$$

$$w\ \frac{\partial \ln\theta_s}{\partial z} \sim \frac{V}{RiRo}\ \frac{\sigma_s}{L} \sim 10^{-5},$$

$$w\ \frac{\partial}{\partial z}\left(\frac{\delta\theta'}{\theta_s'}\right) \sim \frac{V}{L}\ \frac{Fr}{Ro} \sim 10^{-6},$$

where σ_s is the stability parameter of the standard atmosphere and is of the order of 10^{-1}. These results indicate that the validity of the isentropic assumption on this scale is questionable, since the second term is not balanced by either of the others. Thus, we must use the anisentropic form, which is

$$\left(\frac{\partial}{\partial t} + \vec{V}\cdot\nabla + w\frac{\partial}{\partial z}\right) \ln\theta = \frac{Q}{c_p T} ,$$

where Q is the anisentropic heating rate. We shall return to this subject shortly.

In what has just preceded, we have implicitly assumed that the mass continuity equation can be scaled so that

$$\frac{V}{L} \sim \frac{W}{D} .$$

This is not the case for all scales, as shown in all standard texts. Haltiner (op. cit.) shows that in general, the continuity equation implies

$$\frac{W}{D} \sim \frac{1}{RiRo} \quad \frac{V}{L} .$$

In this case, since both Ri,Ro ~ 1, we find that the previous scaling is valid. This also implies that on this scale the vorticity and divergence are of the same order. We should also mention that the relatively shallow nature of our disturbance allows us to ignore safely the effects of vertical density variations in the mass continuity equation for scaling purposes.

Let us now return to our assumption that Ri ~ 1. From our scale analysis so far, we can say that

$$Ri \sim \frac{\frac{g}{D}\frac{\delta\theta}{\theta}}{\frac{V^2}{D^2}} = \frac{gD}{V^2}\frac{\delta\theta}{\theta} \sim 1 \quad .$$

If this is to hold, we must have $\delta\theta/\theta \sim V^2/gD$. But we have

$$\frac{V^2}{gD} \equiv Fr \quad \text{and} \quad \frac{\delta\theta}{\theta} = \frac{Fr}{Ro} \sim Fr \ ,$$

so this assumption is not inconsistent with our analysis. In fact, a substantial body of evidence supports this order of magnitude for Ri. The studies of McGinley (1973) and Sasaki (1973) show clearly that Ri ~ 1 for systems of the sort described here. Additionally, the scale analysis and numerical simulations of Gambo (1970a,b) stress that Ri must be of this order if the medium scale divergence is to be comparable in order to the vorticity -- i.e.,

$$\nabla \cdot \vec{V} \sim \frac{1}{RiRo}\zeta \ ,$$

which is what we have found for our band-pass fields.

Finally, let us turn our attention to the anisentropic heating we mentioned earlier. The dry air to the west of the surface dryline in Great Plains subsynoptic systems is characterized by steep lapse rates over a deep layer (Schaefer, 1973; McFarland, 1975). It is reasonable to propose that a

substantial anisentropic effect would be realized by turbulent mixing in such an air mass. If we neglect the two smallest terms in the anisentropic statement of the First Law:

$$w \frac{\partial \ln \theta_s}{\partial z} = \frac{Q}{c_p T} = \frac{d \ln \theta}{dt} \quad ,$$

where Q is of the order of 3 joule kg^{-1} sec^{-1}. If we say that this is the result of turbulent heat flux divergence then

$$\frac{Q}{c_p T} = \frac{\partial H}{\partial z} \quad ,$$

where $H \sim \overline{w' \theta'}$, the turbulent heat flux. Recall that

$$w \frac{\partial \ln \theta_s}{\partial z} \sim 10^{-5} \quad .$$

If we say that w* is a typical turbulent convective vertical velocity, with a value of 2.5 m sec^{-1}, then we model the heat flux by

$$H \sim w^* \frac{\partial \theta_s'}{\theta_s'} \sim 2.5 \times 10^{-2}$$

If we, in turn, model this via an eddy coefficient hypothesis, we find

$$H \sim K_H \frac{\partial \ln \theta_s}{\partial z} \sim K_H \frac{\sigma_s}{D}$$

Therefore, $K_H \sim 2.5 \times 10^2$ m^2 sec^{-1}. This rather large value can be substantiated, in part by the low Ri associated with the dry air (McGinley, 1973) and in part by direct calculations in a one-dimensional boundary layer model (Burk, personal communication) with input stratification corresponding to typical dry air values. Even though this eddy mixing is large by synoptic scale standards, it is not unreasonable in the low Ri environment behind a dryline.

If we turn our attention to the moist air ahead of the dryline, where we expect severe convection, we propose that latent heat release can account for the anisentropic effect. Suppose C is the condensation rate in the convective areas and L is the latent heat of condensation ($L \sim 2.4 \times 10^6$ joule kg^{-1}). Then the total rate of anisentropic heating per unit mass is simply

$$Q = LC$$

Now by our scale analysis $Q/C_pT \sim 10^{-5}$ sec^{-1} with $c_pT \sim 3 \times 10^5$ joule kg^{-1}, so we must have

$$C \sim 1.25 \times 10^{-6} \text{ sec}^{-1},$$

This condensation rate is actually in kg of water per kg of air, per second, so that this implies

$$C \sim 1.25 \times 10^{-3} \text{ g kg}^{-1} \text{ sec}^{-1},$$

which is the same order of magnitude as the band-pass moisture convergence we have computed for the subsynoptic scale -- i.e.,

$$\nabla\cdot(r\vec{V}) \sim \frac{V}{L}\ r \sim 10^{-3}\ \text{g kg sec}^{-1}\ ,$$

if $r \sim 10$ g kg^{-1}. Hence, we are in substantial agreement with the results of Fritsch (1975) who has pointed out that severe convection cycles both total mass and water mass substantially faster (by an order of magnitude) than can be resupplied by large scale convergence. Our result indicates that subsynoptic moisture convergence is adequate to account for the water mass budget of severe convection and that the latent heat released in the process can account for the anisentropic heating in the moist air required by our scale analysis. That anisentropic effects play a significant role has been suggested by Gall (1976a,b) and Nitta and Ogura (1972).

CHAPTER V

SUBSYNOPTIC SCALE DYNAMICS

As suggested in the introduction, there is a modest amount of dynamical theory available in the literature on this scale. No general agreement exists about the primary mechanism for the systems we observe in severe weather situations. A substantial number of tornadoes and severe thunderstorms develop in association with what could be called "synoptic" scale weather systems. One of the cases we have examined, that of June 8, 1974, is of this variety. The severe weather events in such a situation are widespread and, as Ostby (1975) suggests, are relatively well treated by conventional forecast methods. Other situations, such as the June 18, 1973 event we have examined in Chapter III, are characterized by somewhat isolated clusters of severe thunderstorms. These develop in association with subsynoptic systems that cannot be explained by classical theory of synoptic scale weather systems. The main criterion we use to differentiate between the two types is the presence or absence of

strong upper-level (say 500 mb or above) forcing. As so lucidly explained in Palmén and Newton (op. cit., Ch. 11), upper-level divergence is crucial for the development of an extratropical cyclone. We can generally associate upper-level divergence with positive vorticity advection (PVA) at 500 mb, and it is often not possible to find strong PVA in many tornado-producing weather situations, especially in the Great Plains.

Instead, as suggested by Tegtmeier (op. cit.), we find many severe weather events occur with frontal waves that never go through the full life cycle of an extratropical cyclone. In this sense, they are so-called "stable" frontal waves. However, there is growing evidence that such medium scale (subsynoptic) systems, developing in zones of modest baroclinicity, can and do play an important role in organizing severe convection. The numerical simulations of Gall (1976a,b), Nitta and Oqura (1972), Tokioka (1972) and Gambo (1970a) all suggest that disturbances, primarily confined to the lower troposphere, can develop on a time scale appropriate for our subsynoptic framework, independent of any upper-level developments.

Instability theory, as developed by Stone (1966), Tokioka (1970), and Orlanski (1968), points out that in the range where Ro and Ri are of order unity, a variety of mechanisms can operate. As Ri and Ro vary over this order, theory predicts that Kelvin-Helmholtz (vertical shear),

symmetric, baroclinic, and barotropic (horizontal shear) instabilities are all capable of playing some role. A small variation of either Ri or Ro can cause a large change in the theoretical growth rate for the various modes. Tokioka (op. cit.) and Gall (1976a) point out that for classical baroclinic instability the growth rate increases for decreasing Ri, and shifts toward smaller wavelengths if the lapse rate increases under constant vertical shear. This is precisely the condition we expect for frontal waves of the sort we have been considering. Also, Kung and Tsui (1975) and Gall (op. cit.) have shown that the primary source of subsynoptic scale kinetic energy production seems to be the baroclinic mode. Since the work of Kung and Tsui is observational in nature, we are encouraged to support the baroclinic instability hypothesis. Gambo (1970a) has shown that baroclinic instability on this scale becomes significant for Ri $\sim$ 1, but emphasizes that other mechanisms, such as shearing instability, may arise in this range (Gambo, 1970b).

The numerical simulations of Tokioka (op. cit.) and Nitta and Ogura (op. cit.), as well as the observations of Matsumoto, et al. (1970) have shown that the disturbances they have examined are relatively cold air in the lower troposphere on the south side of the system. However, Nitta and Ogura point out in their case that the opposite is actually observed. The cases seen in this study also show warm air to the south. Thus, as proposed by Gall, the frontal

wave circulation acts to decrease dynamic instability. In the absence of upper-level large-scale forcing, the warm air rising northward and the cold air sinking southward act to suppress further baroclinic development, via an increase of static stability and a decrease of vertical wind shear. It is anticipated that the severe convection developing in association with the subsynoptic wave plays a significant role in this process, as suggested by the scale analyses in the preceding chapter. The budget studies of McGinley (1973) support this hypothesis. His analysis of several cases, including two of the cases shown here, shows that in the vicinity of thunderstorms, subgrid heat sources and kinetic energy sinks exist at high levels, with heat sinks and kinetic energy sources at low levels. This indicates the effect of the severe convection is to relieve the conditions that allowed the subsynoptic circulation to amplify.

We now wish to focus our attention on the vorticity and divergence equations, as applied to our results. These may be written:

$$\frac{\partial \zeta}{\partial t} + \vec{V}\cdot\nabla\ (\zeta+f) + w\frac{\partial \zeta}{\partial z} = -(\zeta+f)\,\delta + \left(\frac{\partial w}{\partial y}\,\frac{\partial u}{\partial z} - \frac{\partial w}{\partial x}\,\frac{\partial v}{\partial z}\right)$$

$$+ \hat{k}\cdot(\nabla \times \vec{F} - \nabla\alpha \times \nabla p)$$

and

$$\frac{\partial \delta}{\partial t} + \vec{V}\cdot\nabla\delta + w\frac{\partial \delta}{\partial z} = -\delta^2 + f\zeta - \alpha\nabla^2 p + 2\hat{k}\cdot\nabla u \times \nabla v +$$

$$- \nabla w\cdot\frac{\partial \vec{V}}{\partial z} - \nabla\alpha\cdot\nabla p + \nabla\cdot\vec{F} + \vec{V}\cdot(k \times \nabla f).$$

These equations apply only to the subsynoptic scale and, as mentioned before, do not include the interaction terms with large scale flow. We shall examine these equations as they apply to our band-pass data to see how well they are satisfied with our surface data as input. We are clearly unable to evaluate those terms that involve vertical motion, since we have no reliable means of estimating such motion. Similarly, we cannot evaluate the terms involving vertical derivatives. Although we cannot readily dismiss the possible effects of terms involving $\nabla\alpha$, we are similarly unable to estimate this reliably, so it is neglected. On the basis of a simple estimate of order of magnitude, we neglect terms involving ∇f immediately. Thus, we may rewrite our equations, also neglecting friction terms, as:

$$\frac{\partial \zeta}{\partial t} = -\vec{V}\cdot\nabla\ (\zeta+f) - (\zeta+f)\,\delta\ ,$$

$$\frac{\partial \delta}{\partial t} = -\vec{V}\cdot\nabla\delta - \delta^2 + f\zeta - \alpha\nabla^2 p + 2k\cdot\nabla u \times \nabla v\ .$$

Upon using the band-pass data to evaluate these equations, we find several remarkable results. First, the observed values of $\partial\zeta/\partial t$ are well correlated with the sum

of $-\vec{V}\cdot\nabla(\zeta+f)$ and $-(\zeta+f)\delta$. This agrees with the conclusions of Matsumoto, et. al. (1967) that on this scale, the vorticity distribution seems to be dominated by the divergence field. This suggests that the vorticity of the subsynoptic system is generated by convergence of already existing low-level vorticity. We do not find, however, a significant need for a contribution from the tilting term, as did Matsumoto, et al. (op. cit.).

A simple scale analysis of the divergence equation implies that the largest terms in the equation ought to be of the order of 10^{-8} sec^{-2}. This is the case for the band-pass data, with the exception of the pressure Laplacian term. Use of observed band-pass data gives values for $-\alpha\nabla^2 p$ of the order of 10^{-7} sec^{-2}. This agrees with the values obtained by Matsumoto and Ninomiya (1967). It is not clear that eddy momentum transport is sufficient to explain the apparent imbalance, as the pressure Laplacian remains the dominant term throughout the day. It would be more likely to suppose that the subsynoptic scale momentum transport over a large area, implied by the terms

$$w\frac{\partial \delta}{\partial z}\ ,\ \nabla w \cdot \frac{\partial \vec{V}}{\partial z} \text{ which are derived from } \nabla\cdot(w\frac{\partial \vec{V}}{\partial z})$$

is responsible, if the effect is to be relatively time independent. Since the pressure term has violated our simple scale analysis, such additional violations would not be unreasonable. It is worth mentioning again that the pressure

used here is already a sort of "perturbation pressure", as the low-pass pressure field has been subtracted out. If one examines the ageostrophic patterns seen in the low-pass fields, it may be noted that we have found that the crossing-angle patterns are remarkably consistent from case to case and from one analysis time to another. This also suggests some relatively large scale, time-independent effect on the flow field, which may be below the scale of the low-pass analysis, but of the same scale as the subsynoptic system. It is not clear at this time that we can isolate the aforementioned terms as those that balance the pressure Laplacian term. But it does seem obvious that if the pressure term is large in comparison to the remaining terms and the effect is not temporally dependent, then friction terms generated by small-scale eddies are probably not responsible for the balance, as proposed by Matsumoto, et al. (op. cit.).

The second problem, which is the lack of balance of the observed divergence tendency with the terms remaining after omission of the (presumably balanced) band-pass pressure Laplacian is also unresolved. It is here that the temporal variation of the friction terms as a result of dry convection may play a role, as suggested by Sasaki (1973). The convergence immediately behind the dryline could be related to this effect, since convective mixing develops rapidly in the morning within the dry air as the morning inversion is eroded by solar heating. There may also be a

pressure perturbation, superimposed on this subsynoptic scale pressure field, which is of subgrid scale and hence, unresolved. This could also contribute to the observed temporal and spatial divergence variations, but we have no data to support small-scale pressure influence at this time.

In summary, it appears that the subsynoptic scale flow field satisfies a special type of "balance" equation with its mass field -- namely,

$$-\alpha\nabla^2 p = \nabla\cdot\left(w\frac{\partial\vec{V}}{\partial z}\right) .$$

When this is satisfied, the observed time changes are at least of the same order as the remaining calculable terms in the horizontal version of the divergence equation. If we assume that the friction term is responsible for the residuals in the revised divergence equation, we have

$$\frac{\partial\delta}{\partial t} = -\vec{V}\cdot\nabla\delta - \delta^2 + f\zeta + 2\hat{k}\cdot\nabla u \times \nabla v + \nabla\cdot\vec{F}$$

where $\vec{F}$ is of the form $\partial/\partial z\ (\overline{u'w'})$.

The corresponding vorticity equation makes use of the fundamental balance we have just described. Since the balanced condition implies

$$-\alpha\frac{\partial p}{\partial x} = w\frac{\partial u}{\partial z} \quad \text{and} \quad -\alpha\frac{\partial p}{\partial y} = w\frac{\partial v}{\partial z} ,$$

when we compute the tilting terms in the vorticity equation, we find that

$$\frac{\partial w}{\partial y}\frac{\partial u}{\partial z} - \frac{\partial w}{\partial x}\frac{\partial v}{\partial z} = 0 .$$

This model agrees well with the calculated results from the band-pass data -- i.e.,

$$\frac{\partial \zeta}{\partial t} = -\vec{V}\cdot\nabla(\zeta+f) + (\zeta+f)\delta \ .$$

Also, the friction term appears not to be necessary in the vorticity equation. This finding also agrees with the work of Matsumoto, et al. (op. cit.), in which the frictional forces are considered irrotational. Thus, we have indications that friction on this scale is predominantly the result of eddy momentum transport, as postulated by Matsumoto, et al.

CHAPTER VI

SUMMARY AND RECOMMENDATIONS

We have developed a band-pass filter which can produce a detailed subsynoptic analysis from relatively noisy surface data. The analyses can be correlated with severe storm events on this scale, provided that the organizing dynamical system is within the resolution limits imposed by the data.

From these results and available theoretical and numerical studies, we have developed a subsynoptic scale analysis which is internally consistent and seems to be verified by the band-pass data. This analysis has suggested that anisentropic effects play a major role in subsynoptic events. The surface data are consistent with the hypothesis that the circulation is a low-level baroclinic instability phenomenon. These circulations can be detected well in advance of thunderstorm development and appear to localize storm activity in such a way that very strong convection results. Indications are that convection is instrumental in causing the decay of this subsynoptic scale circulation. There is evidence that

a subsynoptic scale balance exists between the pressure forces and the momentum transport generated by the vertical circulations of the subsynoptic system. This momentum transport may also influence the larger scale flow, creating characteristic patterns of ageostrophic winds.

As in most research, there remain some unanswered questions. The band-pass filter we have developed is relatively new, and to the author's knowledge, band-pass moisture divergence calculations have only been done by Hylton (1972). Hylton's method of computing moisture divergence differs somewhat from the method used in this study, so it is somewhat difficult to compare results. A method similar to band-pass filtering has been presented by Darkow and Livingston (1973) in which a Shuman (1957) filtered "low-pass" field is subtracted from the analyzed field. But no attempt at analysis of the spectral modification of this technique is made. Also, only pressure and static energy (Krietzberg, 1964) fields are analyzed, with no kinematic analysis.

Because of the lack of previous work in this area, a considerable effort should be made to relate band-pass analysis to a wider range of cases. The work of Charba (1975) or Hudson (1971) has shown that "low-pass" moisture convergence has good correlation to severe weather events. Since this study has substantiated this finding and indicated a possible extension to band-pass moisture convergence, this seems to be a fruitful avenue for further study. A question

of some practical significance exists in this area -- i.e., whether or not the results shown here can be useful in real-time forecasting. If this method can be applied on a real-time basis, we will not only extend the range of test cases, but we will be able to see if the method can be useful for refining the areas of severe weather threat, as suggested by this post-storm study.

Another potentially useful avenue of research is modelling the subsynoptic systems we have isolated with the band-pass filter. The results of the scale analysis provide a preliminary framework for additional numerical simulations. If one can successfully parameterize the anisentropic effects, the results we have shown can be applied to a simplified model, perhaps incorporating the implied balance equation as a diagnostic constraint. The role of diurnal effects in the dry air seem crucial to storm development, but it is not yet clear how the dryline (which is not a baroclinic zone) interacts with the frontal wave. This interaction could be clarified by numerical experiments.

Lack of knowledge of the subsynoptic scale vertical structure is a critical gap which inhibits further elucidation of subsynoptic processes. Available serial soundings in proximity to tornadic storms (Schaefer, personal communication) show deepening of the moist layer and erosion of the capping inversion prior to the onset of convection. This supports our hypothesis of the role of subsynoptic scale

moisture convergence in localizing convection. But we need a broader scope to our knowledge of the time variations of static stability, moisture and wind profiles, etc. to determine the validity of our suggestions about the dynamics of the subsynoptic system, especially in the dry air. Budget studies on the time and and space scales we have considered would be fruitful in answering questions on the nature of energy conversions.

Our examination of the problems inherent in analysis of meteorological data has shown that we need to examine the theory of the information content in our observations. This has a definite impact on the design of future experimental observation networks and the ways in which data are analyzed. We need to develop some means of ensuring that our networks will, in fact, resolve the phenomena that we seek without excessive redundancy, for purely practical reasons. This developing theory will have to account for the variety of physical mechanisms that can give rise to meteorological waves. It should also be able to account for networks that are non-uniform, owing to the relatively random distribution of most meteorological data.

We cannot reasonably expect to have subsynoptic scale data available operationally in the foreseeable future, so we need to examine how motions on this scale interact with other scales. Our analysis has suggested several possible interactions and it is likely that continuing research in the

dynamics of these subsynoptic scales of motion will indicate more interactions. Since this scale is intermediate between the complex mesosystems seen in experimental data and the standard large-scale analysis, it is possible that it plays an important intermediary role between the scales. In any event, subsynoptic systems represent an exciting area of study that is accessible with more or less conventional data. It is hoped that this work will stimulate further efforts to examine subsynoptic scale processes.

REFERENCES

Barnes, S. L. "A Technique for Maximizing Details in Numerical Weather Map Analysis," Journal of Applied Meteorology, 3, 1964, pp. 396-409.

Barnes, S. L. "Mesoscale Objective Map Analysis Using Weighted Time-Series Observations," NOAA Technical Memoranda ERL-NSSL-62, Norman, Oklahoma, 1973, 60 pp.

Bedient, H. A., and G. P. Cressman. "An Experiment in Automatic Data Processing," Monthly Weather Review, 85, 1957, pp. 333-340.

Bengtsson, L. "4-Dimensional Assimilation of Meteorological Observations. GARP Publication Series No. 15, WMO, Geneva, Switzerland, 1975, 76 pp.

Blackman, R. B., and J. N. Tukey. The Measurement of Power Spectra (from the Point of View of Communications Engineering), New York: Dover Publications, 1958, 190 pp.

Brown, R. A. (Editor). "The Union City, Oklahoma Tornado of 24 May 1973," NOAA Technical Memoranda (in preparation), Norman, Oklahoma, 1976.

Charba, J. P. "Operational Scheme for Short Range Forecasts of Severe Local Weather," Preprints, Ninth Conference on Severe Local Storms, Norman, Oklahoma, 1975, pp. 51-57.

Charney, J. G., and A. Eliassen. "On the Growth of the Hurricane Depression," Journal of the Atmospheric Sciences, 21, 1964, pp. 68-75.

Darkow, G. L., and R. L. Livingston. "Hourly Surface Static Energy Analysis as a Delineator of Thunderstorm Outflow areas," Preprints, Eighth Conference on Severe Local Storms, Denver, Colorado, 1973, pp. 232-237.

Eddy, A. "The Objective Analysis of Atmospheric Structure," Journal of the Meteorological Society of Japan, Ser. II, 51, 1973, pp. 450-457.

Fritsch, J. M. "Synoptic-Meso Scale Budget Relationships for a Tornado Producing Squall Line," Preprints, Ninth Conference on Severe Local Storms, Norman, Oklahoma, 1975, pp. 165-172.

Gall, R. "A Comparison of Linear Baroclinic Instability Theory with the Eddy Statistics of a General Circulation Model," Journal of the Atmospheric Sciences, 33, 1976a, pp. 349-373.

Gall, R. "Structural Changes of Growing Baroclinic Waves," Journal of the Atmospheric Sciences, 33, 1976b, pp. 374-390.

Gambo, K. "The Characteristic Feature of Medium-Scale Disturbances in the Atmopshere (I)," Journal of the Meteorological Society of Japan, Ser. II, 48, 1970a, pp. 173-184.

Gambo, K. "The Characteristic Feature of Medium-Scale Disturbances in the Atmosphere (II)," Journal of the Meteorological Society of Japan, Ser. II, 48, 1970b, pp. 314-330.

Gandin, L. S. "Objective Analysis of Meteorological Fields," (English Translation, 1965): Program for Scientific Translations, Jerusalem, Israel, 1963, 242 pp.

Haltiner, G. J. Numerical Weather Prediction. New York: John Wiley, 1971, 317 pp.

Haurwitz, B. "Comments on the Sea-Breeze Circulation," Journal of Meteorology, 4, 1947, pp. 1-8.

Hudson, H. R. "On the Relationship Between Horizontal Moisture Convergence and Convection Cloud Formation," Journal of Applied Meteorology, 10, 1971, pp. 755-762.

Hylton, D. A. "The Application of Low-Pass and Band-Pass Filtering Techniques to Surface and Upper Air Wind Fields," Master's Thesis, University of Oklahoma, Norman, Oklahoma, 1972, 87 pp.

Jenkins, G. M., and D. G. Watts. Spectral Analysis and Its Applications. San Francisco: Holden-Day, 1968, 525 pp.

Krietzberg, C. W. "The Structure of Occlusions as Determined from Serial Ascents and Vertically Directed Radar," Air Force Cambridge Research Laboratory, Research Report 64-26, Cambridge, Massachusetts, 1964, 121 pp.

Kung, E. C., and T. L. Tsui. "Subsynoptic-Scale Kinetic Energy Balance in the Storm Area," Journal of the Atmospheric Sciences, 32, 1975, pp. 729-740.

Lewis, J. M. "Variational Subsynoptic Analysis With Applications to Severe Local Storms," Monthly Weather Review, 99, 1971, pp. 786-795.

Lumley, J. L., and H. A. Panofsky. The Structure of Atmospheric Turbulence. New York: John Wiley Interscience, 1964, 239 pp.

Maddox, R. A., and W. M. Gray. "A Frictionally Driven Model for Tornado Genesis with Similarities to Hurricane Genesis," Preprints, Eighth Conference on Severe Local Storms, Denver, Colorado, 1973, pp. 203-206.

Matsumoto, S., and K. N. Ninomiya. "On the Role of Convective Momentum Exchange in the Mesoscale Gravity Wave," Journal of the Meteorological Society of Japan, Ser. II, 47, 1969, pp. 75-85.

Matsumoto, S., K. N. Ninomiya, and T. Akiyama. "A Synoptic and Dynamic Study on the Three-Dimensional Structure of Mesoscale Disturbances Observed in the Vicinity of A Cold Vortex Center," Journal of the Meteorological Society of Japan, Ser. II, 45, 1967, pp. 64-82.

McFarland, M. J. "Sasaki's Variational Optimization Analysis of Temperature and Moisture Advection in a Severe Storm Environment," Preprints, Ninth Conference on Severe Local Storms, Norman, Oklahoma, 1975, pp. 158-164.

McGinley, J. A. "Environmental Energy Fields Associated With Severe Storms," Master's Thesis, University of Oklahoma, Norman, Oklahoma, 129 pp.

McGinley, J. A., and Y. K. Sasaki. "The Role of Symmetric Instabilities in Thunderstorm Development on Drylines," Preprints, Ninth Conference on Severe Local Storms, Norman, Oklahoma, 1975, pp. 173-180.

Miller, R. C. "Notes on Analysis and Severe-Storm Forecasting Procedures of the Air Force Global Weather Central," Air Weather Service Technical Report 200 (Rev.), Air Weather Service, Scott Air Force Base, Illinois, 1972, approximately 190 pp.

Nitta, T., and Y. Ogura. "Numerical Simulation of the Development of the Intermediate-Scale Cyclone in a Moist Atmosphere," Journal of the Atmospheric Sciences, 29, 1972, pp. 1011-1024.

Orlanski, I. "Instability of Frontal Waves," Journal of the Atmospheric Sciences, 25, 1968, pp. 178-200.

Ostby, F. P., Jr. "An Application of Severe Storm Forecast Techniques to the Outbreak of June 8, 1974," Preprints, Ninth Conference on Severe Local Storms, Norman, Oklahoma, 1975, pp. 7-12.

Palmén, E., and C. W. Newton. Atmospheric Circulation Systems. New York: Academic Press, International Geophysics Series, 13, 1969, 603 pp.

Sasaki, Y. "An Objective Analysis Based on the Variational Method," Journal of the Meteorological Society of Japan, Ser. II, 36, 1958, pp. 77-88.

Sasaki, Y. "An Objective Analysis for Determining Initial Conditions for the Primitive Equations," Technical Report Project 208, 1960, Texas A&M University, College Station, Texas, 22 pp.

Sasaki, Y. "Some Basic Formalisms in Numerical Variational Analysis," Monthly Weather Review, 98, 1970, pp. 875-883.

Sasaki, Y. K. "Mechanism of Squall-Line Formation as Suggested from Variational Analysis of Hourly Surface Observations," Preprints, Eighth Conference on Severe Local Storms, Denver, Colorado, 1973, pp. 300-307.

Saucier, W. J. Principles of Meteorological Analysis. Chicago: University of Chicago, 1955, 438 pp.

Schaefer, J. T. "The Environment Near the Dryline," Proceedings, Opening Meeting for SESAME, Boulder, Colorado, 1974 (Published 1975), pp. 206-216.

Seibers, J. O., F. Hidalgo, S. A. Tegtmeier, and M. Young. "Guide for Using GOES/SMS Imagery in Severe Weather Forecasting," USAFETAC, Andrews Air Force Base, Maryland, 1975, 56 pp.

Sheets, R. C. "Analysis of STORMFURY Data Using The Variational Optimization Approach," NOAA Technical Report, 1973, ERL 264-WMPO 1, Boulder, Colorado, 92 pp.

Shuman, F. G. "Numerical Methods in Weather Prediction: II Smoothing and Filtering," Monthly Weather Review, 85, 1957, pp. 357-361.

Stephens, J. J. "On Definable Scale Reduction by Simultaneous Observations," Journal of Applied Meteorology, 10, 1971, pp. 23-25.

Stephens, J. J., and J. M. Stitt. "Optimum Influence Radii for Interpolation with the Method of Successive Corrections," Monthly Weather Review, 98, 1970, pp. 680-687.

Stone, P. "On Non-Geostrophic Baroclinic Instability," Journal of the Atmospheric Sciences, 23, 1966, pp. 390-400.

Tegtmeier, S. A. "The Role of the Surface, Subsynoptic, Low Pressure System in Severe Weather Forecasting," 1974, Master's Thesis, University of Oklahoma, Norman, Oklahoma, 66 pp.

Tidwell, L. G. "A Synoptic and Sub-Synoptic Study of the 8 June 1974 Severe Thunderstorm and Tornado Outbreak in Oklahoma," Master's Thesis, University of Oklahoma, Norman, Oklahoma, 1975, 65 pp.

Tokioka, T. "Non-Geostrophic and Non-Hydrostatic Stability of a Baroclinic Fluid," Journal of the Meteorological Society of Japan, Ser. II, 48, 1970, pp. 503-520.

Tokioka, T. "A Numerical Experiment of Medium-Scale Disturbances: Dry Model," Journal of the Meteorological Society of Japan, Ser. II, 50, 1972, pp. 259-270.

APPENDIX A

SOURCES OF ERROR IN THE ANALYSIS

Meteorological observations contain many sources of error, which we can summarize in three basic categories: measurement, interpolation, and sampling errors.

By measurement errors, we include such problems as bias, lag, hysteresis, and system noise in the instrument used to measure a quantity of interest. Also included are any human errors in operating the measurement system and external influences (e.g. -- lightning strikes, mechanical shock, etc.). Aside from the gross error check of the data described above, there will be no treatment of this subject here. There is not much that can be done in the immediate future to improve the quality of measurement in the operational surface data network. This is not to be construed as a statement of satisfaction with the quality of these data, as improvements are indeed desired. For the moment it is reasonable to assume that more serious errors will arise, meteorologically speaking, in the second two categories. In a sense, Bengtsson (1975) concurs in this assessment by

pointing out that the interpolation error will generally be larger than the measurement error, if the latter is uncorrelated. This implies that measurement error is potentially less serious (owing its random nature), as a result of the smoothing effect of interpolation.

The subject of interpolation error has been treated extensively by Gandin (1963) and his work on so-called optimum interpolation is the basis of Eddy's (1973) work. For our purposes, however, interpolation error will also not be treated in any depth here. Gandin himself states (op. cit., p. 67), "For a dense network of stations, any reasonable interpolation method will have an accuracy which is only slightly lower than the accuracy of optimum interpolation." Although not explicitly defined by Gandin, a network is dense when it samples the phenomena of interest at a frequency well above the Nyquist.

The final source of error in meteorological observations is sampling error -- i.e., the errors introduced by the finite, discrete nature of our data. There are several aspects to this problem, some of which have received relatively little attention. A series of tests using the interpolation methods of this paper have been made under various conditions of data sample size, density and so forth. The input is a known, analytic function and the output is compared to this standard with the intent to provide a qualitative estimate of the sampling error of this analysis method.

Except where noted, the input data contain two harmonics, one just below the spatial Nyquist frequency and one well above it, superimposed on a mean field. The field mean is 10^3 (arbitrary units) and each harmonic has an amplitude of 20.

The first aspect considered is comparison of a data sample distributed pseudo-randomly in space with one spaced at regular intervals. The regularly spaced data locations are shown in Fig. A1(a), while the random data locations, given by

$$x_r = x_o + \frac{N_1^{*2}}{2} \Delta s \quad ,$$

$$y_r = y_o + \frac{N_2^{*2}}{2} \Delta s \quad ,$$

(where $(\ )_r$ is the coordinate in the random mesh, $(\ )_o$ is the coordinate of a point in the regular data mesh, N_1^* and N_2^* are pseudo-random numbers uniformly distributed from -1 to +1, and s is constant grid spacing in the regular data mesh) are illustrated in Fig. A2(a). We see the resulting interpolated fields in Figs. A3 and A4. The influence radius used is 18 s. Two observations can be made. First, the regular network has somewhat underestimated the theoretical amplitude that is to be passed by the band-pass filter while the low-pass results are about correct in terms of the amplitude of the long harmonic. No obvious aliasing of the short harmonic appears in either analysis. Second, the results for the

random mesh show a substantial degradation of the "true" field, for both the low- and band-pass analysis, although some of the basic features come through. The negative aspects of a random distribution may be the result of spatial variations in the aliasing of the shorter harmonic. This subject is discussed somewhat more below.

Another aspect that has received relatively little attention is the effect of edges and corners. As the edge of the analysis grid is approached, unless data from outside the grid is considered, the number of points used for the weighted average falls off markedly. If the data mesh is uniform, an edge grid point considers half the points that an interior point uses. In the corner, the average is over one-fourth the data points. This can lead to serious biases. An estimate of the effect depends, of course, on the weight function used and the radius of influence. Figures A5 and A6 show the results on a grid which has three fewer grid points along each side, but uses the original data mesh. This results in a grid which has data well outside of the units of the grid. The influence radius is 11 grid lengths and the weight function used is the one which samples the center of the band 8 times. The data grid is regularly spaced.

Low-pass results show that exclusion of data outside the grid has seriously contaminated the analysis, giving about 10 units of gradient across the grid where no gradient really exists. The band-pass analysis shows a similar

degradation, but the effect diminishes rapidly toward the center of the mesh, as expected. The band-pass error along the boundaries is of the order of 5 units or more, but more important is the substantial change in pattern.

The third aspect under consideration is the effect of variable data density, particularly that associated with a boundary where a dense data mesh gives way to a sparse one. This problem of variable aliasing is related to the question of random vs. regular data samples as well as the typical situations on coastlines or where data networks are "nested". In an effort to show the effect, the standard regular mesh of data as seen in Fig. A1(a) is used for the first 6 columns of data in the mesh -- about halfway across the analysis grid. Then the data spacing in both the x and y directions is tripled. The data mesh appears in Fig. A1(b). Results, shown in Fig. A7 should be compared to Fig. A3, which is otherwise identical (except for the "coarse" data mesh part). It can be seen that the quality of the analysis is degraded almost immediately at the edge of the dense network and considerable noise appears in the form of shorter wavelengths. The patterns are distorted and strong gradients are developed, especially along or near the edges of the grid. Clearly, aliasing has significantly altered the analysis. Figure A8 shows the same test on a randomly distributed data mesh (shown in Fig. A2(b). The problems that show up for the "regular" grid are even more acute when the data are distributed randomly.

It appears from the tests seen so far that a data mesh which allows the aliasing/truncation effect to vary spatially (or temporally) has difficulty with returning the input signal. The implications for network design are serious but no recommendations can be made on the basis of the limited testing done here. It does seem clear from what we see in these simple tests that an average data density is not adequate to describe the resolving power of a randomly spaced data mesh.

Aliasing is one of the key concepts in the general topic of sampling error and is discussed in broad terms in almost any text on spectral analysis (see Jenkins and Watts, 1968). If one considers the frequency at which standard meteorological observations are taken it is clear that if instantaneous data (such as would be the result of automatic digital observing) were taken at hourly intervals, severe aliasing would result, especially for winds. The normal wind field contains large amounts of power at high frequencies and this would be folded and refolded until a nearly white noise spectrum can result if the observations are instantaneous and at hourly intervals. However, human observers currently record the winds manually and, fortuitously, do what amounts to a time averaging process on the instruments' output. The amplitude of high frequency modes in temperature, pressure, and moisture observations is normally low enough to allow some hope that the folded part of those observations

falls mainly in the high-frequency portion of the spectrum where a low-pass filter can eliminate the noise. As a consequence, some hope exists for using the standard surface observations, provided proper filtering is done (which, of course, is the part of the point of this work).

A second key concept in sampling is the truncation error. If we sample a wave at or near the Nyquist interval, we have "resolved" the wave in terms of simple sampling theory, but we really know little or nothing about the wave. In particular, if we compute spatial or temporal derivatives of the wave, we cannot rely on our results. Truncation error is generally taken to mean the difference between the "true" derivative and its finite difference analog. Consider the standard centered difference operation on a function of one independent variable, f(x), where

$$\frac{df}{dx} \doteq \frac{f(x+\Delta) - f(x-\Delta)}{2\Delta} \quad ,$$

where Δ is the difference interval. If we let f be a wave of the form

$$f(x) = A \sin \frac{2\pi}{L} x \quad ,$$

where A is the amplitude of the wave and L is its wavelength, then

$$\frac{df}{dx} = \frac{2\pi A}{L} \cos \frac{2\pi}{L} x \ .$$

If we consider the difference form

$$\frac{f(x+\Delta) - f(x-\Delta)}{2\Delta} = \frac{A}{2\Delta} 2 \cos \frac{2\pi x}{L} \sin \frac{2\pi \Delta}{L} ,$$

which simplifies to

$$\frac{f(x+\Delta) - f(x-\Delta)}{2\Delta} = \frac{A}{\Delta} \cos \frac{2\pi x}{L} \sin \frac{2\pi \Delta}{L} .$$

When Δ is small in comparison to L, then

$$\sin \frac{2\pi \Delta}{L} \approx \frac{2\pi \Delta}{L} ,$$

and the finite difference form becomes identical to the true form. Suppose that L is at the Nyquist interval, however. Then $L = 2\Delta$ and

$$\frac{f(x+\Delta) - f(x-\Delta)}{2\Delta} = \frac{A}{\Delta} \cos \frac{2\pi x}{L} \sin \pi = 0.$$

Clearly, then, we can compute derivatives of our analyzed fields properly only for wavelengths long enough so that truncation error is not a problem.

Having examined the qualitative effects of the sampling error, there remain two questions of interest before we turn to the results of the filtering. The first of these questions concerns the radius of influence to be used for the weighted average. If we were using the successive corrections interpolation scheme of Bedient and Cressman (1957), the influence

radius would be the parameter that determined the weight function; but our interpolation weight function is exponential and, in principle, extends to infinite radius. Clearly, we have to set some finite limit to its extent. In his paper on the method, Barnes (1963, op. cit) points out that beyond some limit that depends on the analysis parameters (the κ_i), the weights are so small that we may safely exclude points outside that limit. Barnes' work is directed toward reproducing the initial input as accurately as possible by choosing the analysis parameter in a specific way and making successive passes until the interpolation error is acceptable. In this work, the analysis parameters are chosen to derive a specific band-pass filter and, having established them, it is expected that we may lose some of the amplitude of intermediate-scale waves in the low-pass filtered analysis. Our interest in the radius of influence is, in fact, only to choose a large enough radius so that we do not effect the analysis significantly by further increase of the radius. Accordingly, our standard test program has been used to assess the effect of the influence radius. The same basic data as before is used here with the only change being the influence radius. The dense data mesh with regular spacing is our data base and the results for influence radii of 6Δs, 11Δs, and 18Δs are shown in Figs. A9, A10, and A3. The smallest influence radius clearly gives unsatisfactory results, apparently a result of the aliasing of the short wavelength input. The

radius of 11Δs is nearly satisfactory in the band-pass result, but the low-pass is somewhat noisy (although the amplitude is reasonable). From these results, an influence radius of 18Δs is chosen for all actual analysis.

The final question considered is the homogeneity and isotropy of the weight function. A simple spatial spectral analysis has shown that the real waves that will be considered are not symmetric (in general) and the asymmetry is not constant in time. The question can be stated simply: Is an homogeneous, isotropic weight function able to give reasonable results for inhomogenous, anisotropic waves? In an effort to evaluate this, a final test has been run in which a wave with only x-dependence is input to the analysis test program. Results, shown in Fig. A11, demonstrate that the analyzed fields accurately portray the lack of y-dependence.

In summary, if enough knowledge of the waves can be gathered (either by physical understanding or through statistical study) then an inhomogenous, anisotropic weight function can be constructed that will be optimum in some sense (see the remarks in the beginning of this chapter). But it seems likely that a simple symmetric weighted average interpolation of the sort used here is capable of giving acceptable results for a wide class of problems, with considerable computational economy. When developing an interpolation scheme, care should be taken to include data from outside the mesh whenever possible and to choose the influence radius wide enough to include all points which effect a datum point significantly.

APPENDIX B

OTHER CASE STUDIES

An outbreak of severe weather associated with synoptic scale forcing occurred in Oklahoma and Kansas on June 8, 1974. This event has been described in some detail by Ostby (1975) and is somewhat atypical for severe weather in the Great Plains. These data have been subjected to the same band-pass filtering methods developed in this study. Results are shown in Figs. B1 and B2. We see that the low-pass fields are dominated by the effects of a large cyclone, which has moved from northeast New Mexico. This cyclone is near, but not centered in a low pressure center -- the trend during the analyses period is for the circulation to approach this low pressure area. There is a trough of low pressure from the main low, in which exists a streamline confluence region. This is roughly coincident with the surface dryline, as seen in the moisture pattern. As in the June 18, 1973 case, we find that the kinematic convergence in the dry air lags behind the moisture convergence zone along the dryline. We

also find that the pressure center and trough line are again characterized by minimum ageostrophic wind speed, with the ageostrophic speed maxima in the moist air (with low crossing angles) and in the dry air (with high crossing angles).

The band-pass analysis shows a dramatic wind speed maximum in the dry air, which has developed rapidly during the mid-morning. The band-pass moisture field shows a good correlation with the momentum maxima, both in the dry air and in the moist, southerly flow ahead of the dryline. The combination of a strong surface temperature maximum in west central Oklahoma with the moisture field suggesta a local surface static stability minimum in central Oklahoma. A striking feature is the relative minimum in moisture convergence in Oklahoma, between the maxima in Texas and along the Kansas-Oklahoma border.

The satellite photo valid at 1452 CST (Fig. B3) shows that severe storms have developed (several tornadoes have already touched down in the vicinity of Oklahoma City) in the relative moisture convergence minimum of the band-pass fields. These storms are in the low pass moisture convergence maximum. These results can be interpreted as indicating that the dynamics that trigger and maintain thunderstorms in this event are probably on a scale well below the resolution of the data. As seen in the chapter on scale analysis, moisture convergence on the large scale is inadequate to supply the thunderstorms (Fritsch, op. cit.). Since the band-pass data

seem unable to explain the observed storms, we suspect the presence of smaller scale systems.

A final case study is May 24, 1973, the day of the well-known Union City tornado. This storm has been the subject of intensive study at NSSL and the overall synoptic picture can be obtained from Brown, et al. (1976). When comparing the low-pass results for May 24, 1973 (Fig. B4) with those of June 18, 1973, one is immediately struck with their similarity. The major difference between them is in the moisture pattern. Even the ageostrophic winds and isobaric crossing angle patterns are remarkably alike!

It is only when we examine the band-pass fields (Fig. B5) that differences become apparent. The orientation of the dryline is markedly different, the magnitude of the moisture discontinuity is substantially lower, the configuration of the moisture convergence reflects the different orientation of the features, and so forth. The time history of this case also departs from June 18 -- the intensity of the severe weather parameters decreases rapidly from 1500 CST onwards (not shown) while the severe weather and analyzed patterns of June 18, 1973 remain strong on this scale for a longer time. This is reflected in the events of the day -- the Union City storm produced the only major tornado of the day and this individual storm is only poorly related to the band-pass parameters (see the radar photo in Fig. B6). The conventional surface data seem unable to resolve the system

that produced the Union City storm. As we shall see, there are data available which nearly provide the required resolution. However, some of the features of the day's analyses are well-depicted in the band-pass fields. As an example, compare the shape of the thunderstorm line in Fig. B6 with the shape of the moisture convergence zone in Fig. B5.

APPENDIX C

COMPARISON WITH OTHER ANALYSES

The analyses we have seen have put the center of the band at three times the Nyquist interval in space and time. This is pushing the truncation error, since at $L = 6\Delta$

$$\frac{2\pi\Delta}{L} = 1.047 , \quad \sin \frac{2\pi\Delta}{L} = 0.866;$$

whereas at $L = 8\Delta$ we have

$$\frac{2\pi\Delta}{L} = 0.785 , \quad \sin \frac{2\pi\Delta}{L} = 0.707.$$

Results of a revised analysis using a band centered at four times the Nyquist show that as one might have anticipated, the fields are smoother. Many of the "details" are damped out, while basic features show a reduction in amplitude. An obvious conclusion, based on the truncation error argument, is that the smoother analysis should give more

reliable results. If we push the data to its useful limits, we can expect a certain amount of contamination. We can also expect to eliminate more signal along with the noise if we try to be conservative with the data. Without more cases to examine, the question of where a useful limit point is reached remains unanswered.

Turning to analyses done using other methods, we find that Tidwell (1975) has used the analysis package at NSSL developed by Barnes to examine the evolution of the surface fields for June 8, 1974. Results of that method are seen in Fig. C1 for 1200 CST. The basic data set is more detailed in that it contains the special NSSL surface subsynoptic stations. This yields a smaller average station separation near the center of the grid. However, only observations valid at map time are used -- no time-weighted averaging is done.

It is immediately apparent that fundamental similarities exist between the methods, but some substantial differences exist, as well. Qualitative comparison of the streamlines indicates that the low-pass field shown by Tidwell is roughly intermediate to the band- and low-pass results of Figs. B4 and B5. This is borne out by comparison of the kinematic divergence and vorticity patterns. The results presented here show considerably less "detail", even in the band-pass results. It is difficult to assess the extent to which the fine scale features seen in Tidwell's results are true signal on the subsynoptic

scale. The temporal continuity of Tidwell's results (not shown) is generally inferior to the results of the filtering presented here. The greater station density used by Tidwell may be in part compensated for by the time-weighting we have used. This is not to imply that the transient features shown in Tidwell's paper are not real -- only that the data do not allow good continuity when time-weighting is not used.

We now turn to a second comparison; namely, with so-called subjective analysis. In a sense, the skill and experience brought to bear by an experienced hand analyst is a standard by which we may compare our results. The results of hand analysis are not reproducible, which is the main drawback. Also, the expertise is neither quantitative nor easily acquired. Nonetheless, we would like our analysis to be able to do most of what an experienced synoptic meteorologist can do.

If we compare our results for June 18, 1973 with Figs. 8a and 8b in Siebers, et al. (1975) we find a very good relationship. The distinction between the activity developed in association with the cyclonic circulation and that developed further southwest along the dryline is clearly portrayed. As we have seen, this case and the one for May 24, 1973 both support the contentions of Tegtmeier (which form the basis of the Siebers, et al. paper). The objective depiction of these cases shows the ability of this method to support the subjective results of skilled hand analysts. An obvious advantage

of objective techniques is the possibility of actual calculation of kinematic properties, which adds a dimension to the depiction of the situation.

Next, let us compare another application of the analysis package at NSSL (using a low-pass Barnes technique, somewhat modified), this time on the May 24, 1973 case. As seen in Fig. C2, at 1600 CST there are two strong vorticity maxima in Oklahoma portrayed by this analysis. These are not shown as dramatically in the band-pass filtered results. However, by examination of the preceding analysis at 1500 CST (Fig. C3) we see that the vorticity pattern does not have good time continuity. The fact that the Union City tornado is associated with one vorticity maximum (and the weakest one, at that) which has little time continuity implies that the phenomenon which is driving the particular storm that struck Union City is on such a small scale that even the NSSL subsynoptic station network is nearly unable to resolve it. The fact that the "details" of this pattern are smoothed over in our band-pass fields is not surprising. In fact, as in the June 8, 1974 case, we find that the detailed behavior of severe weather outbreaks often cannot be resolved by conventional observations -- a conclusion that is not particularly surprising.

Finally, we compare our results for May 24, 1973 at 1200 CST with an analysis based on the paper by Stephens and Stitt (1970). The method is basically a successive corrections

technique but includes post-interpolation smoothing of the fields. The same stations that are used for our results have been used for this successive corrections analysis. As may be seen in Fig. C4, this smoothing pass results in smooth fields throughout the analysis. As with all comparisons to our results, we see similarities (e.g., compare the streamlines with the band-pass streamlines of Fig. B5) and differences (e.g., location of the fronts, as seen in the streamlines). Successive corrections analysis shows little detail in the thermal field, whereas the band-pass thermal field has several distinct features. On the other hand, the band-pass moisture convergence shows fewer features than successive corrections along the Red River. It is not the intent of this comparison to say which is the "better" analysis -- however, the dual-pass (low- and band-) nature of the current work is obviously better at depicting medium-scale features, since it has been designed to do so.

On the basis of these comparisons, we conclude that hand analysis cannot be used reliably to obtain kinematic properties of the flow although qualitative features may be represented. A second conclusion from these comparisons is that asking a low-pass filter to do the whole job is asking too much, regardless of the particulars of that filter. If one uses a low-pass filter to portray subsynoptic events as well as larger scales, one may run the risk of contamination from "noise" -- noise from signal below the level of reliable

detectability or noise of a more random nature. However, if the results are too smooth, one may have eliminated useful signal along with the noise.

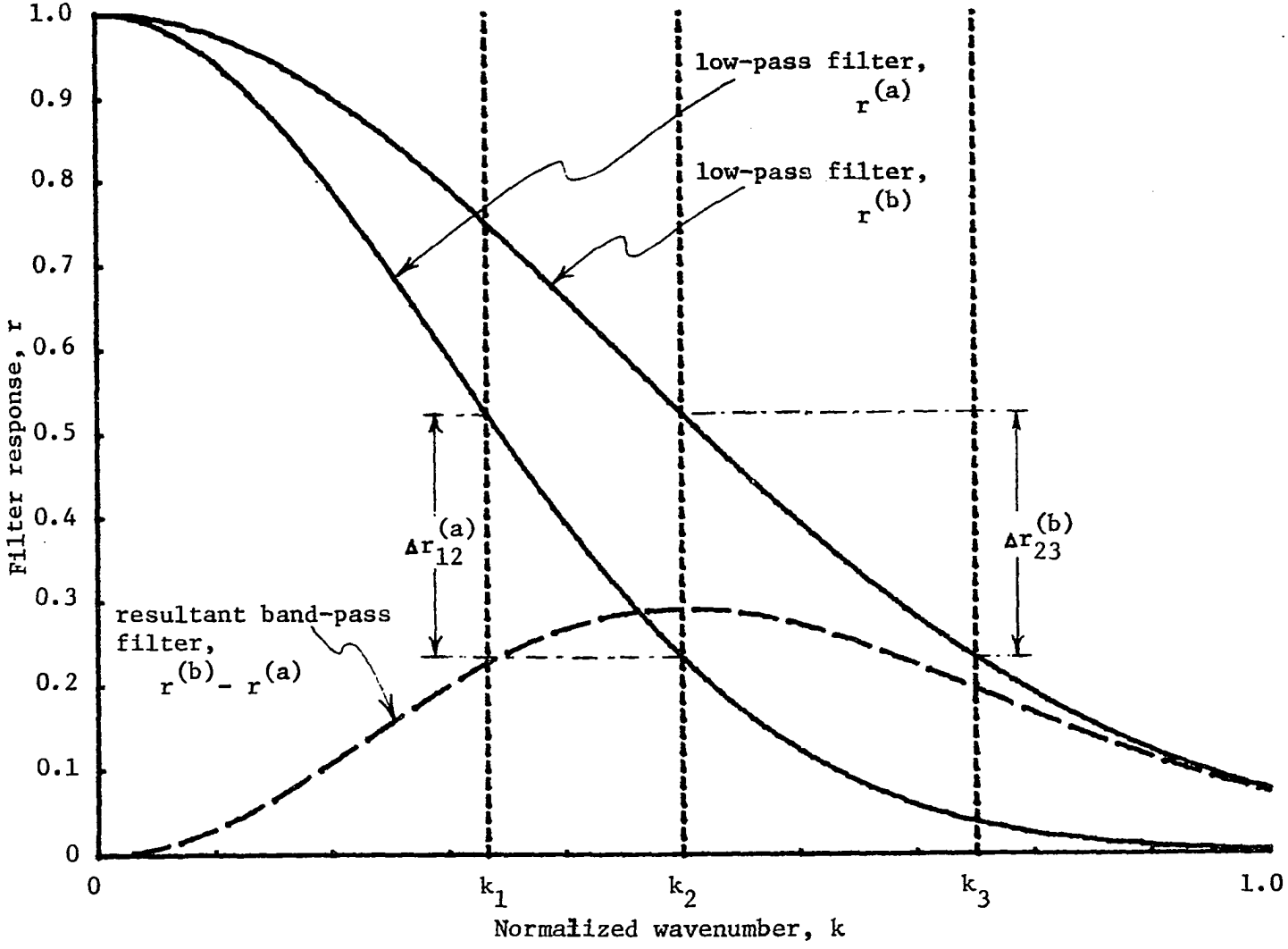


Figure 1. Schematic illustration of development of band-pass filter as difference between two low-pass filters.

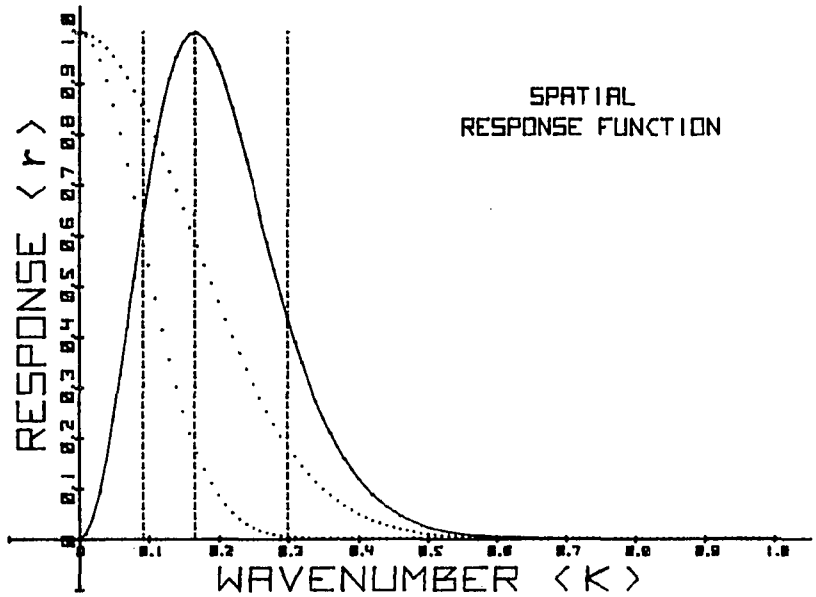


Figure 2. Spatial response function with band-pass peak centered at 12Δs.

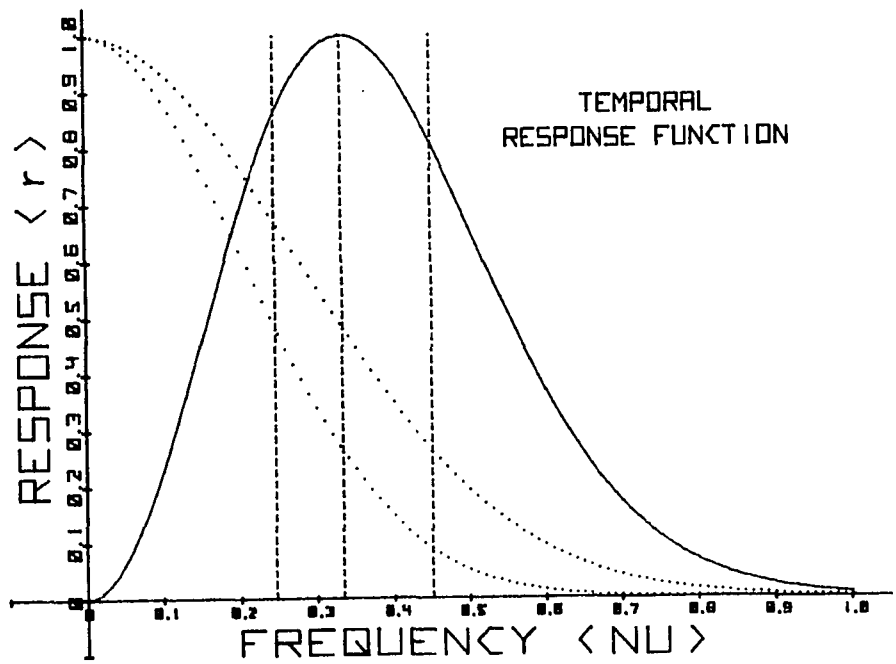


Figure 3. Temporal response function with band-pass peak centered at 6Δt.

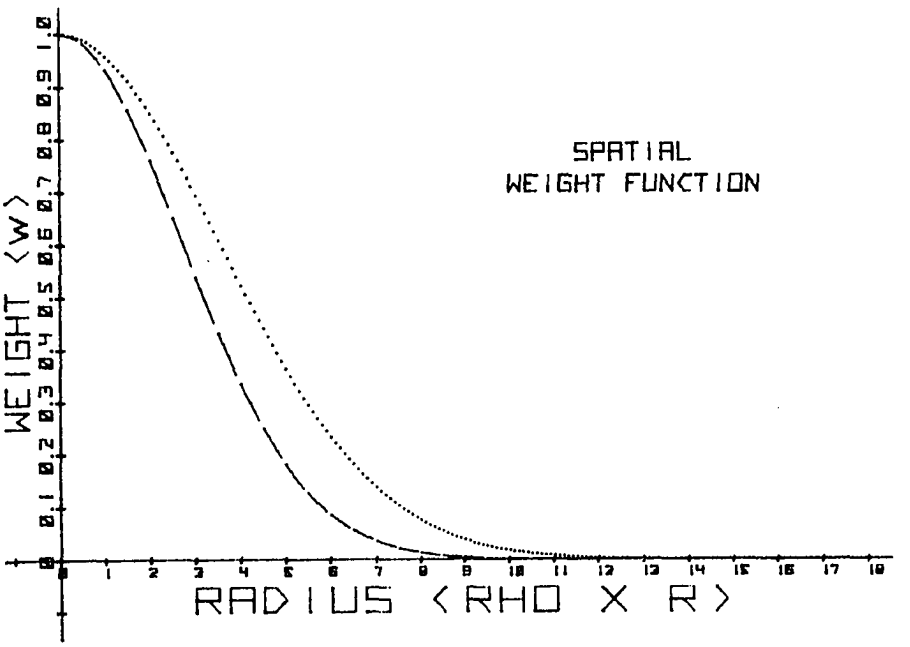


Figure 4. Spatial weight functions for low-pass filters shown in Fig. 2.

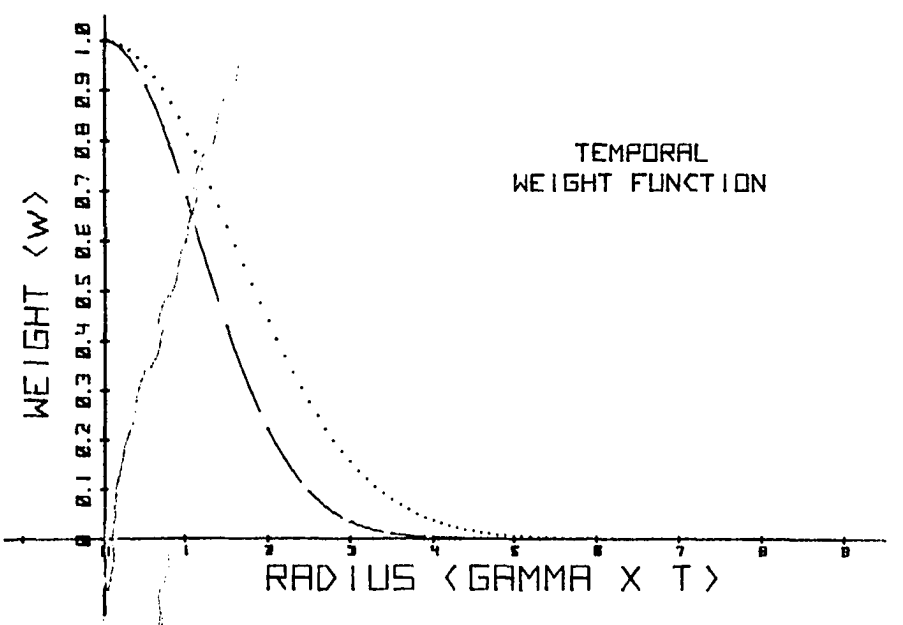


Figure 5. Temporal weight functions for low-pass filters shown in Fig. 3.

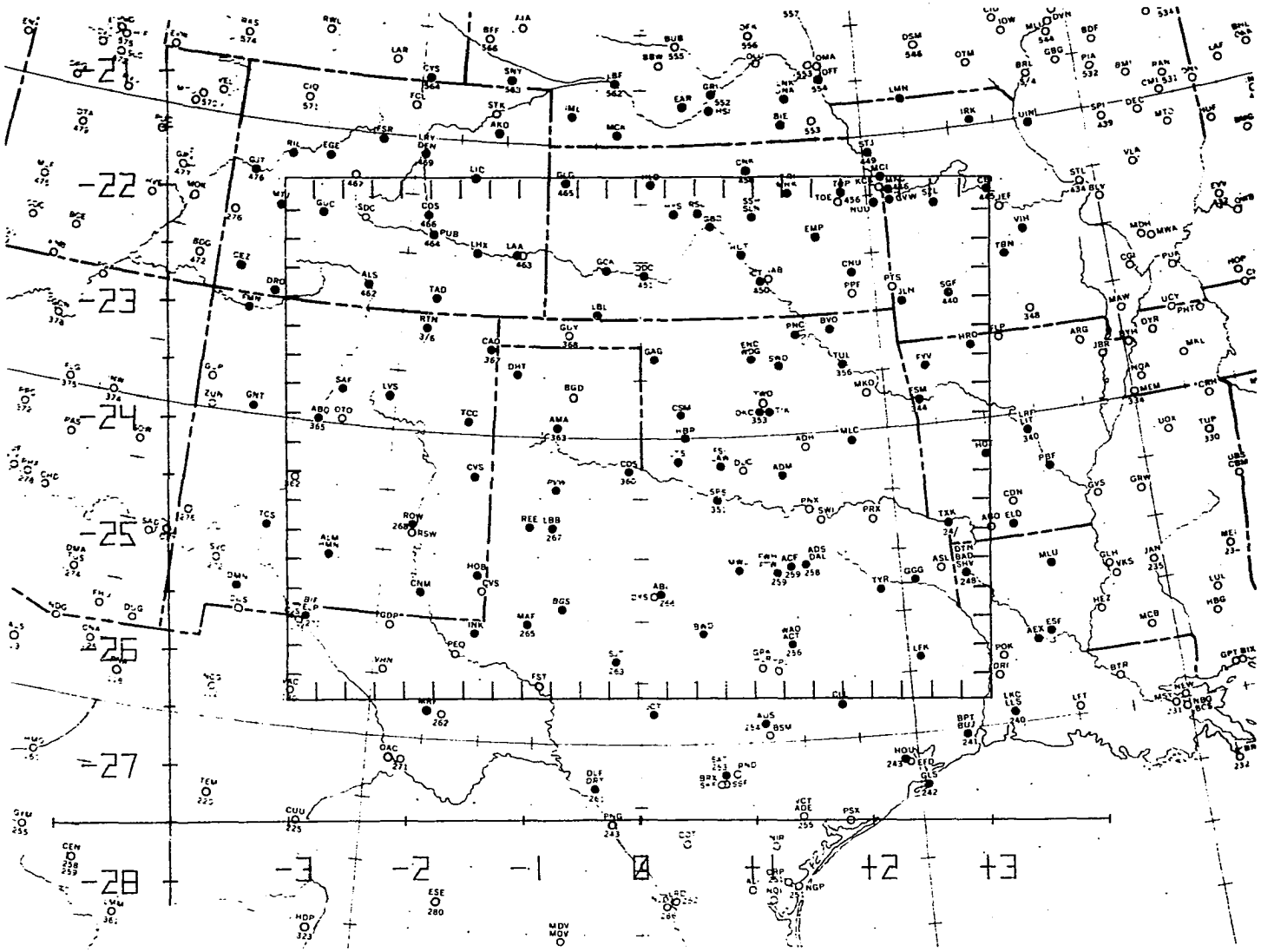


Figure 6. Map showing analysis grid, map coordinate system, and spatial distribution of data points (black circles) used for interpolation.

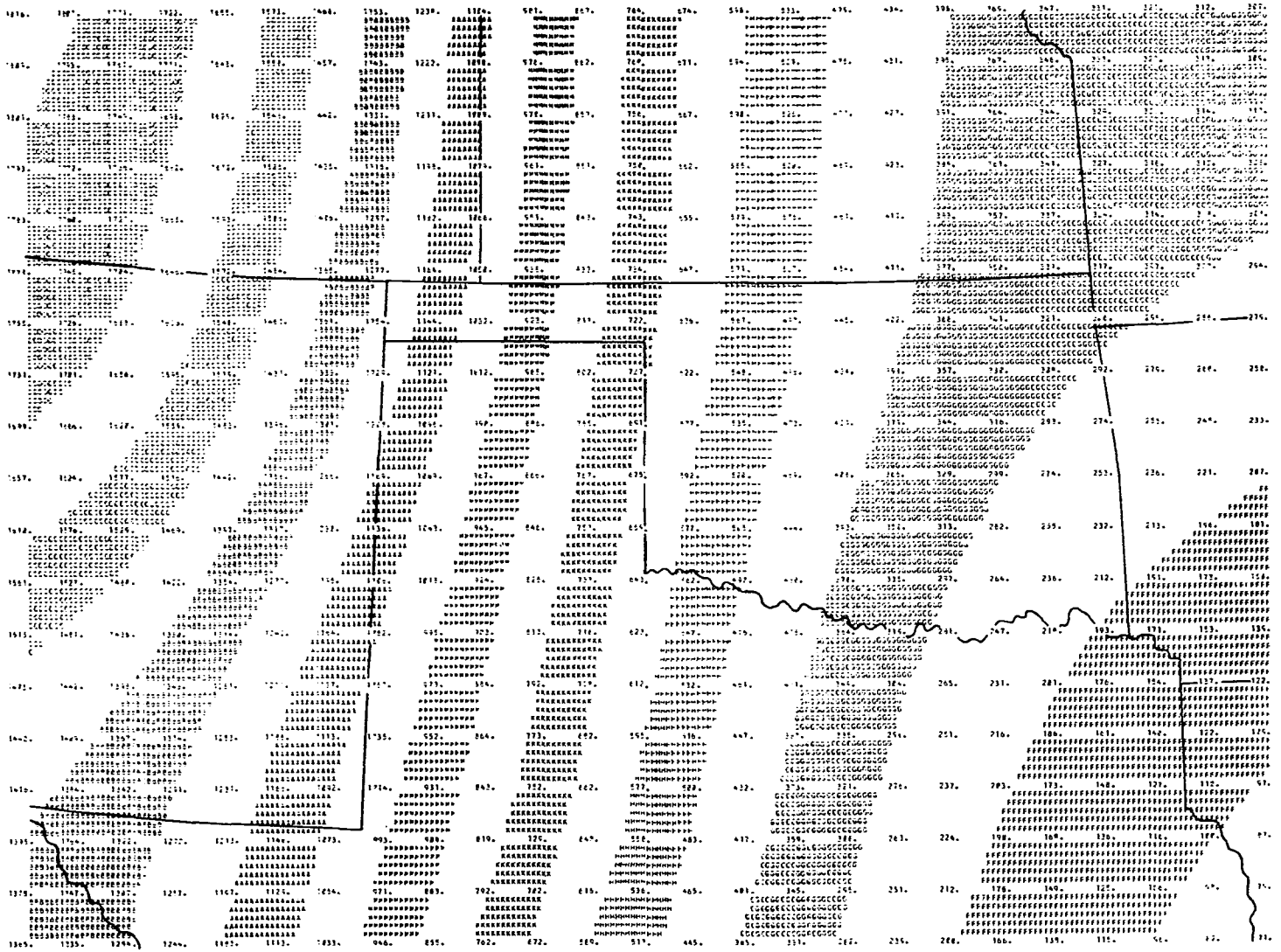


Figure 7. Smoothed terrain analysis based on station heights, in meters.

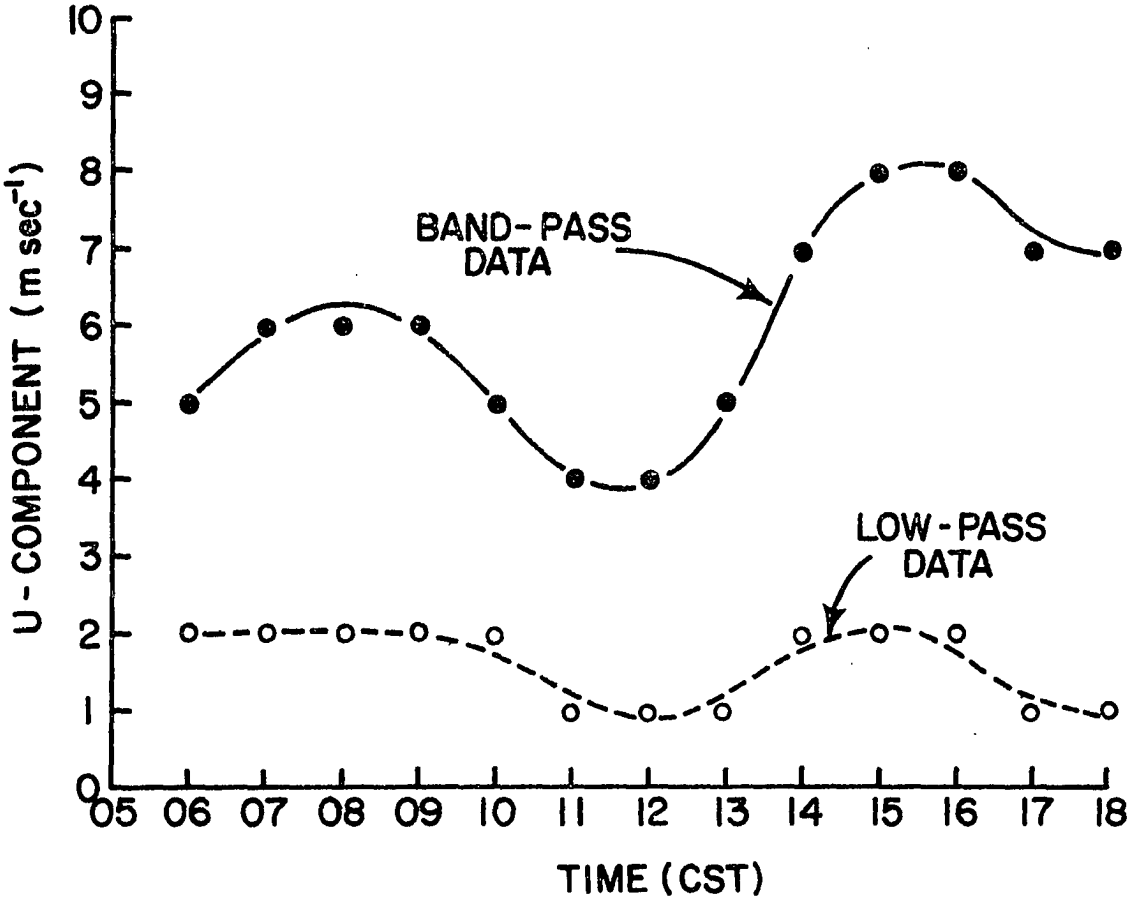
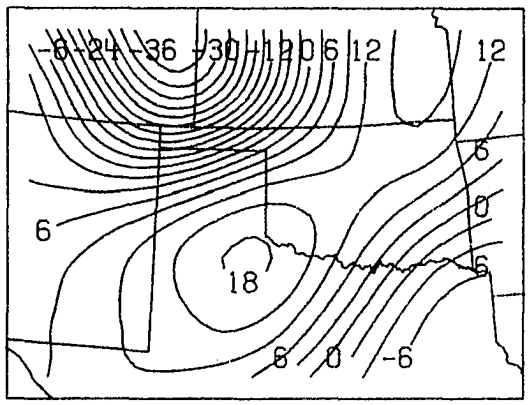
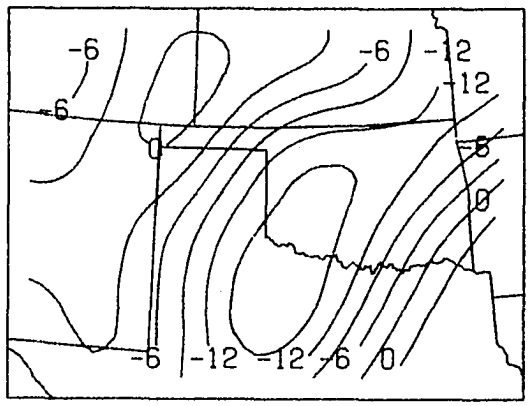


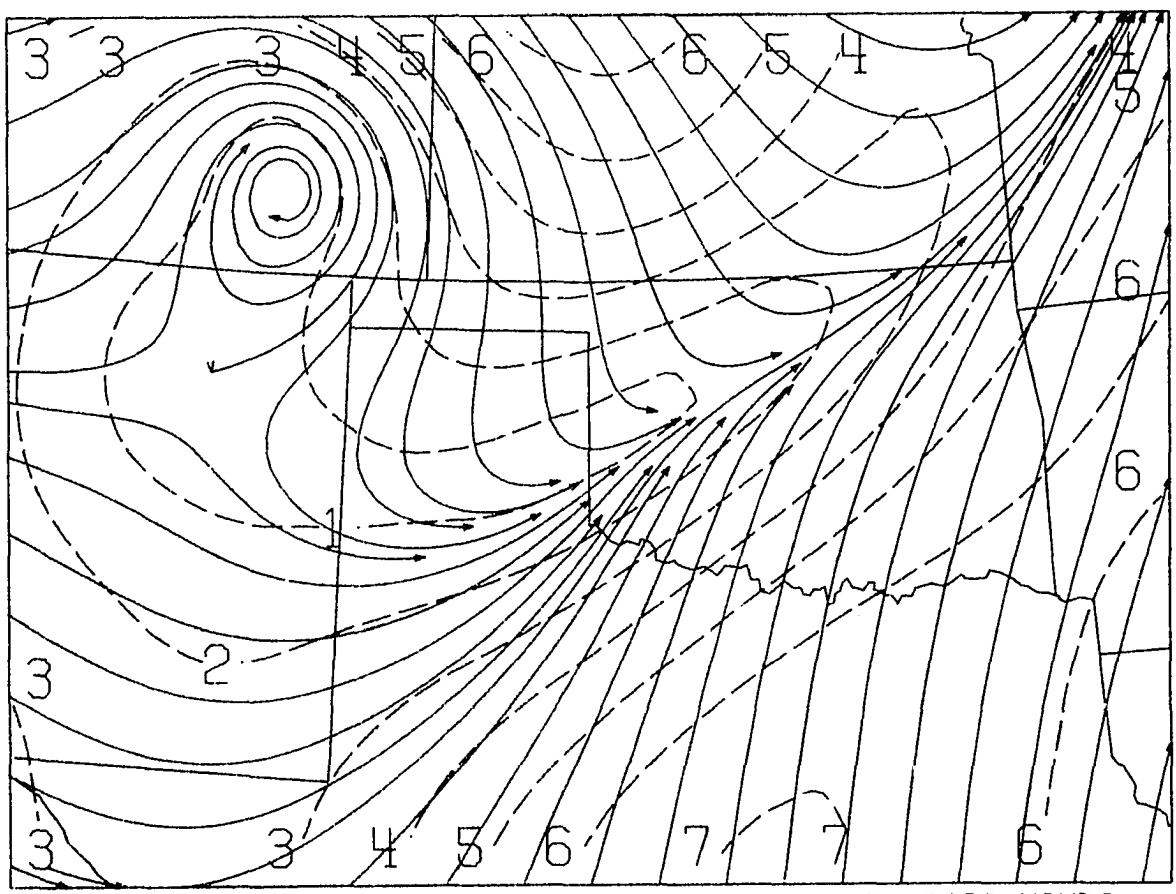
Figure 8. Hourly values of u-component (to the nearest m sec^{-1}) for low-pass data (open circles) and band-pass data (dark circles). The curves show an approximate continuous interpolation.



LOW-PASS VORTICITY

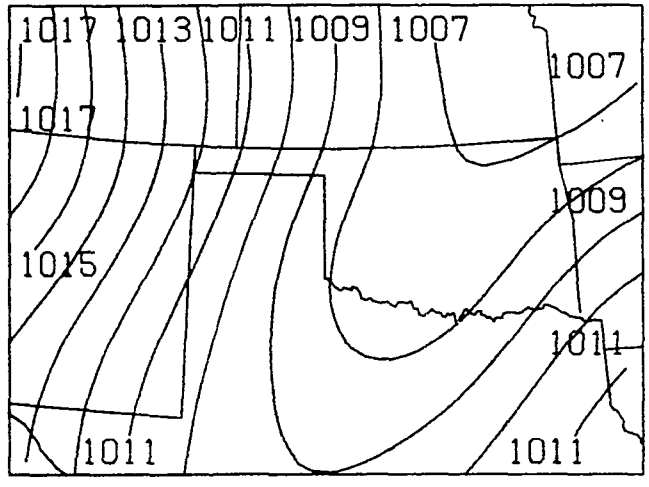


LOW-PASS DIVERGENCE

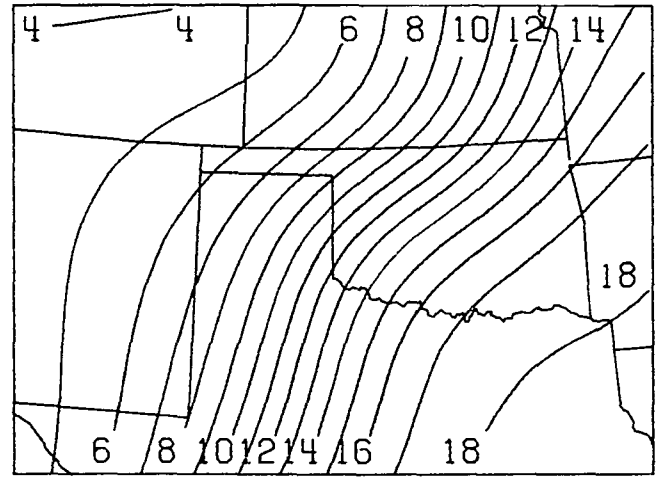


STREAMLINES AND ISOTACHS (M PER SEC) -- LOW-PASS WINDS

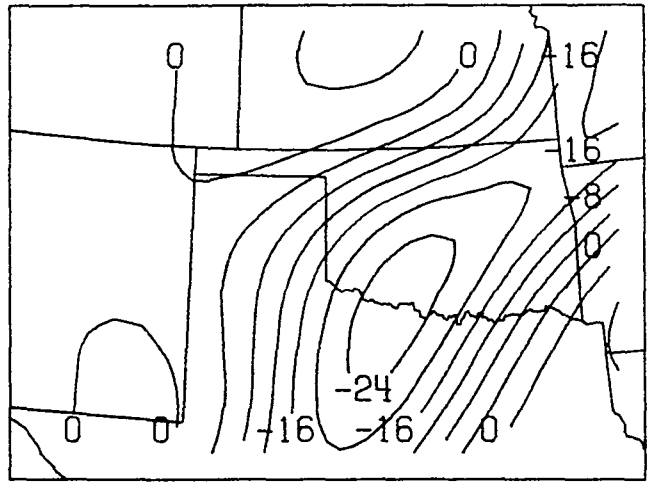
Figure 9a. Low-pass results for June 18, 1973 at 1200 CST. Vorticity and divergence are multiplied by 10^5 and units are sec^{-1}.



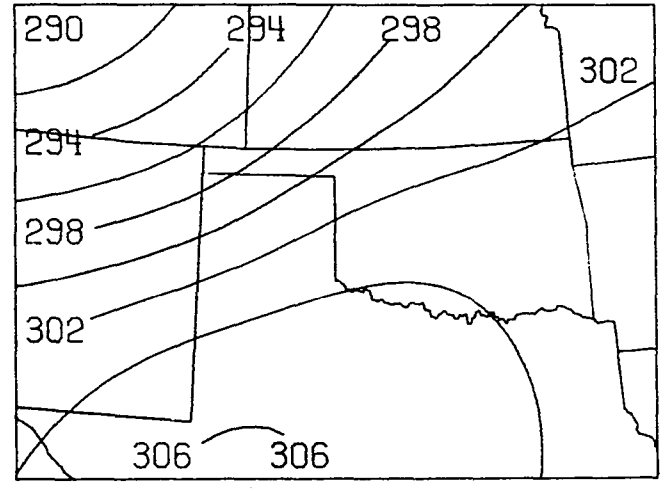
LOW-PASS ALTIMETER SETTING



LOW-PASS MIXING RATIO

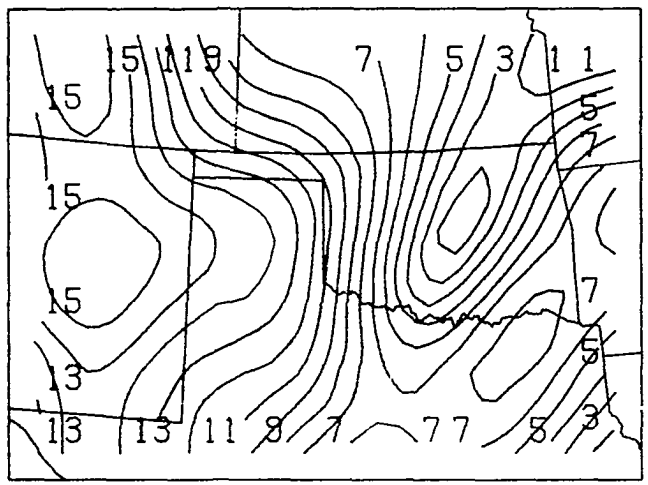


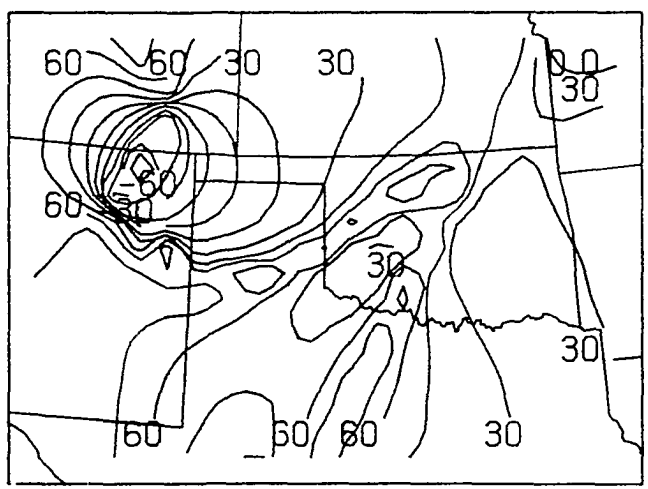
LOW-PASS MOISTURE DIVERGENCE



LOW-PASS TEMPERATURE

Figure 9b. Altimeter setting in mb, mixing ratio in g kg^{-1}, moisture divergence is multiplied by 10^4 and has units of g kg^{-1} sec^{-1}, temperature in deg k.





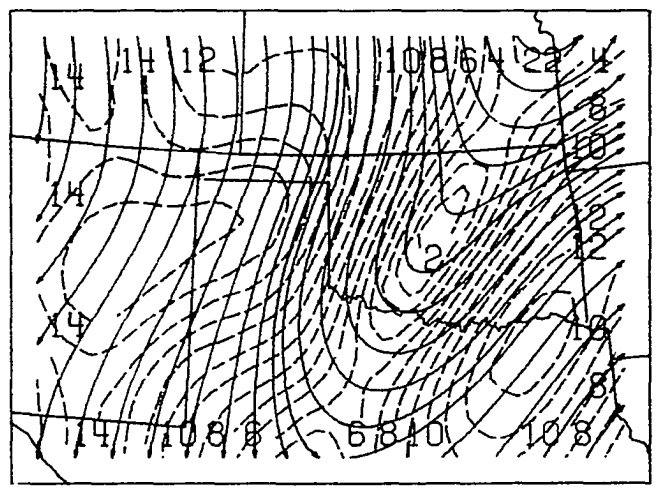
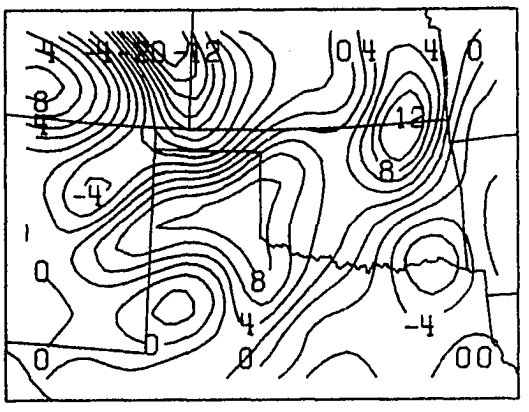
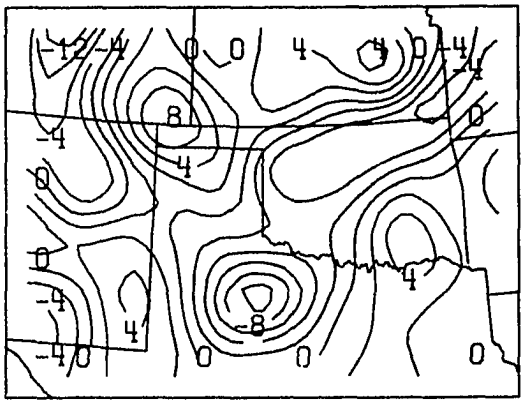


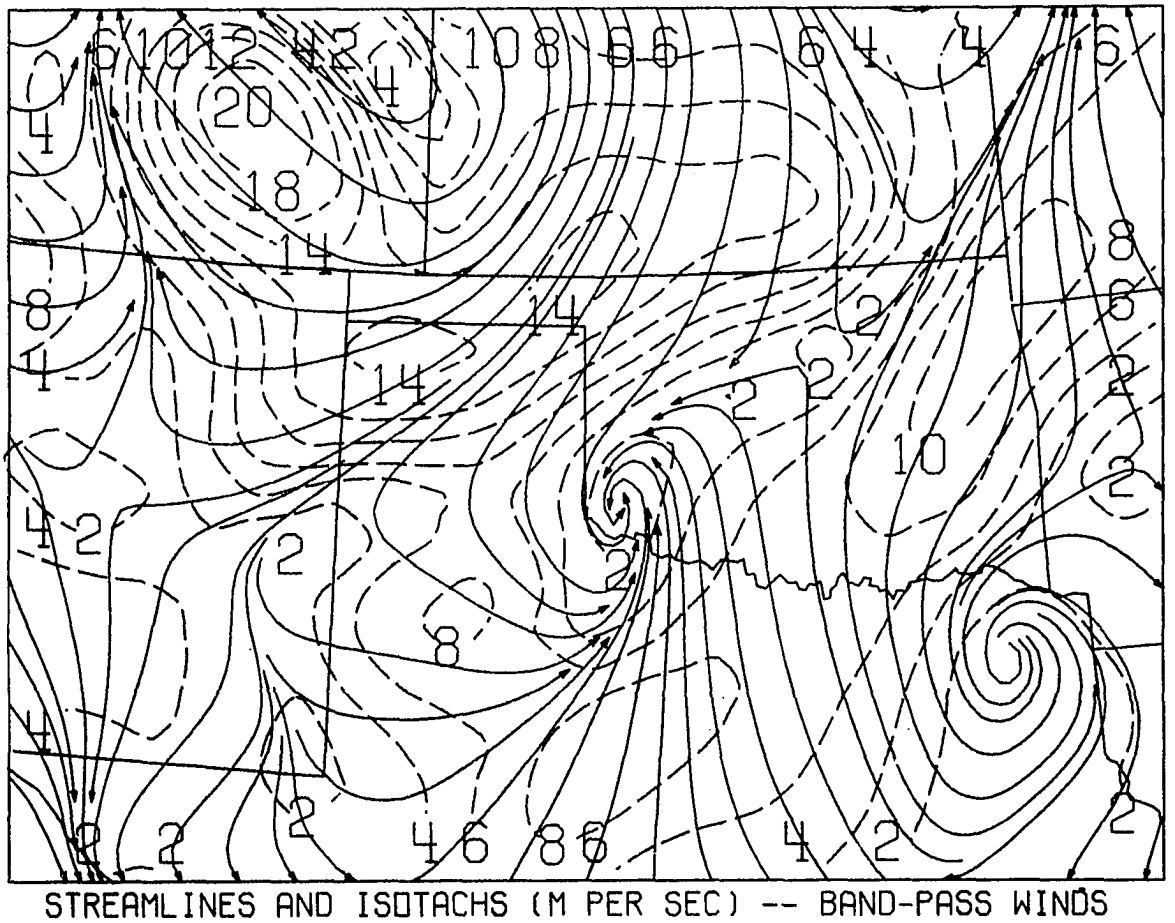
Figure 9c. Ageostrophic speed in m sec^{-1}, isobaric crossing angle in degrees with positive angles toward low pressure, geostrophic isotachs in m sec^{-1}.



BAND-PASS VORTICITY

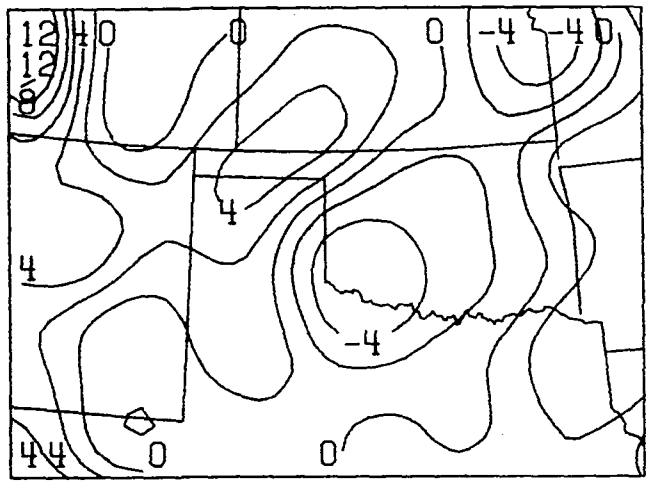


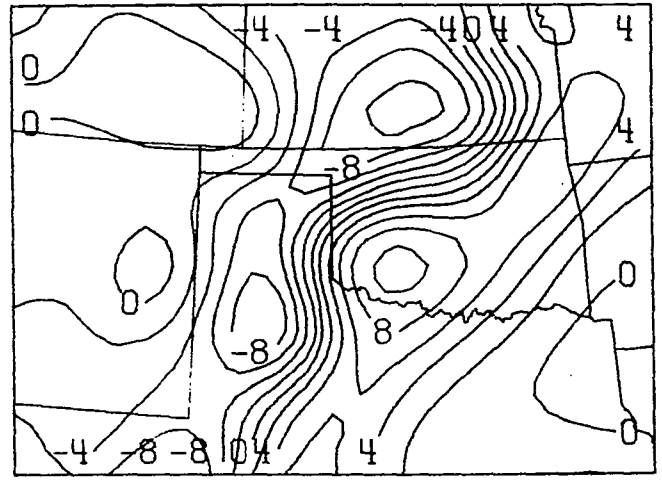
BAND-PASS DIVERGENCE

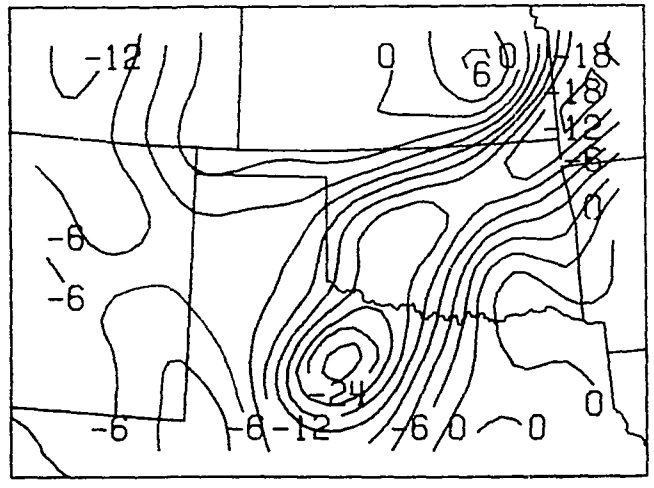


STREAMLINES AND ISOTACHS (M PER SEC) -- BAND-PASS WINDS

Figure 10a. Band-pass results for June 8, 1974 at 1200 CST. Vorticity and divergence are multiplies by 10^4 and units are sec^{-1}.







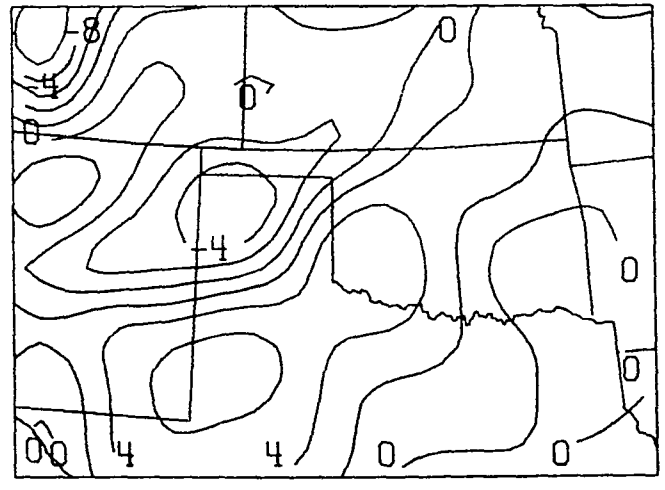


Figure 10b. Same as Fig. 8, except for band-pass results and moisture divergence is multiplied by 10^3.



Figure 11. Satellite photo at 1221 CST on June 18, 1974.



Figure 12. Satellite photo at 1642 CST on June 18, 1974.

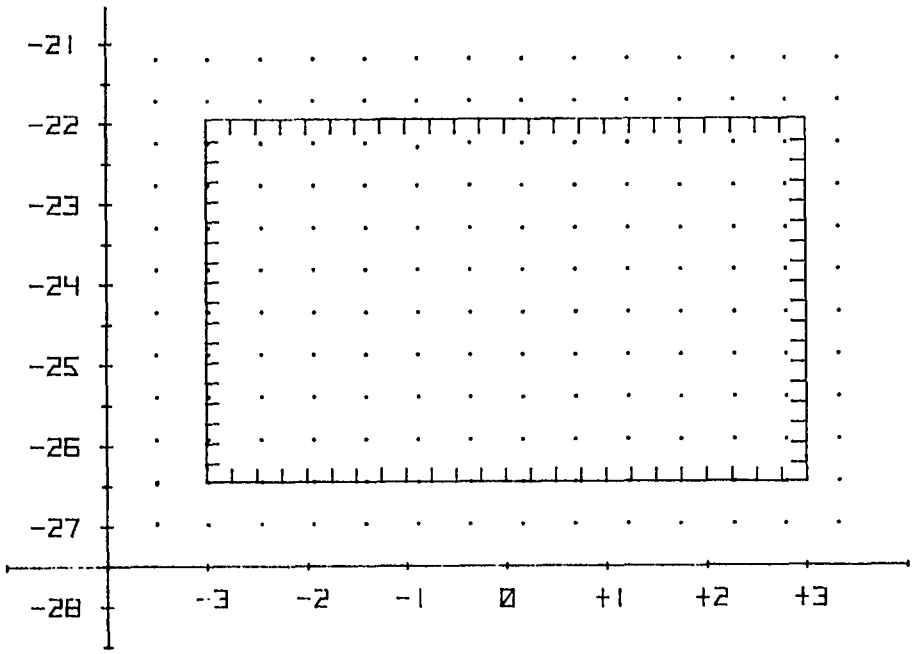


Figure A1(a). Hypothetical uniform grid with roughly the same average spacing as real data.

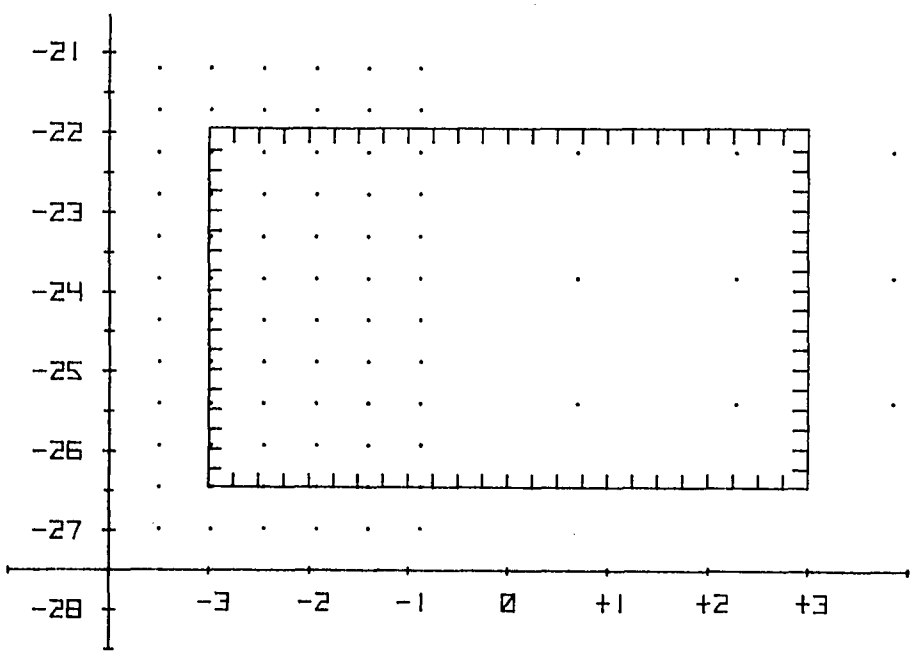


Figure A1(b). Hypothetical uniform grid with dense and coarse distribution of stations.

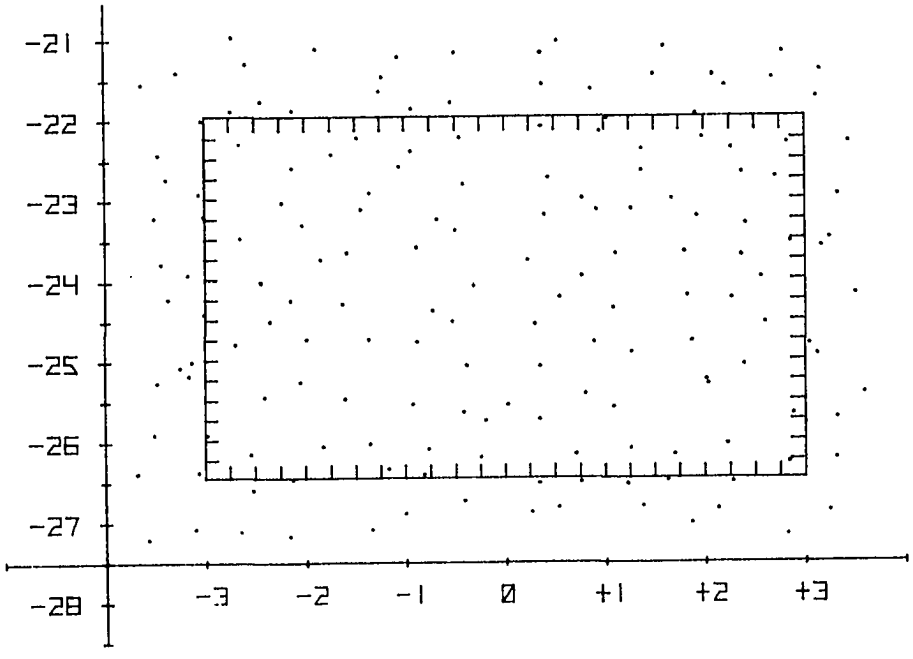


Figure A2(a). Same as Fig. A1(a), except for pseudo-random distribution of data.

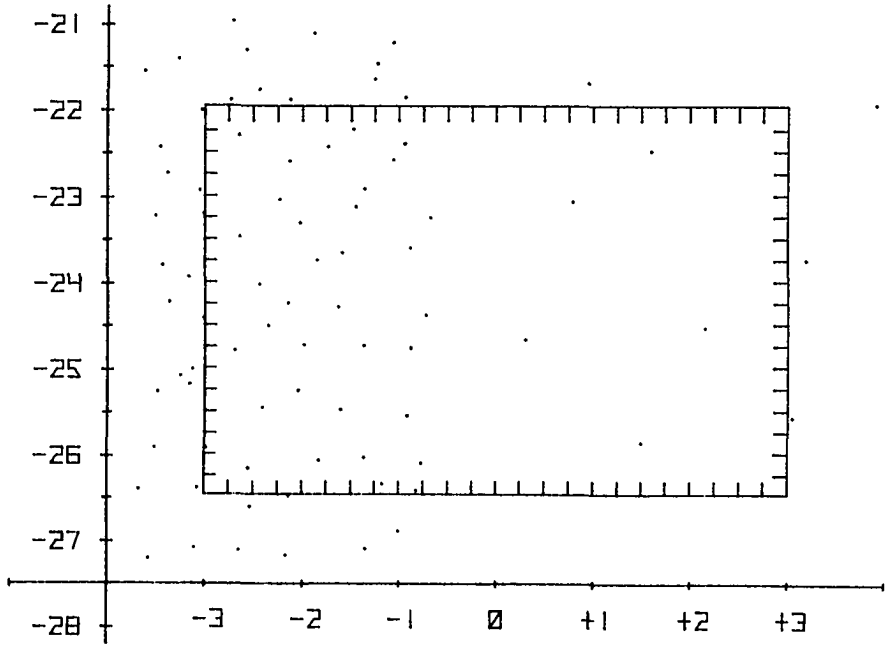


Figure A2(b). Same as Fig. A1(b), except for pseudo-random distribution of data.

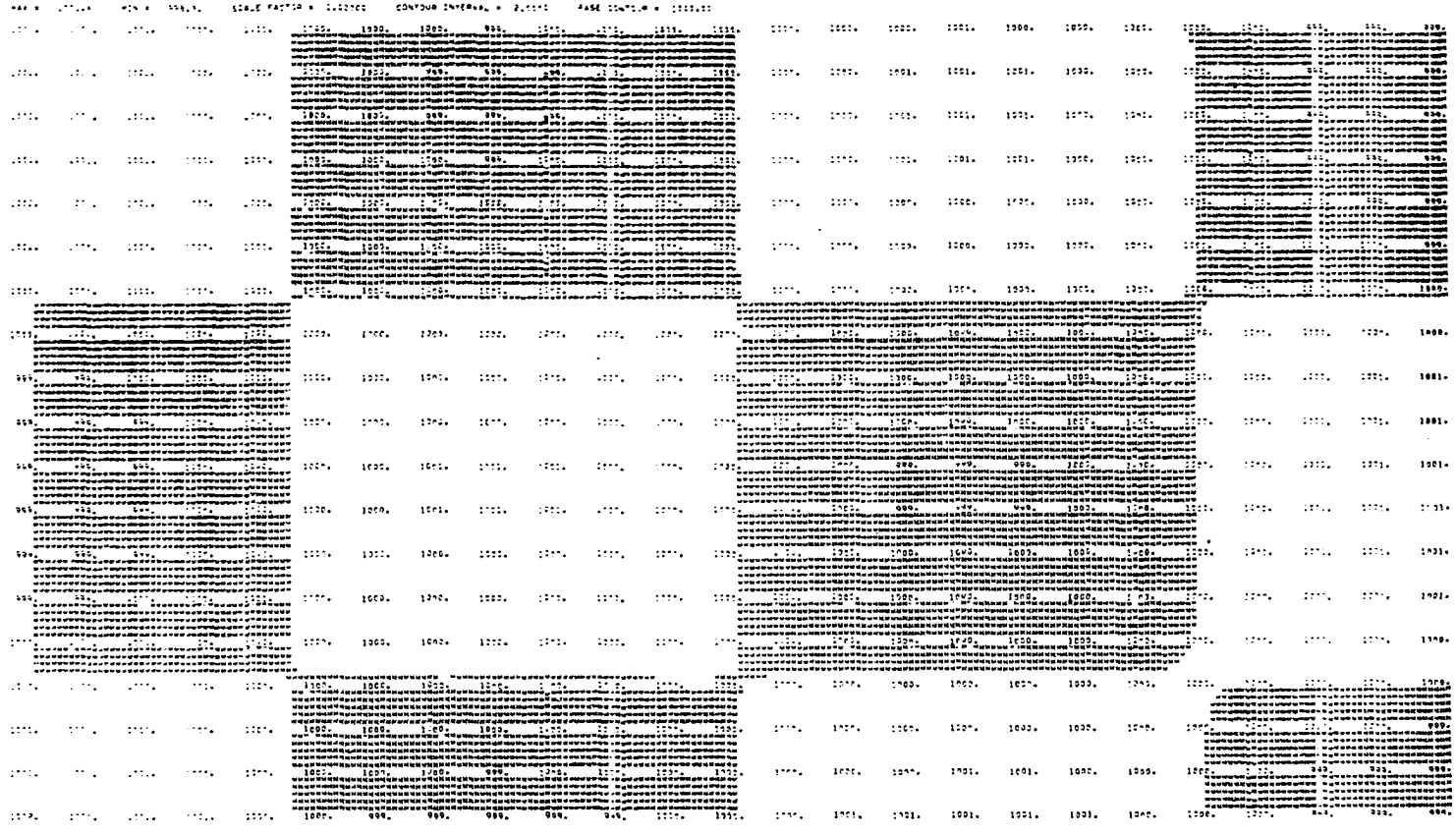


Figure A3(a). Low-pass results of regular data mesh with influence radius of 18Δs.

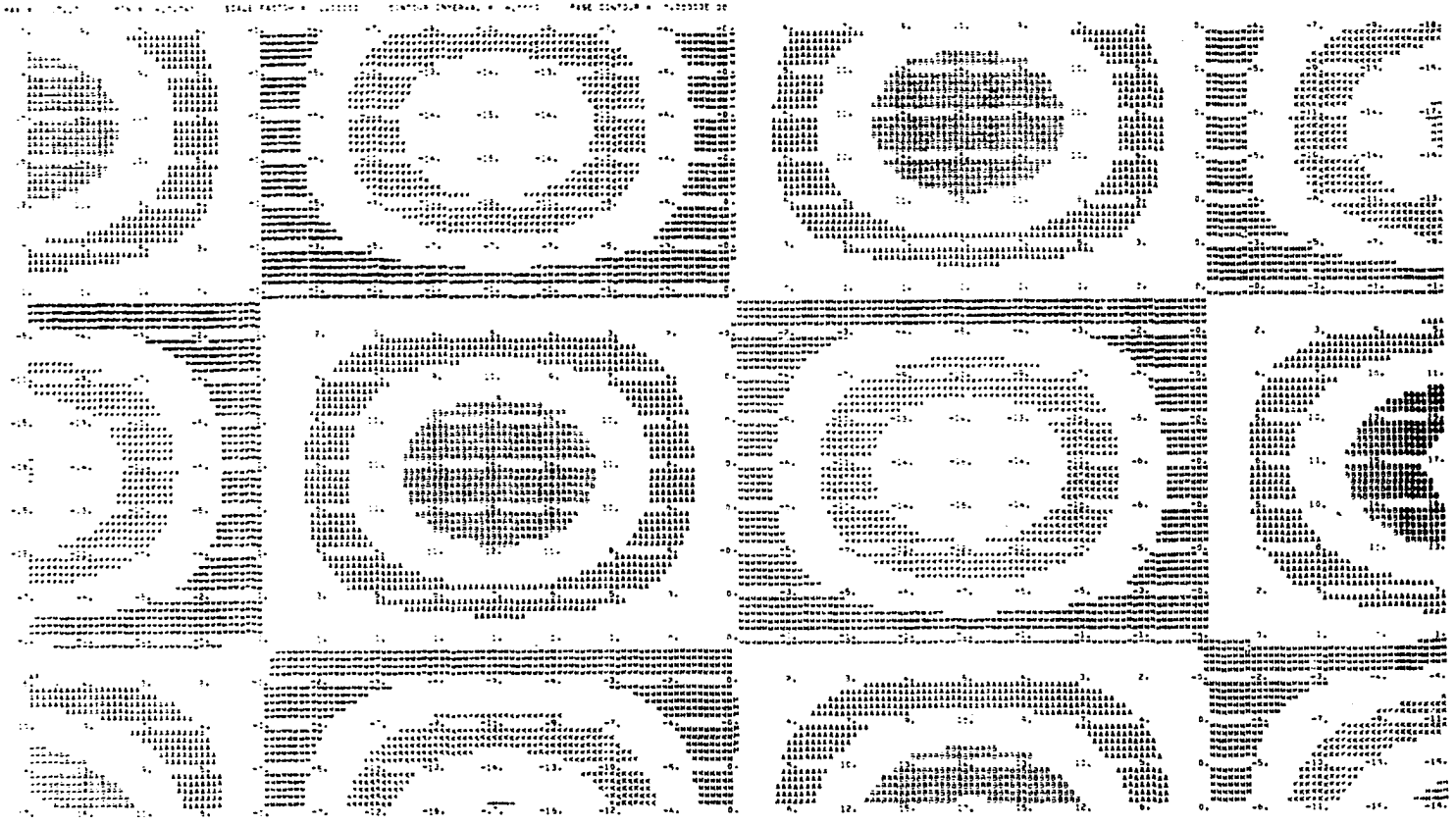


Figure A3(b). Same as Fig. A3(a), except for band-pass results.

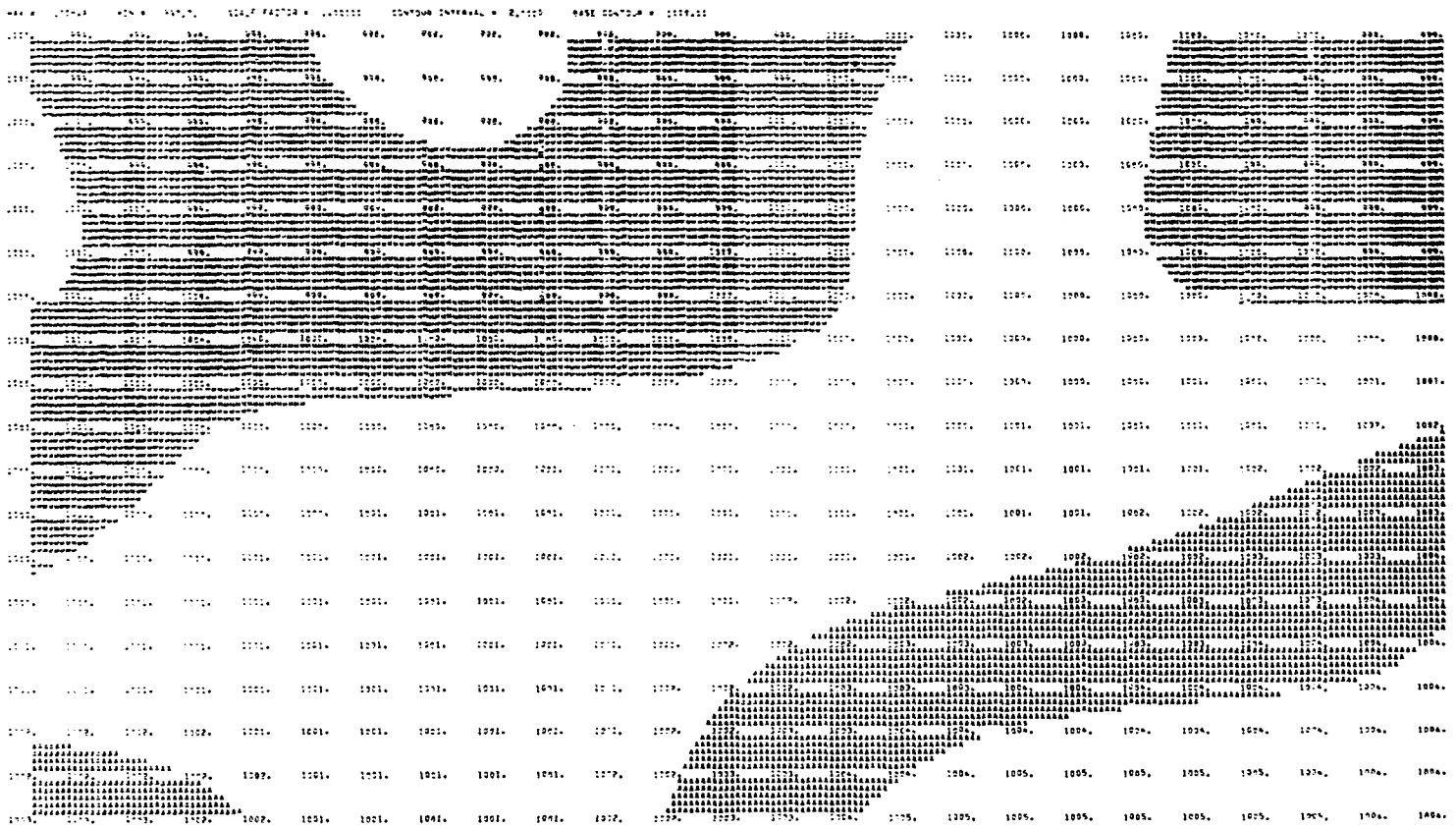


Figure A4(a). Same as Fig. A3(a), except for random data mesh.

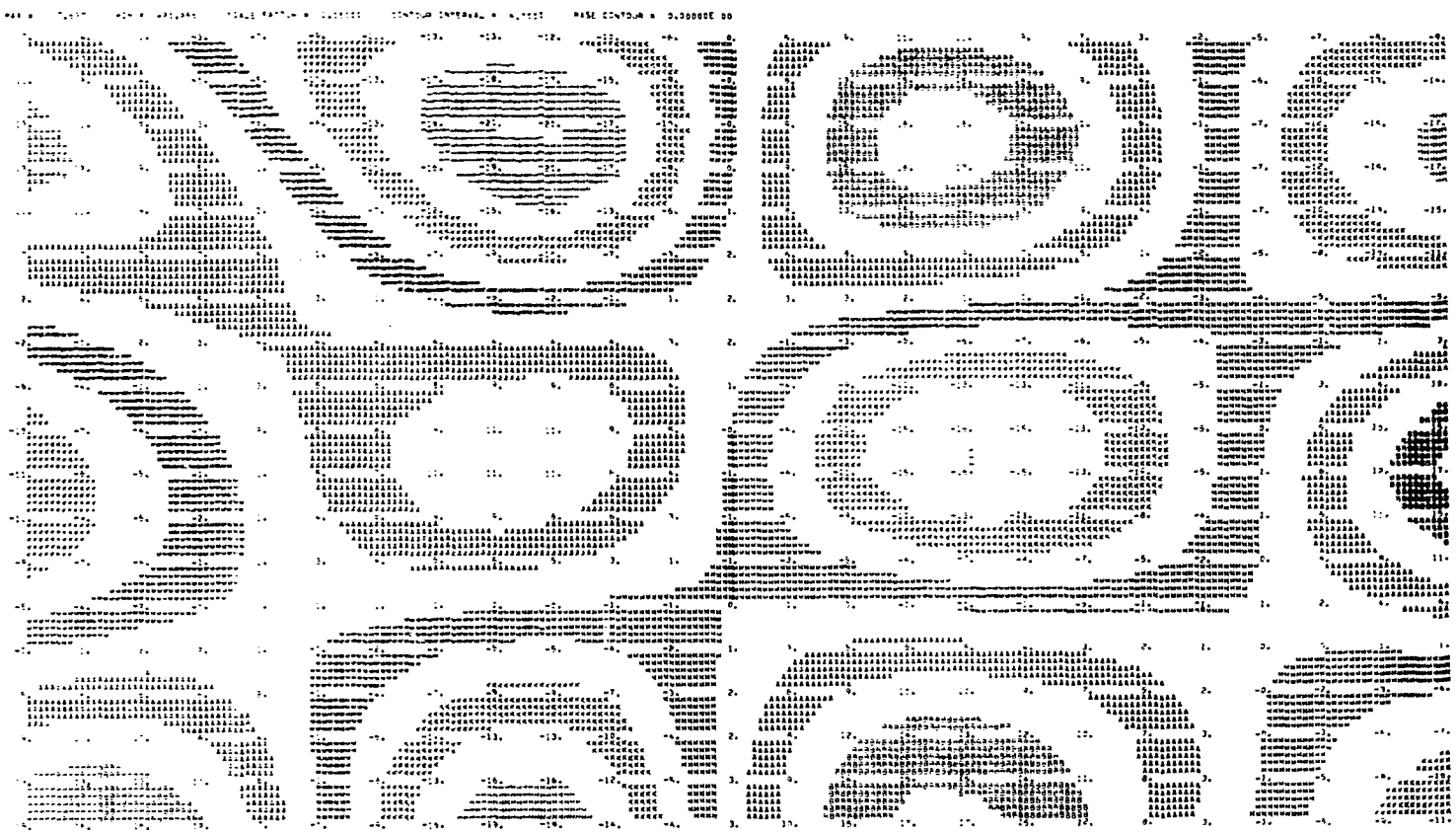


Figure A4(b). Same as Fig. A4(a), except for band-pass results.

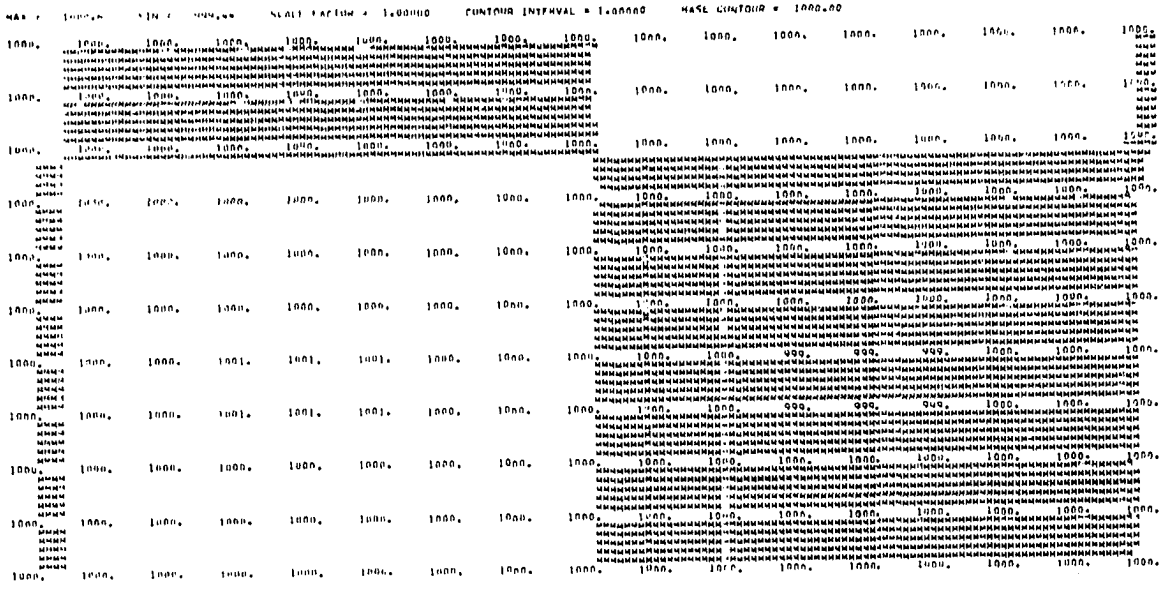


Figure A5(a). Same as Fig. A3(a), except uses grid one inch (on map-4 grid points) smaller on all sides. Includes data outside grid.

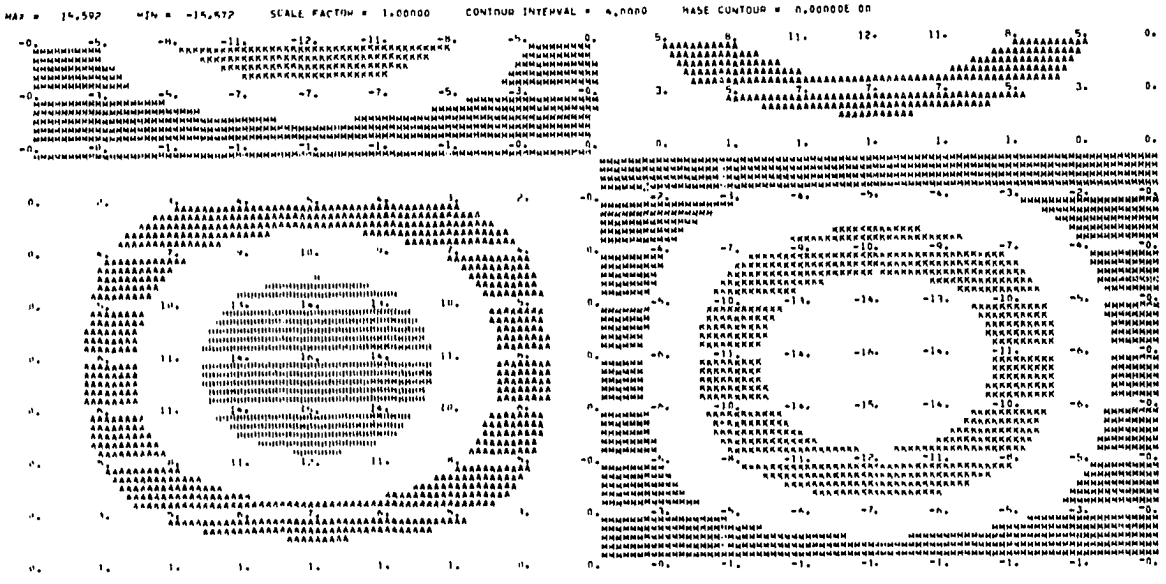


Figure A5(b). Same as Fig. A5(a), except for band-pass results.

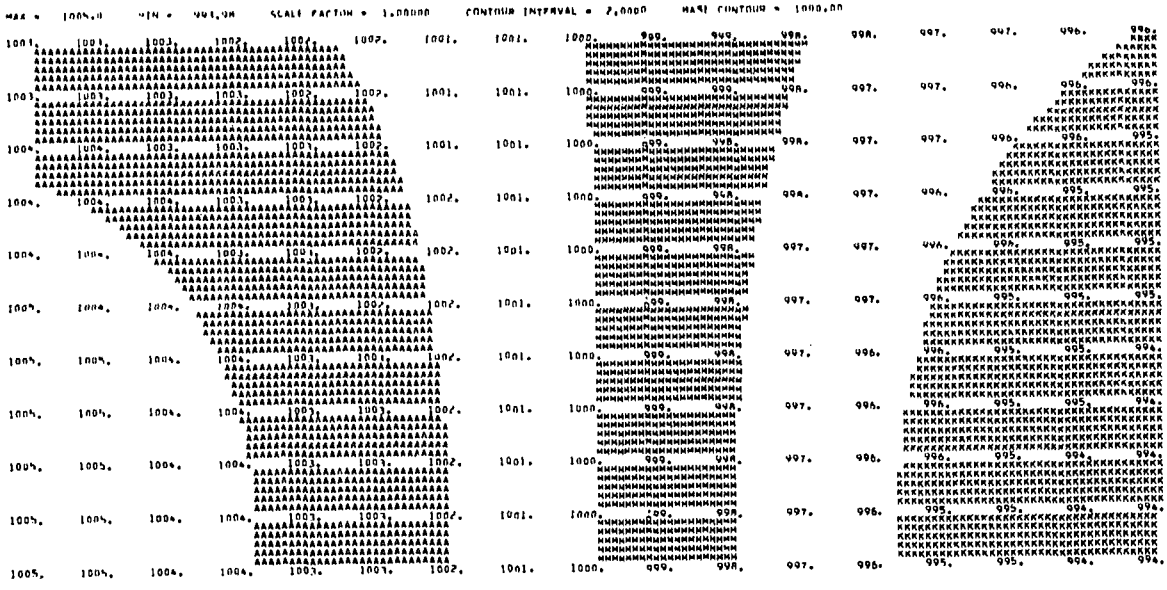


Figure A6(a). Same as Fig. A5(a), except excludes data from outside grid.

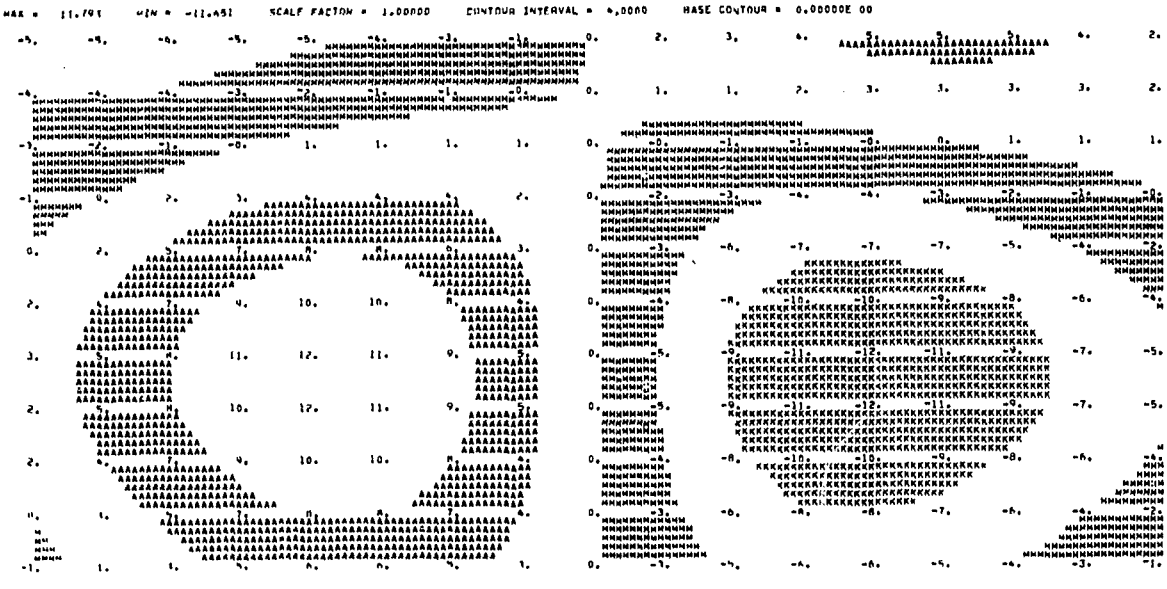


Figure A6(b). Same as Fig. A5(b), except excludes data from outside grid.

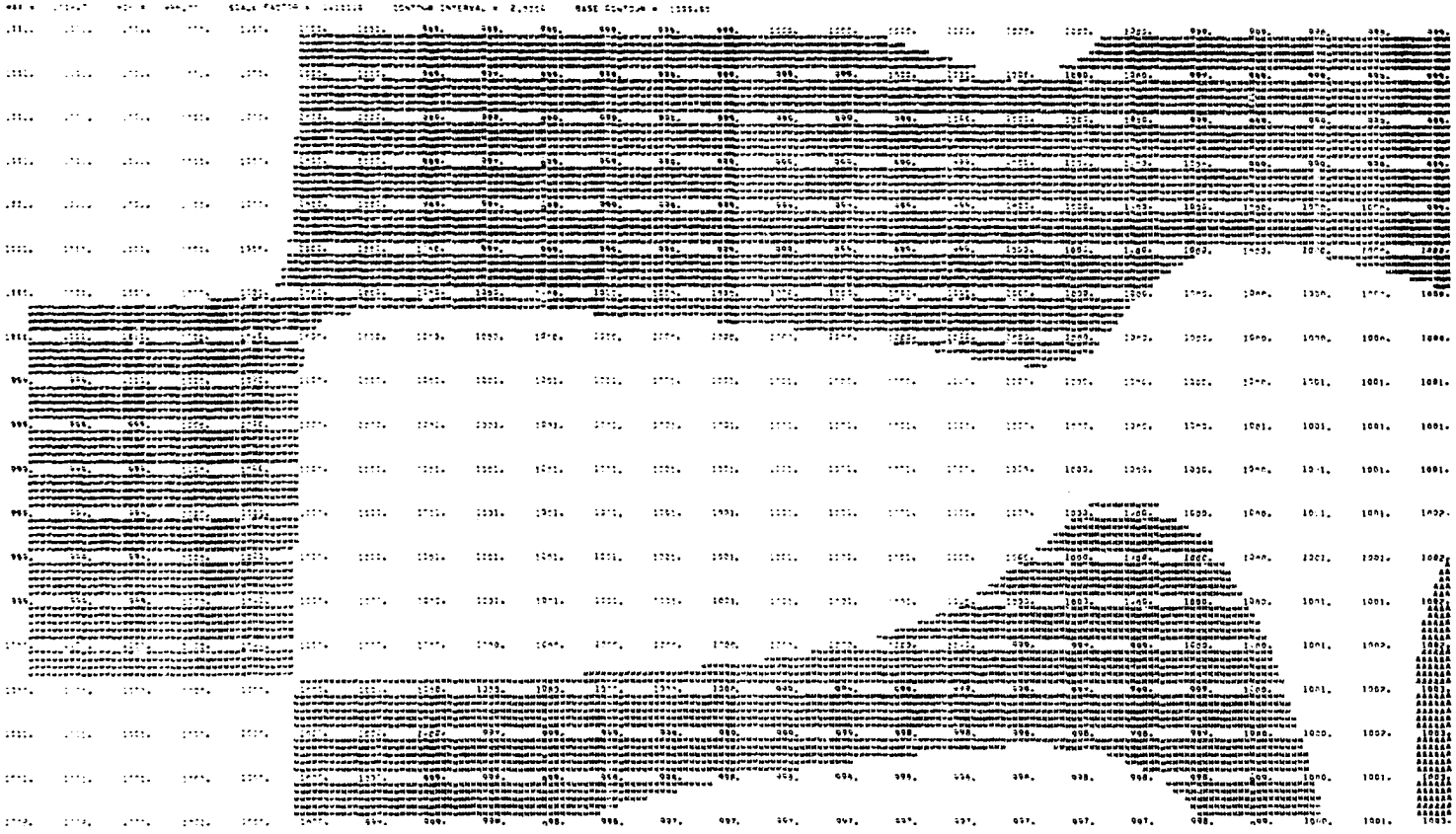


Figure A7(a). Low-pass results, using data grid shown in Fig. A1(b).

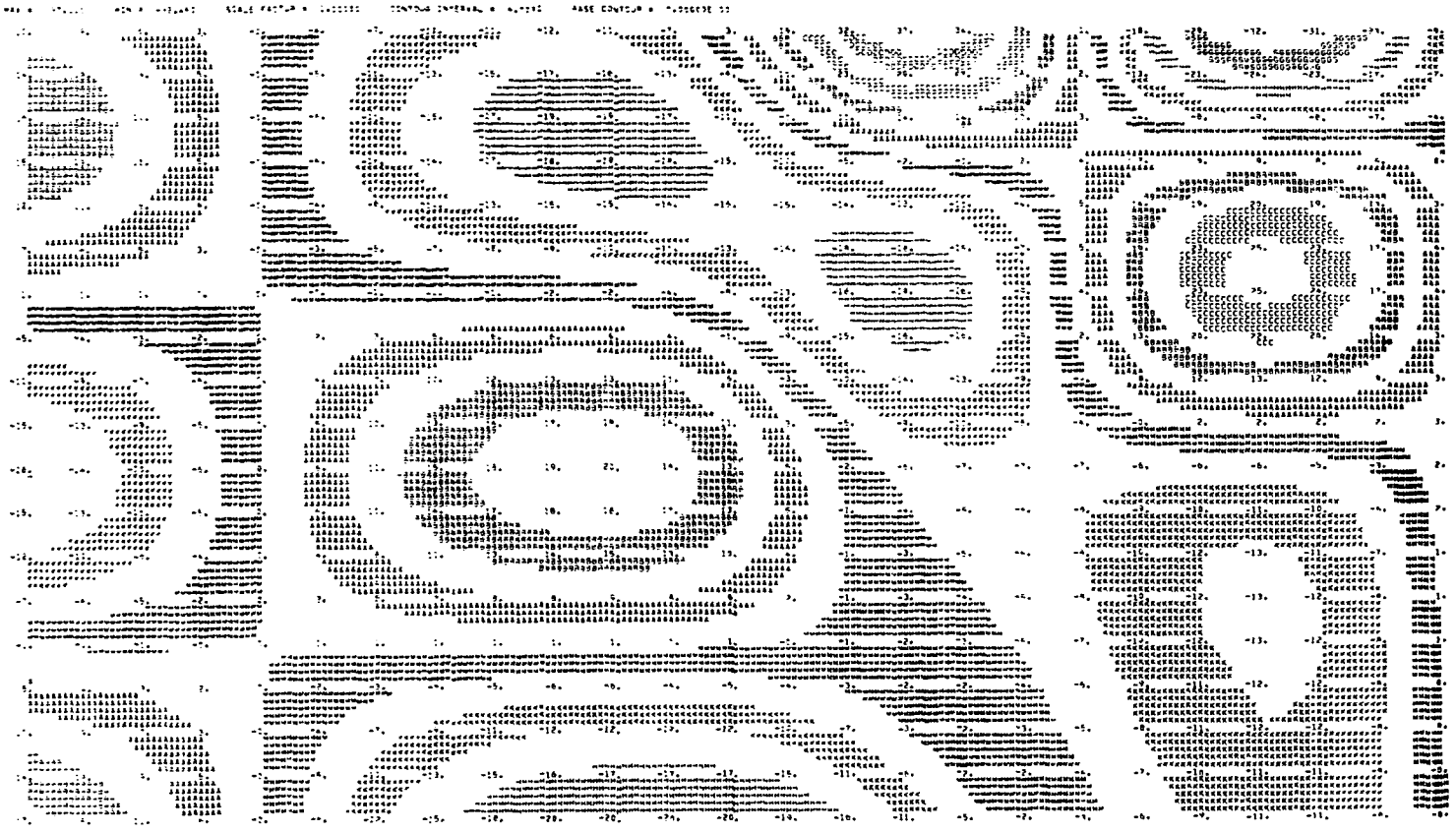


Figure A7(b). Same as Fig. A7(a), except for band-pass results.

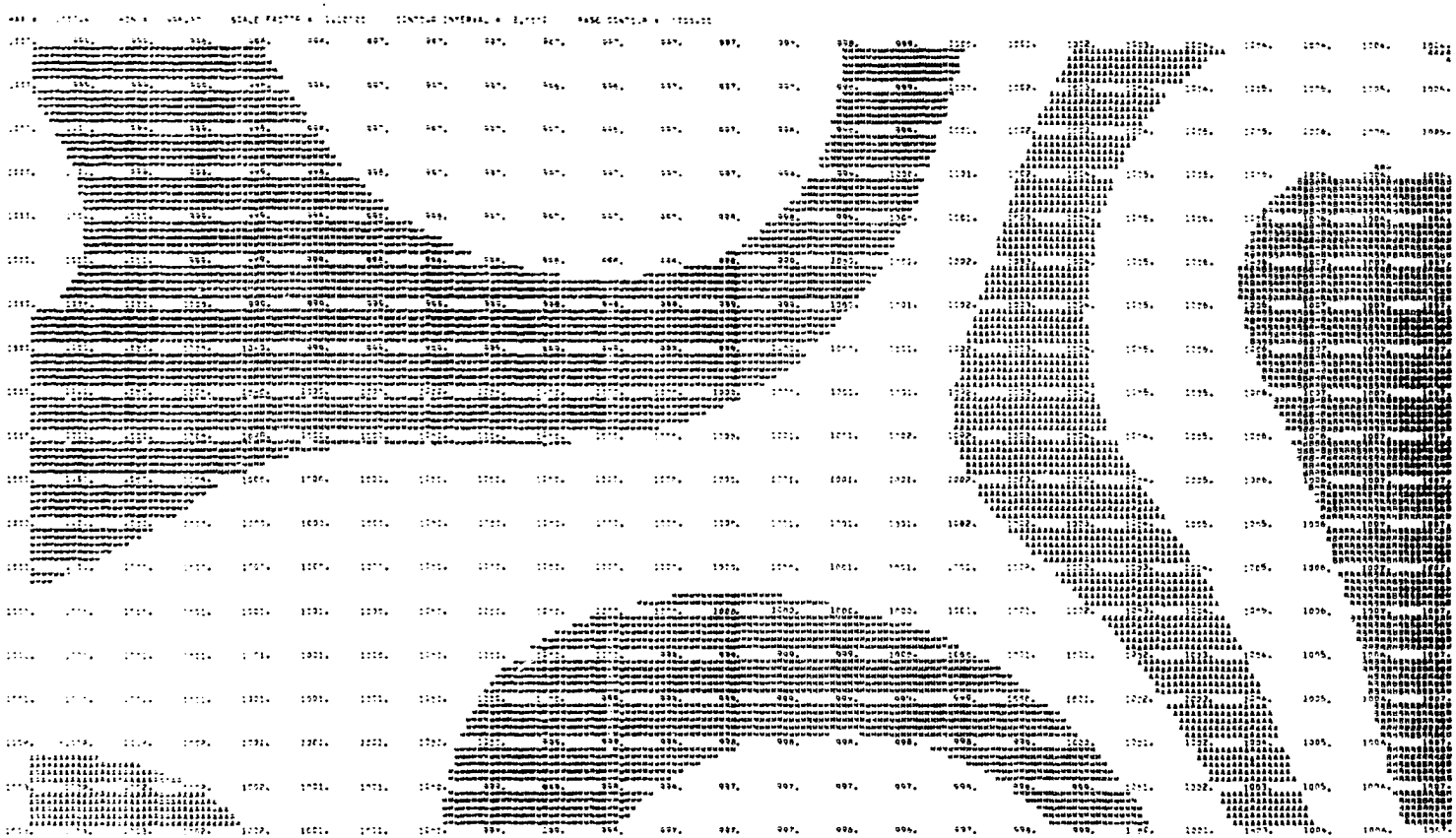


Figure A8(a). Same as Fig. A7(a), except for grid shown in Fig. A2(b).

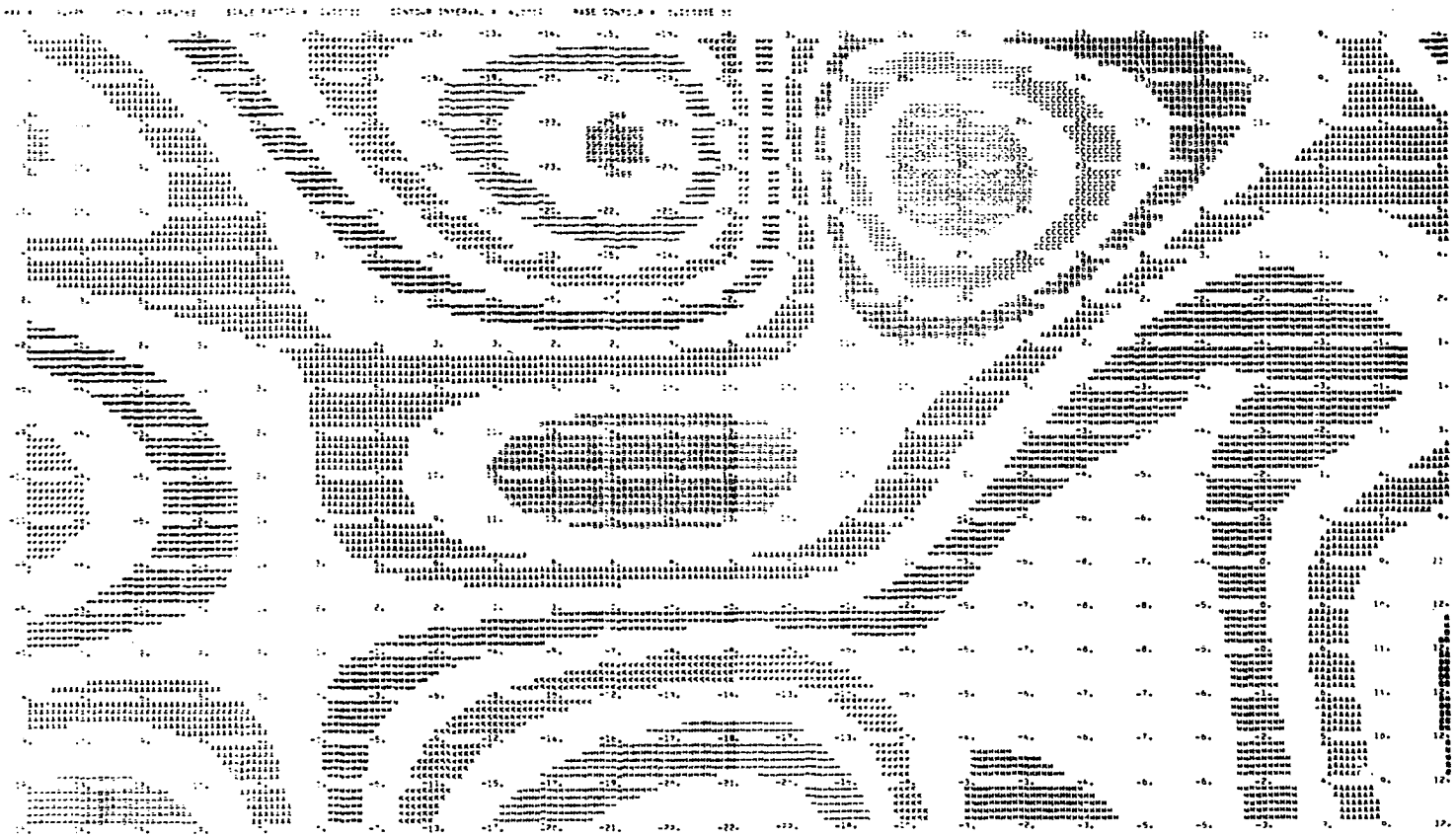


Figure A8(b). Same as Fig. A8(a), except for band-pass results.

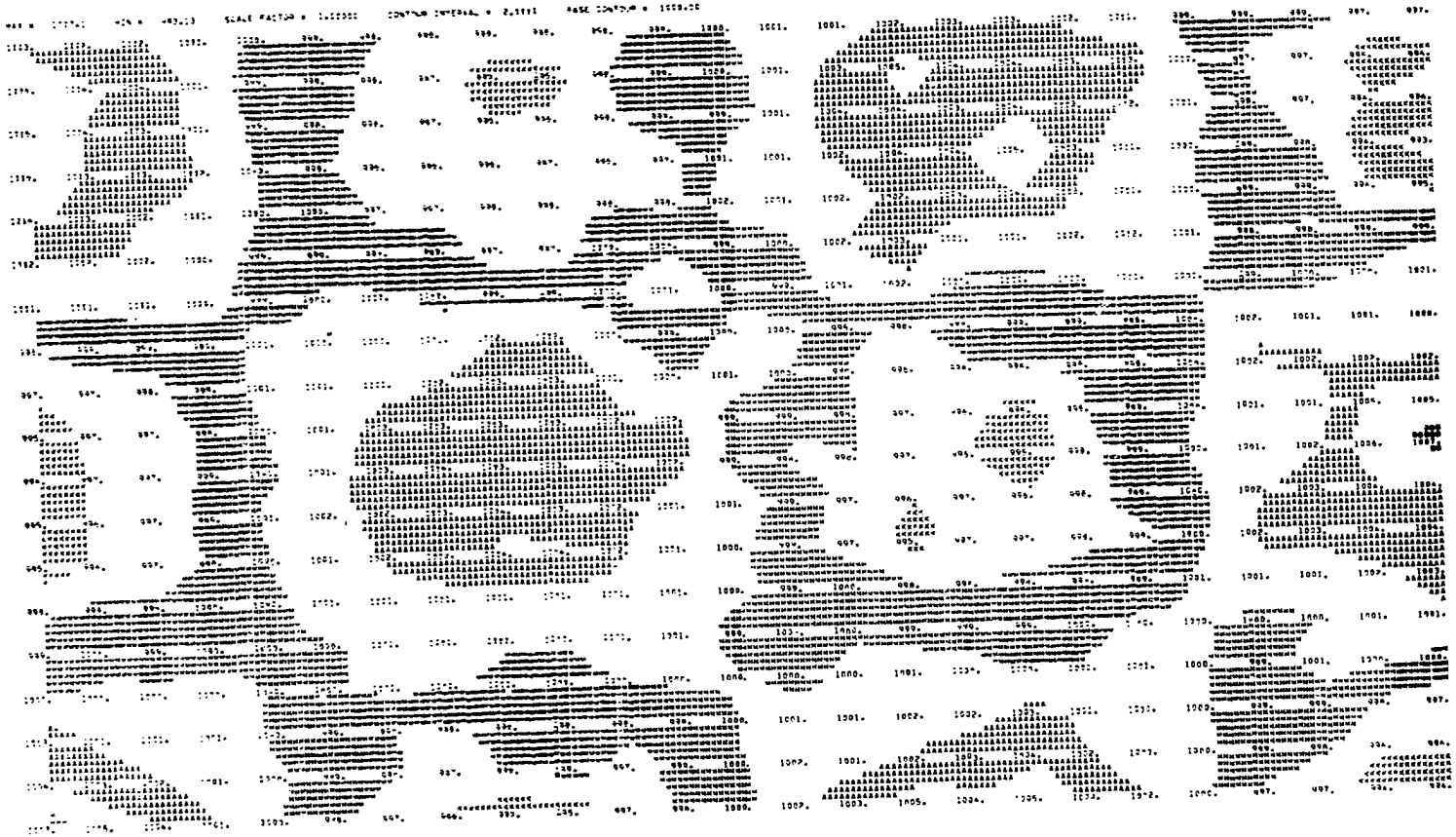


Figure A9(a). Same as Fig. A3(a), except for influence radius of 6Δs.

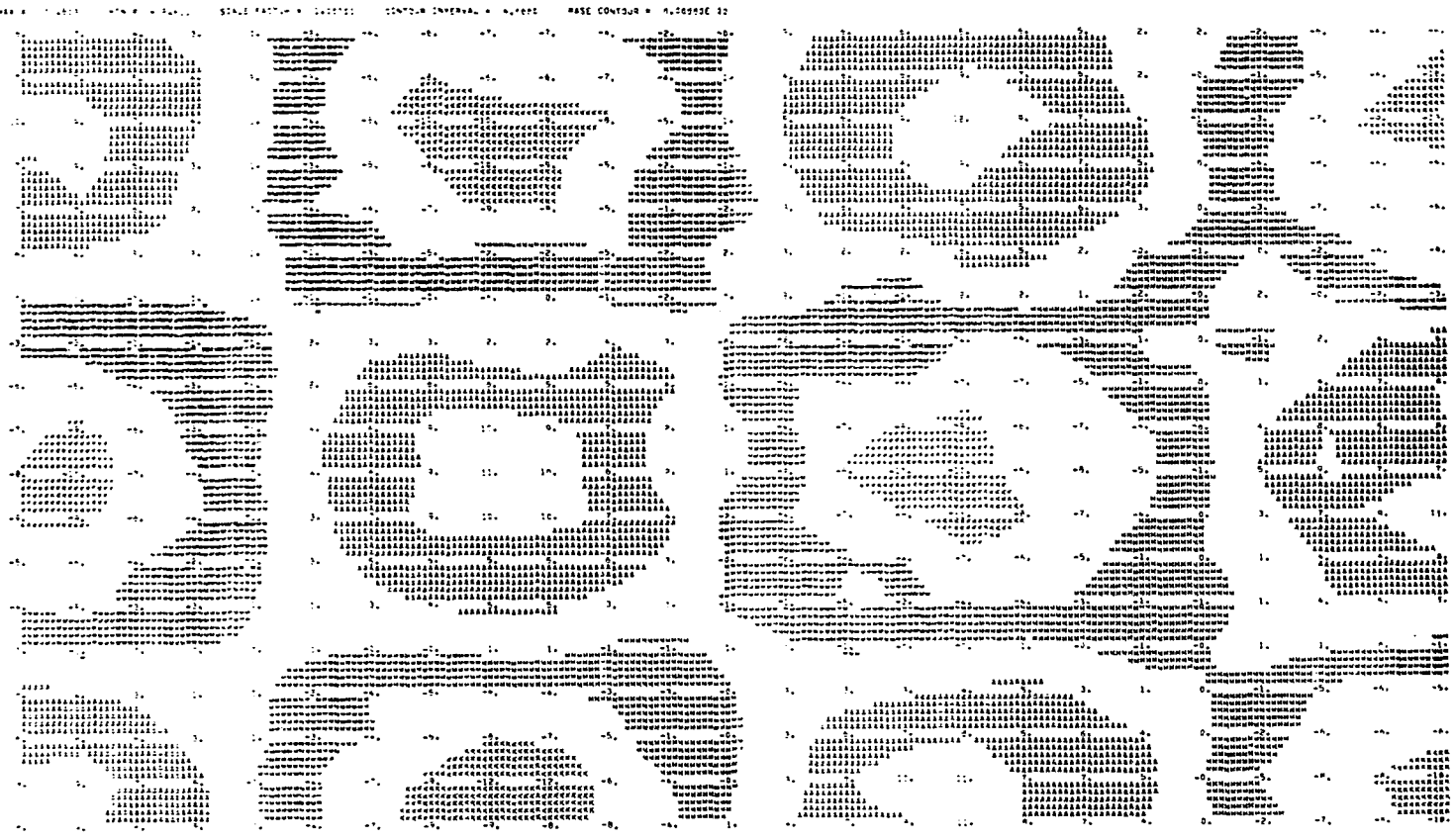


Figure A9(b). Same as Fig. A9(a), except for band-pass results.

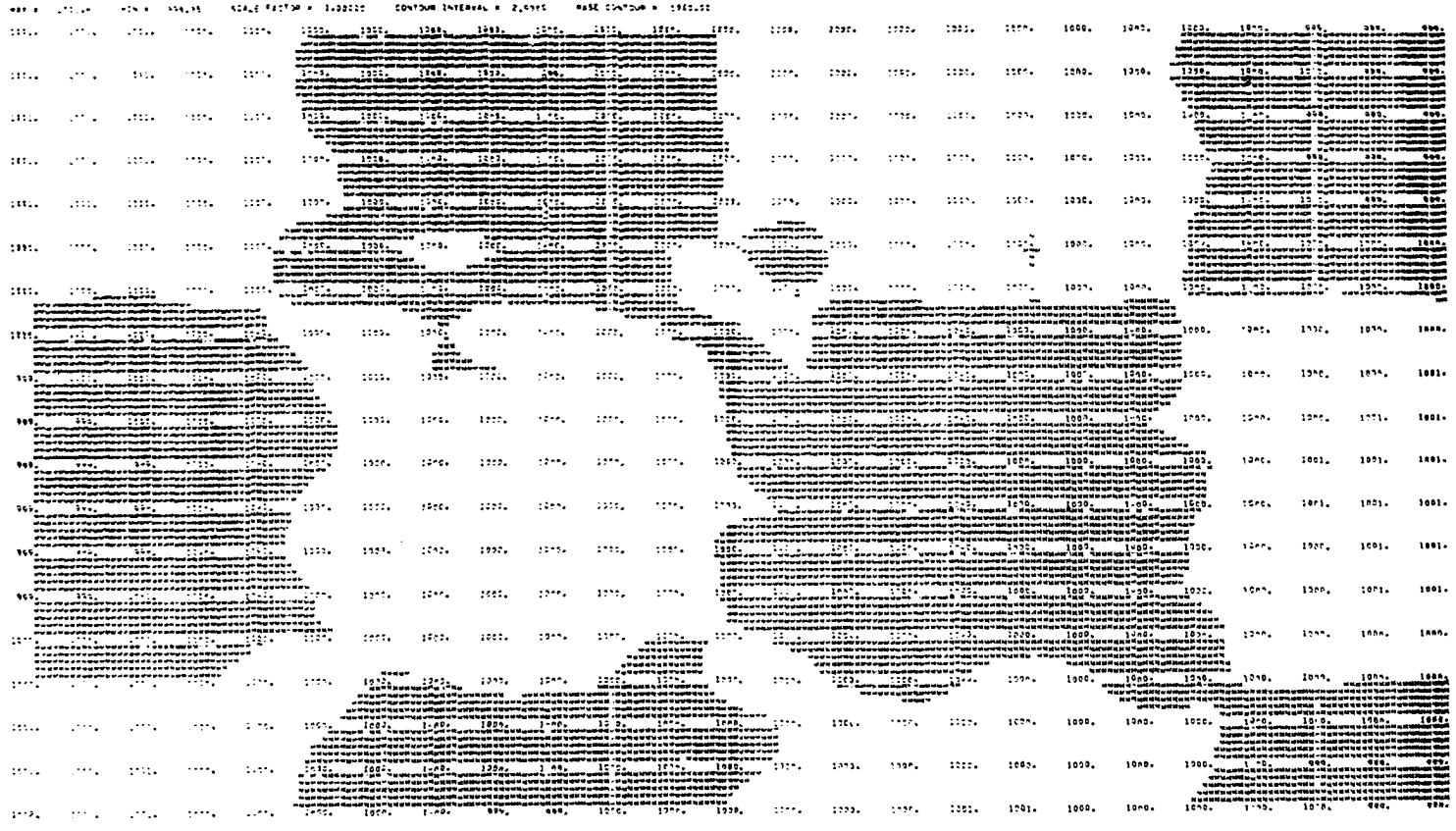


Figure A10(a). Same as Fig. A3(a), except for influence radius of 11Δs.

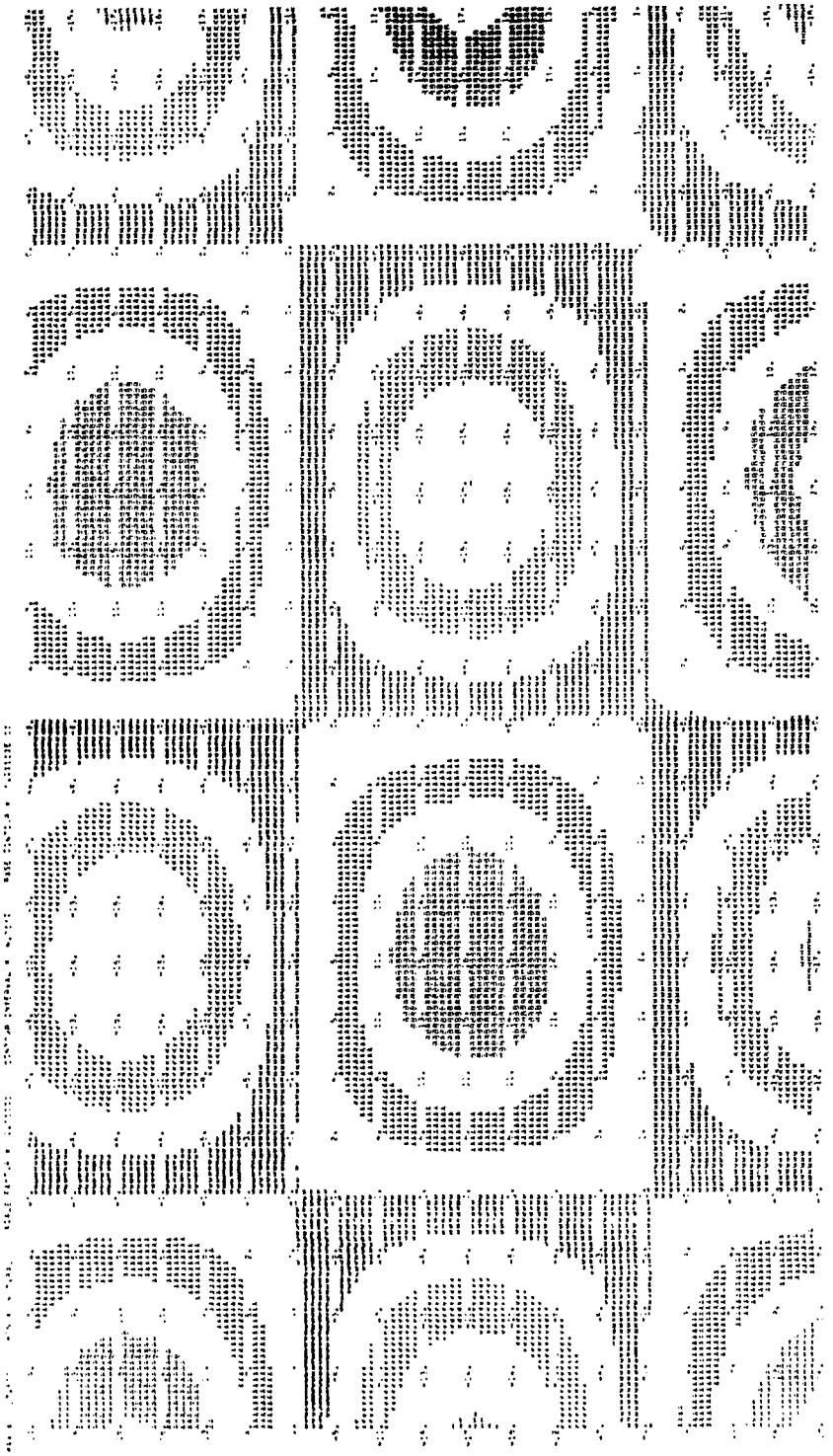


Figure A10(b). Same as Fig. A10(a), except for band-pass results.

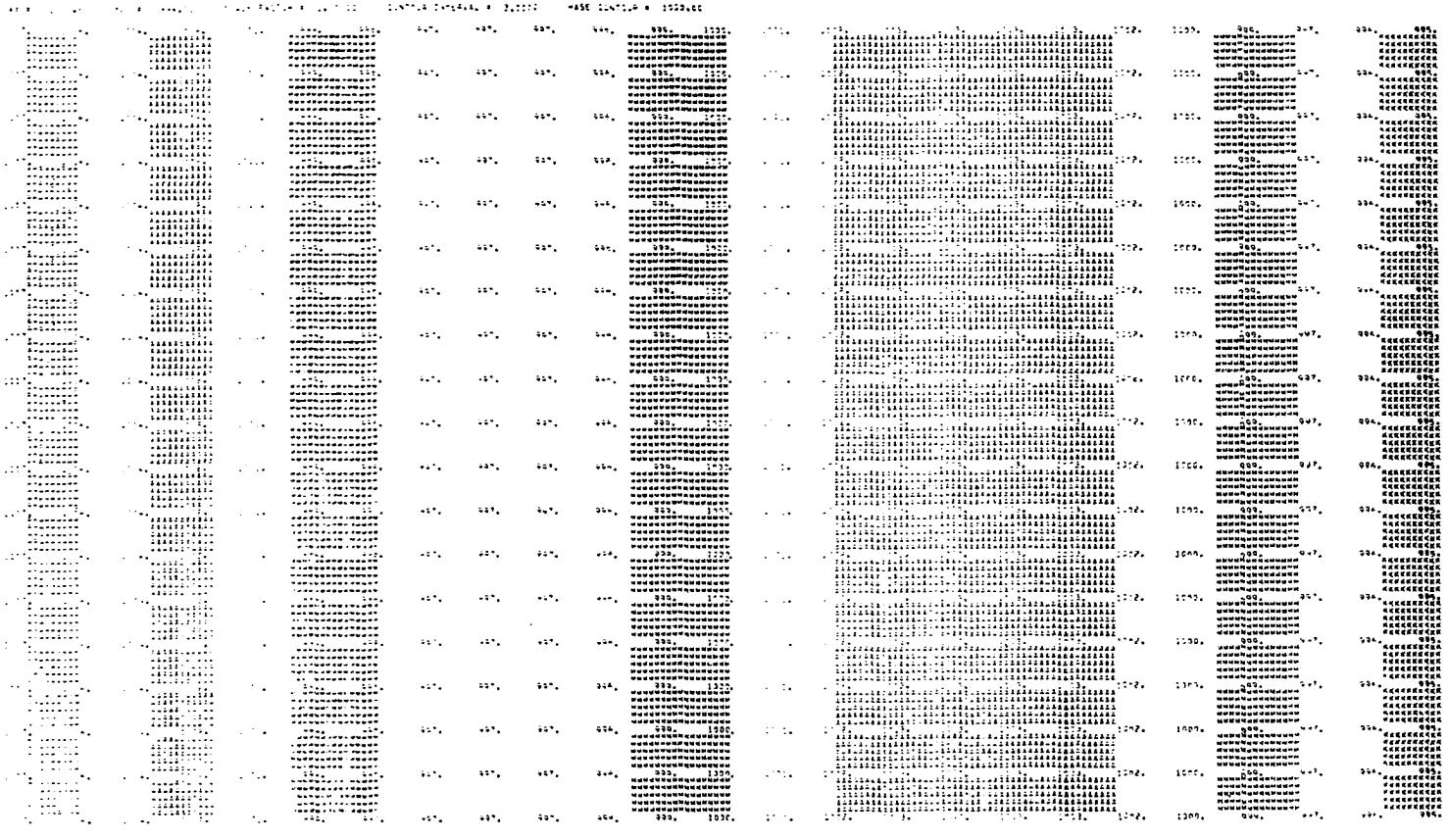


Figure A11(a). Same as Fig. A3(a), except for input with no y-dependence.

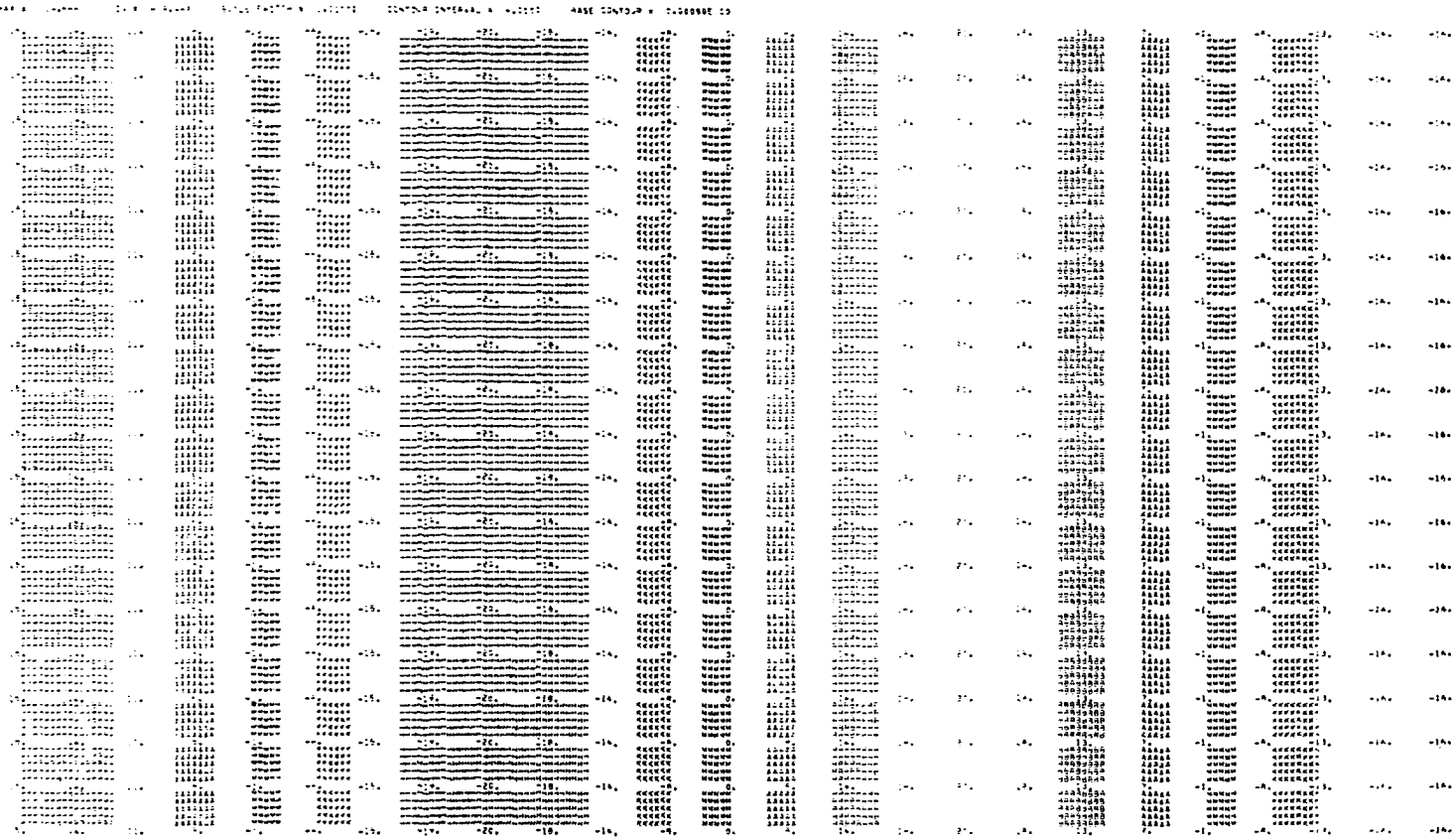


Figure A11(b). Same as Fig. A11(a), except for band-pass results.

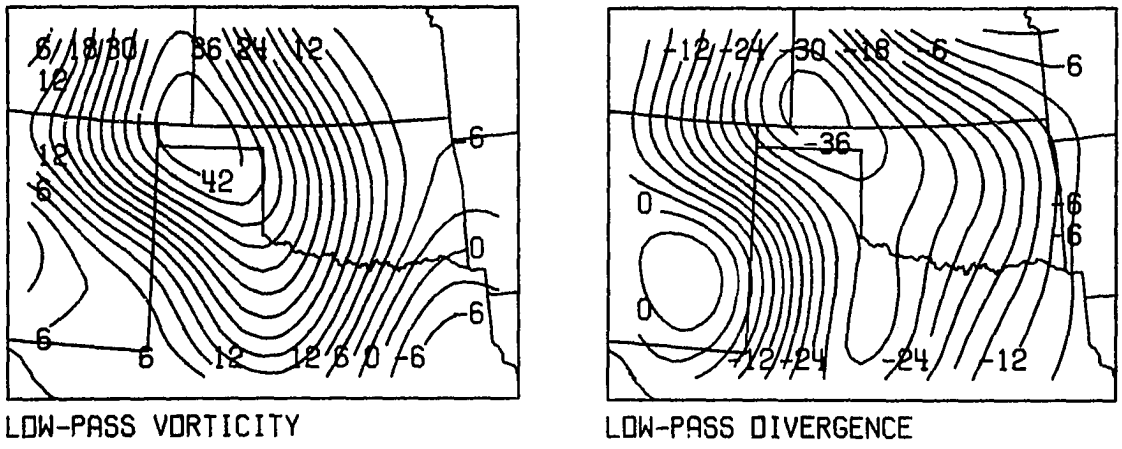
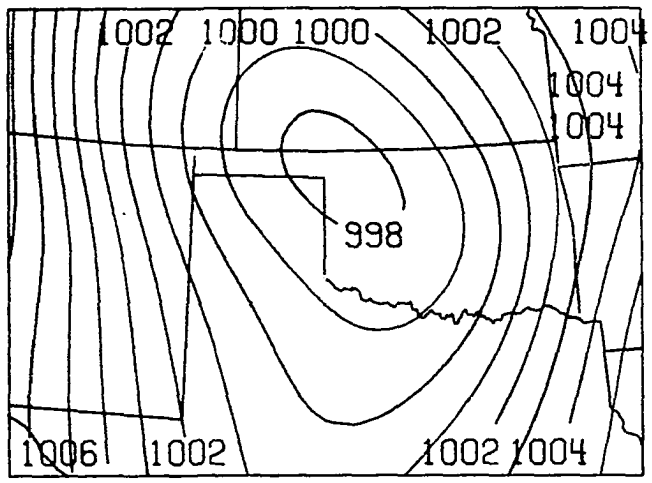
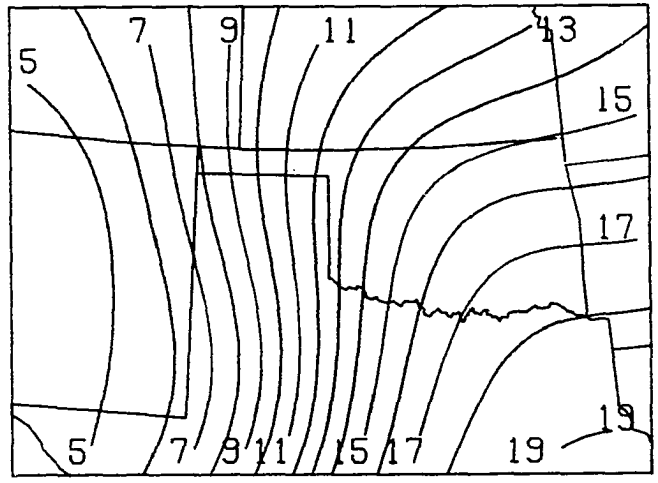


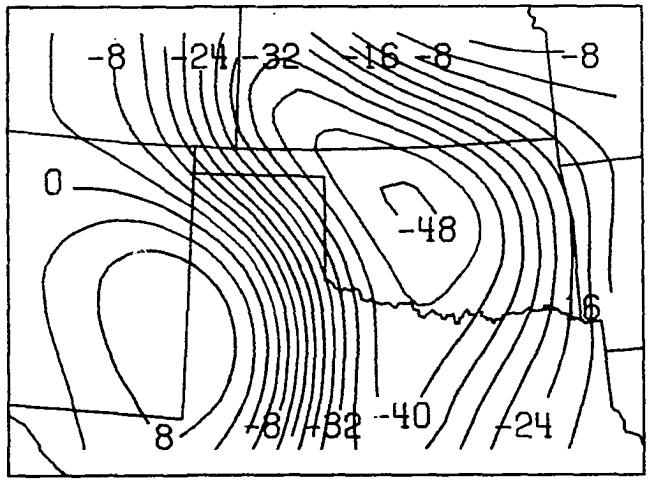
Figure B1(a). Same as Fig. 9a, except for 1200 CST on June 8, 1974.



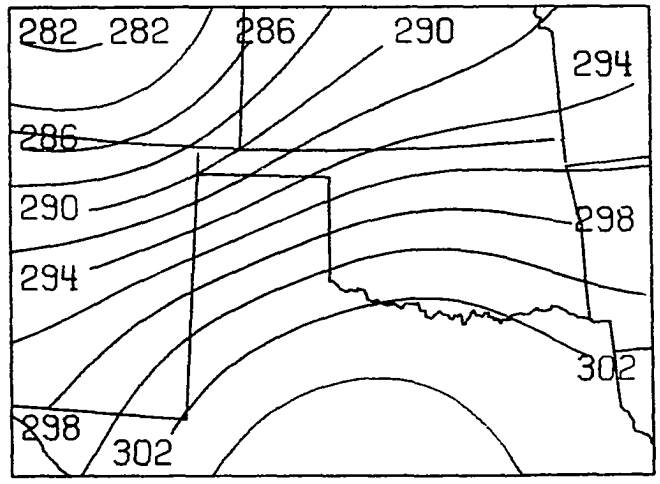
LOW-PASS ALTIMETER SETTING



LOW-PASS MIXING RATIO

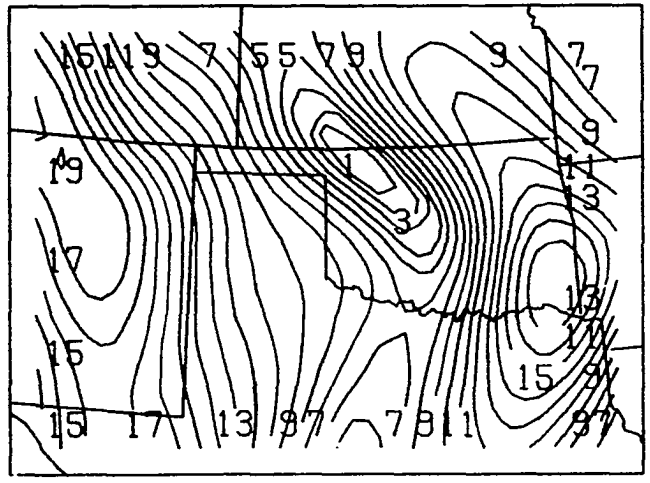


LOW-PASS MOISTURE DIVERGENCE

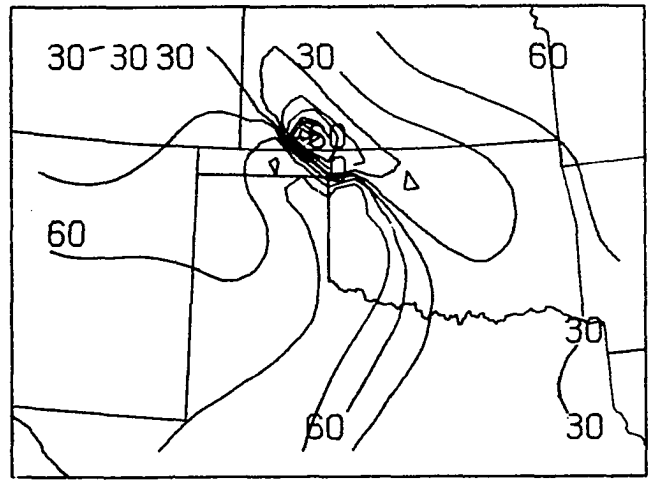


LOW-PASS TEMPERATURE

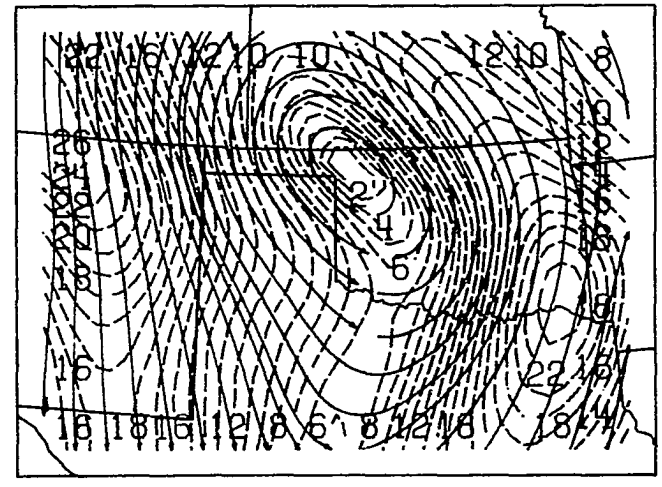
Figure B1(b). Same as Fig. 9b, except for 1200 CST on June 8, 1974.



AGEOSTROPHIC WIND SPEED

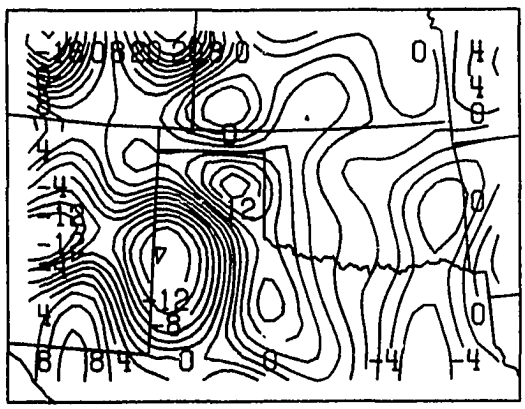


ISOBARIC CROSSING ANGLE

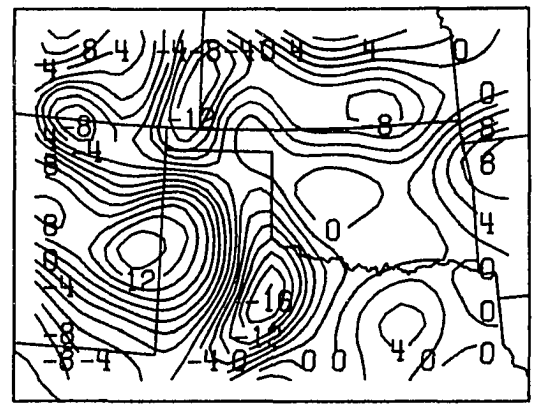


GEOS. STREAMLINES AND ISOTACHS

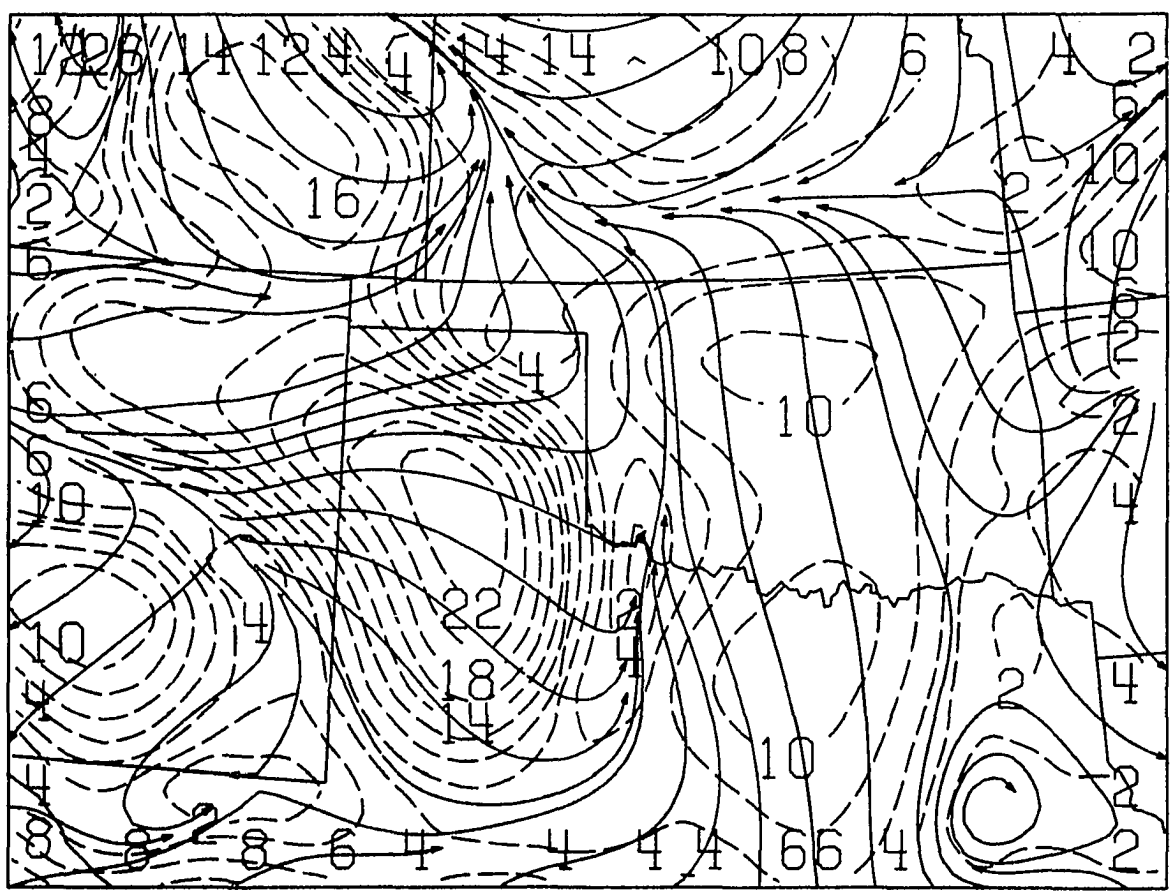
Figure B1(c). Same as Fig. 9c, except for 1200 CST on June 8, 1974.



BAND-PASS VORTICITY

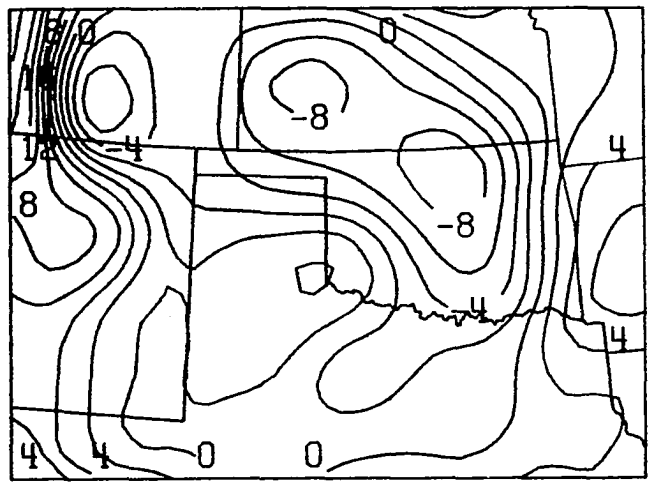


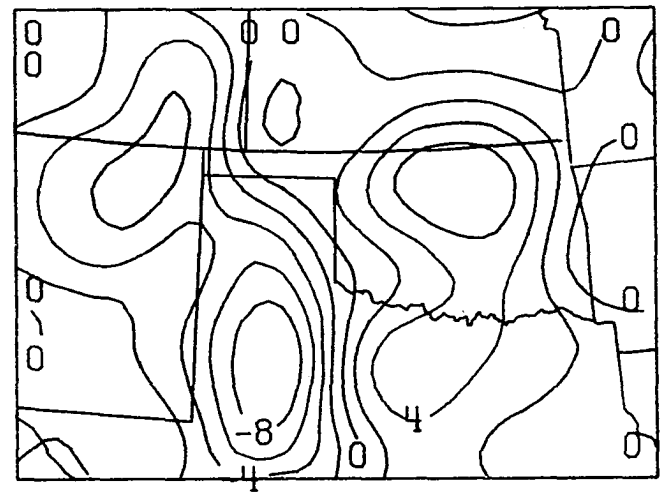
BAND-PASS DIVERGENCE

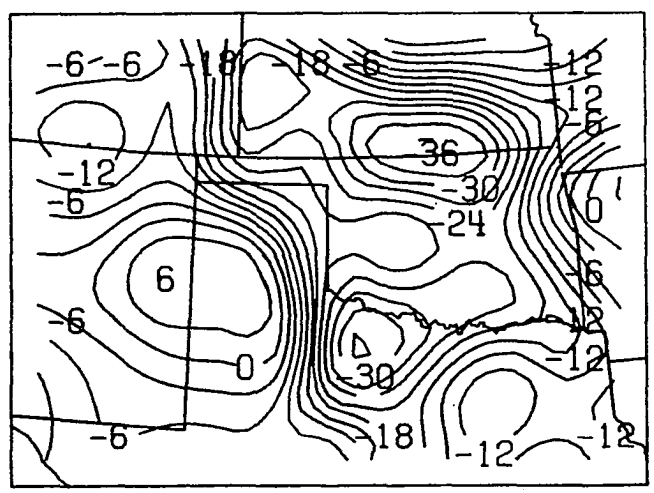


STREAMLINES AND ISOTACHS (M PER SEC) -- BAND-PASS WINDS

Figure B2(a). Same as Fig. 10a, except for 1200 CST on June 8, 1974.







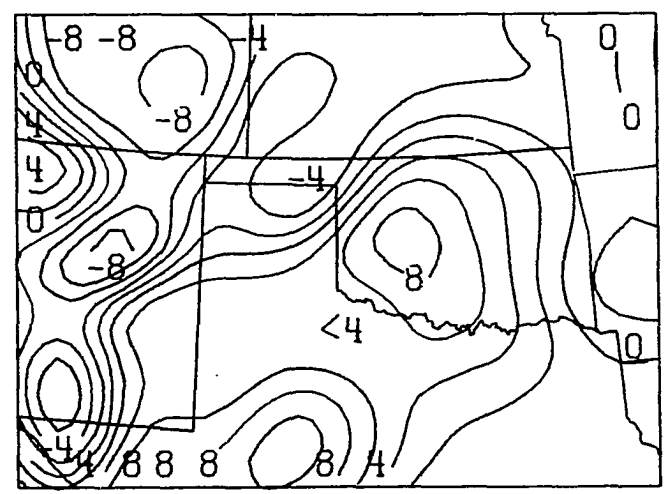


Figure B2(b). Same as Fig. 10b, except for 1200 CST on June 8, 1974.

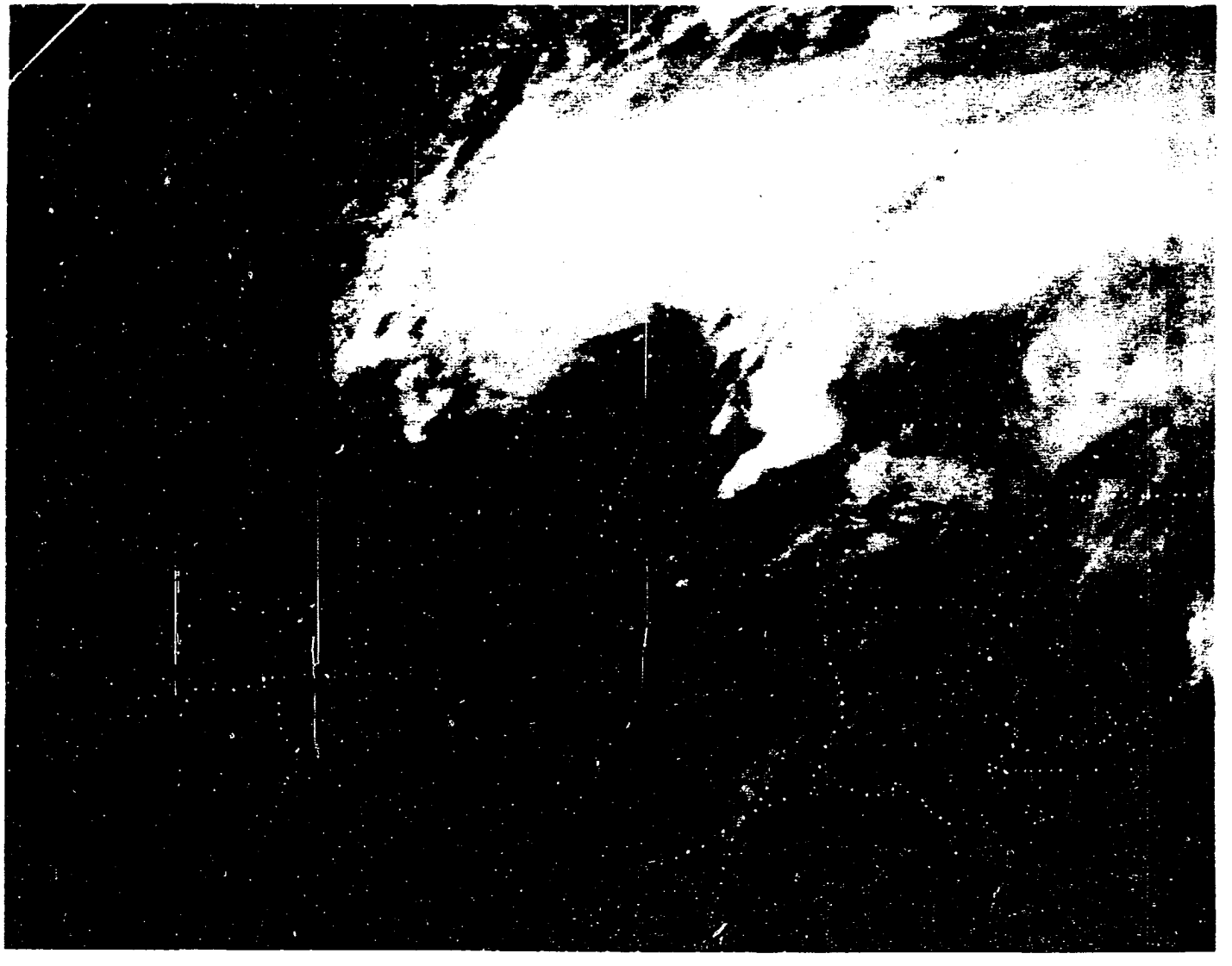


Figure B3. Satellite photo at 1452 CST on June 8, 1974.

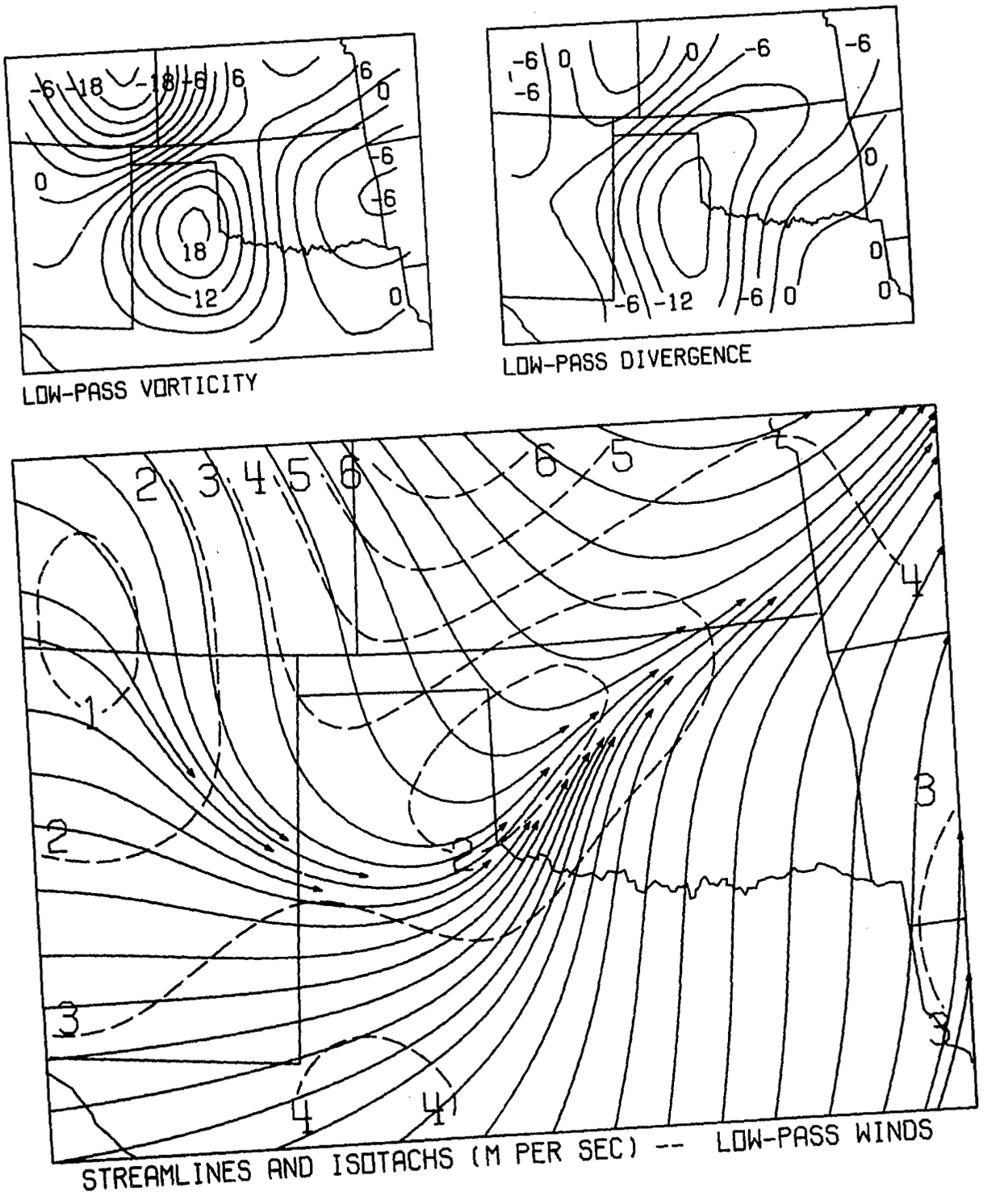
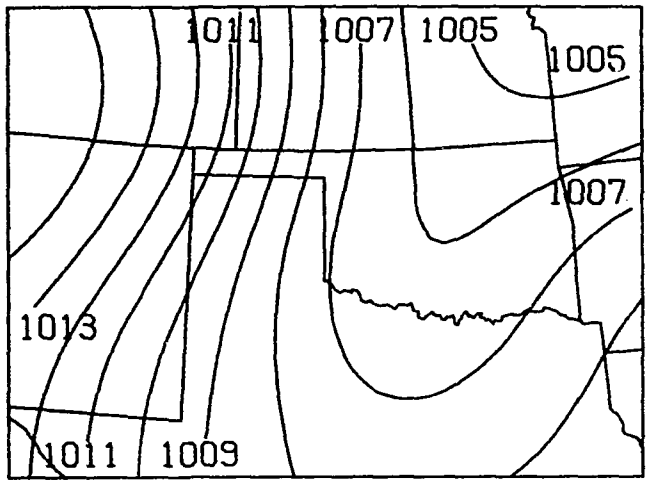
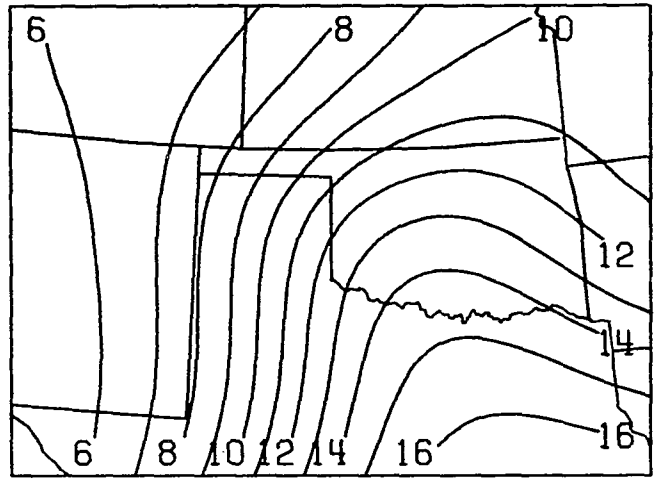


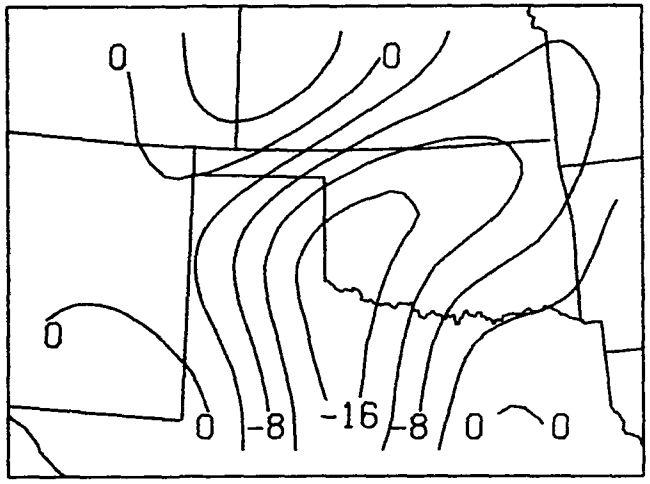
Figure B4(a). Same as Fig. 9a, except for 1200 CST on May 24, 1973.



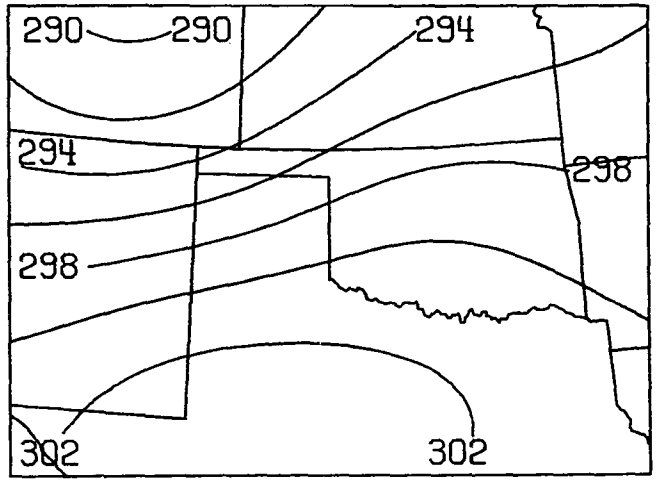
LOW-PASS ALTIMETER SETTING



LOW-PASS MIXING RATIO

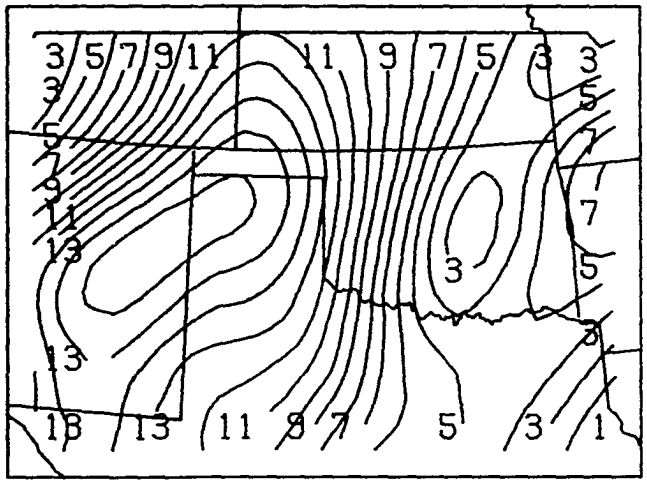


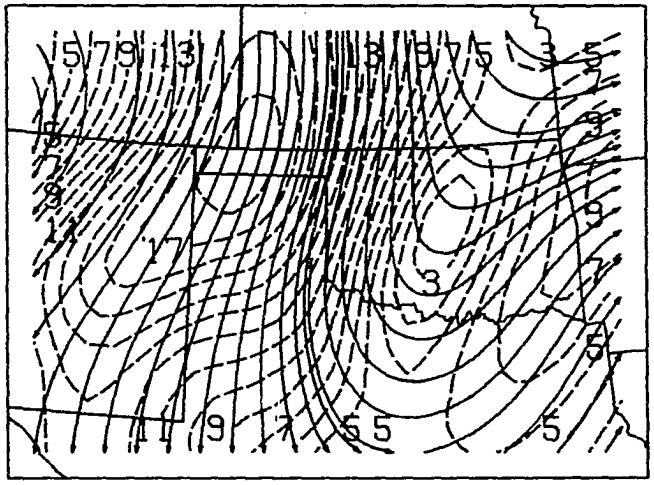
LOW-PASS MOISTURE DIVERGENCE



LOW-PASS TEMPERATURE

Figure B4(b). Same as Fig. 9b, except for 1200 CST on May 24, 1973.





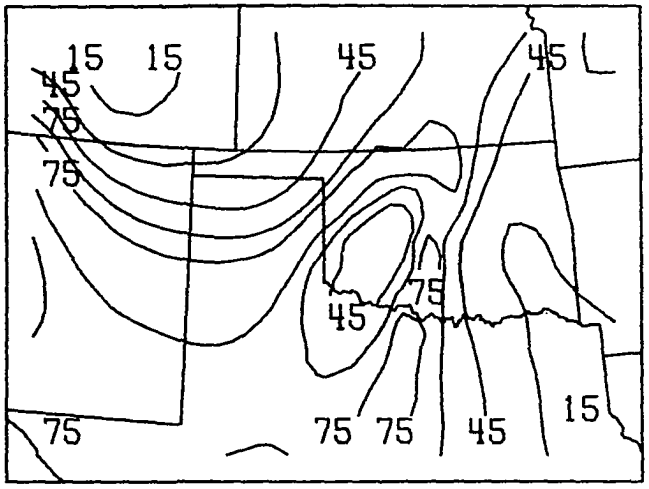
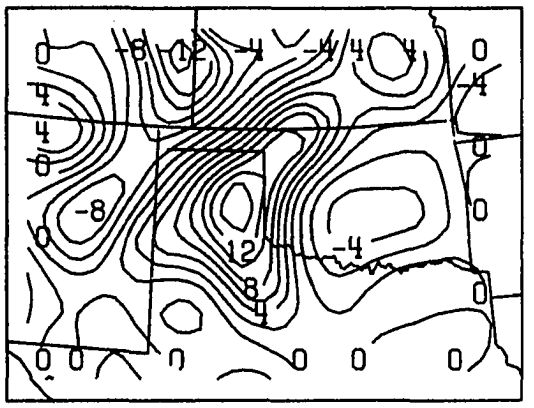
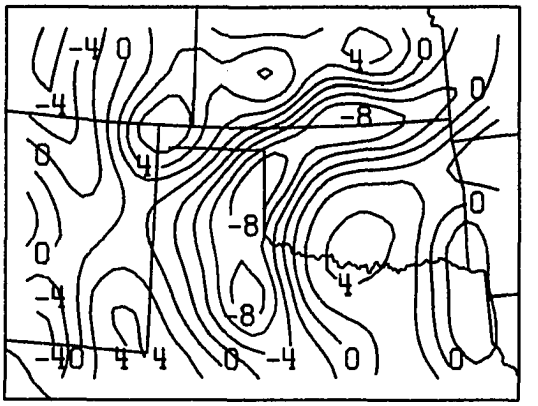


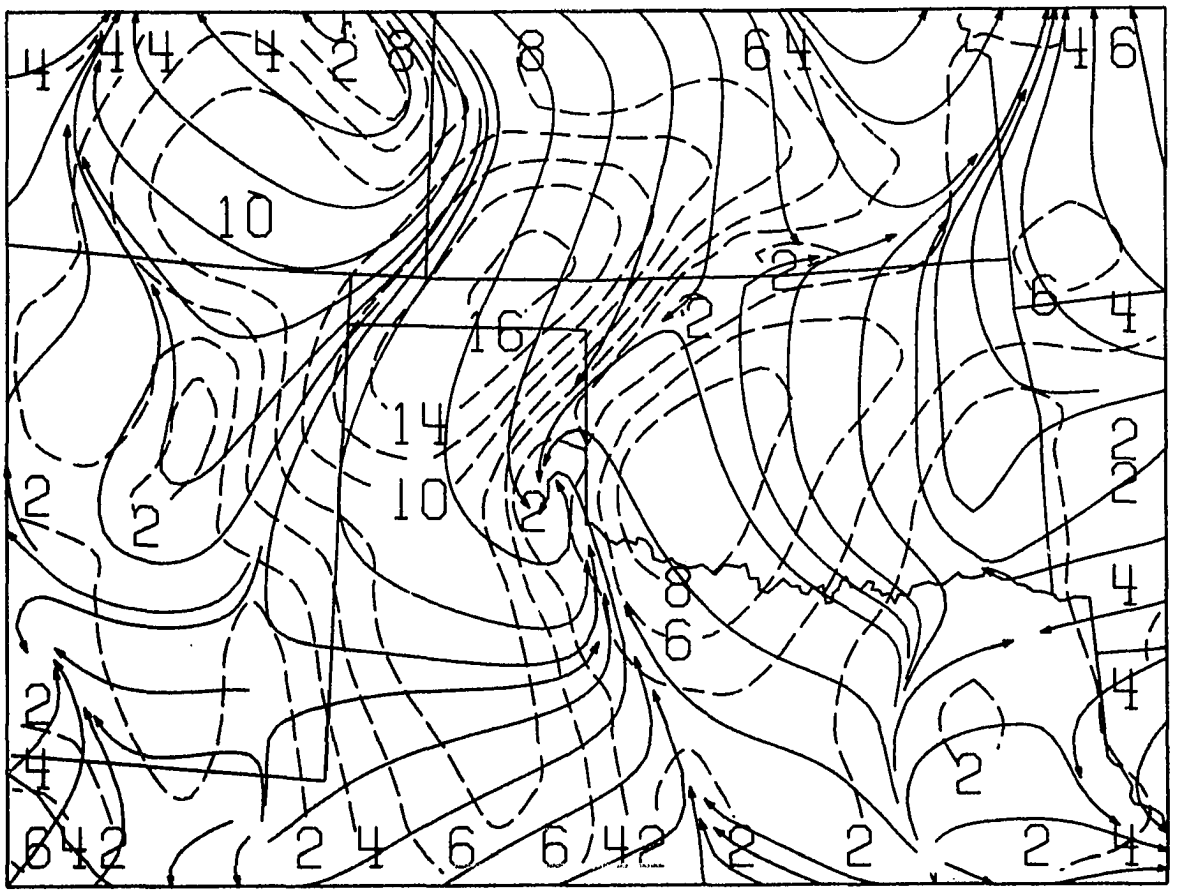
Figure B4(c). Same as Fig. 9c, except for 1200 CST on May 24, 1973.



BAND-PASS VORTICITY

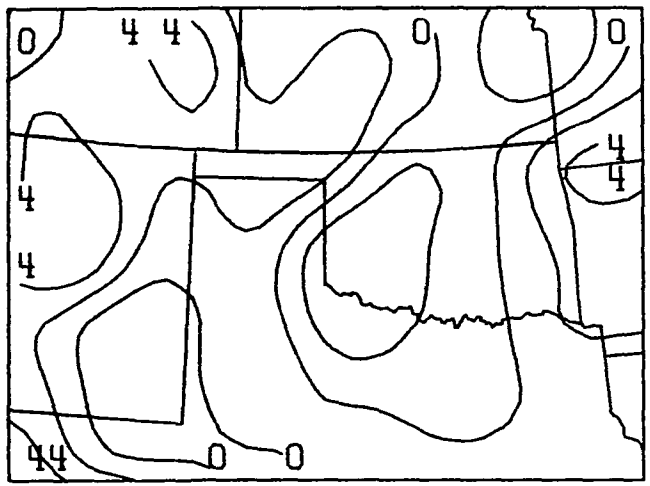


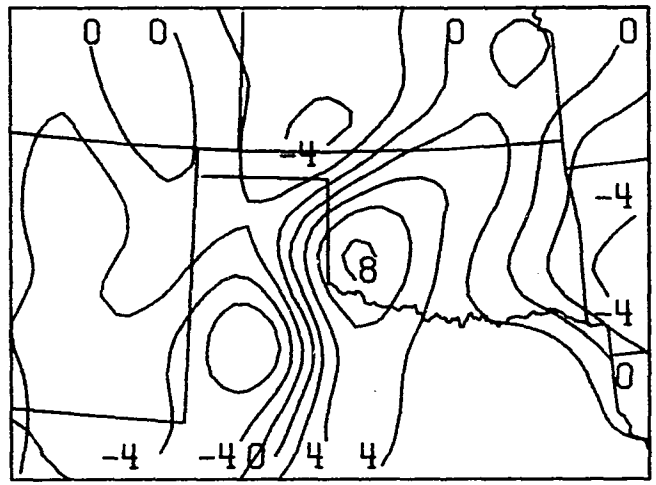
BAND-PASS DIVERGENCE

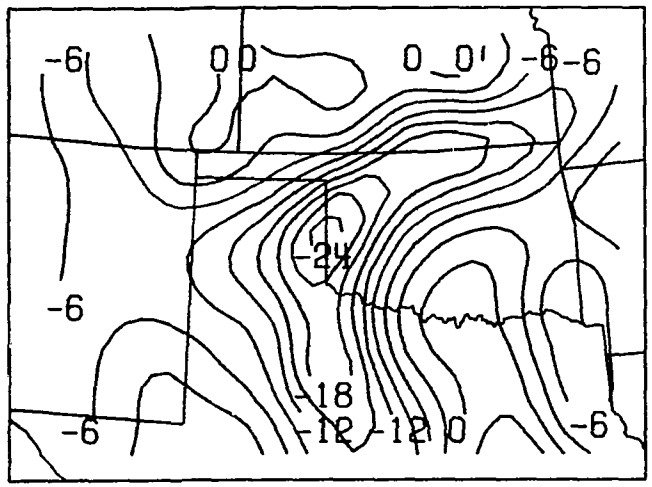


STREAMLINES AND ISOTACHS (M PER SEC) -- BAND-PASS WINDS

Figure B5(a). Same as Fig. 10a, except for 1200 CST on May 24, 1973.







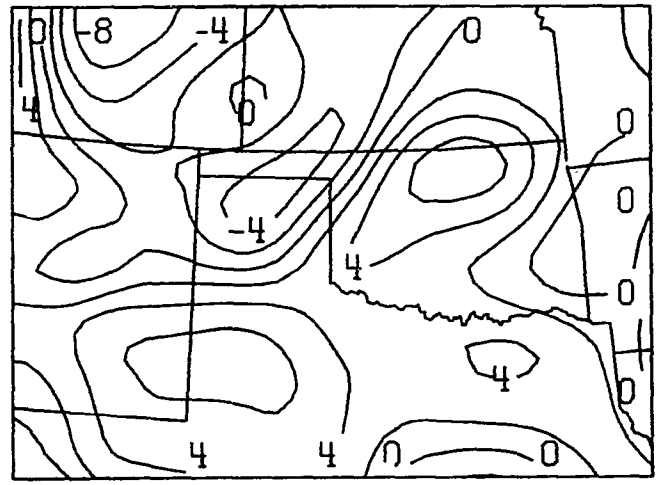


Figure B5(b). Same as Fig. 10b, except for 1200 CST on May 24, 1973.

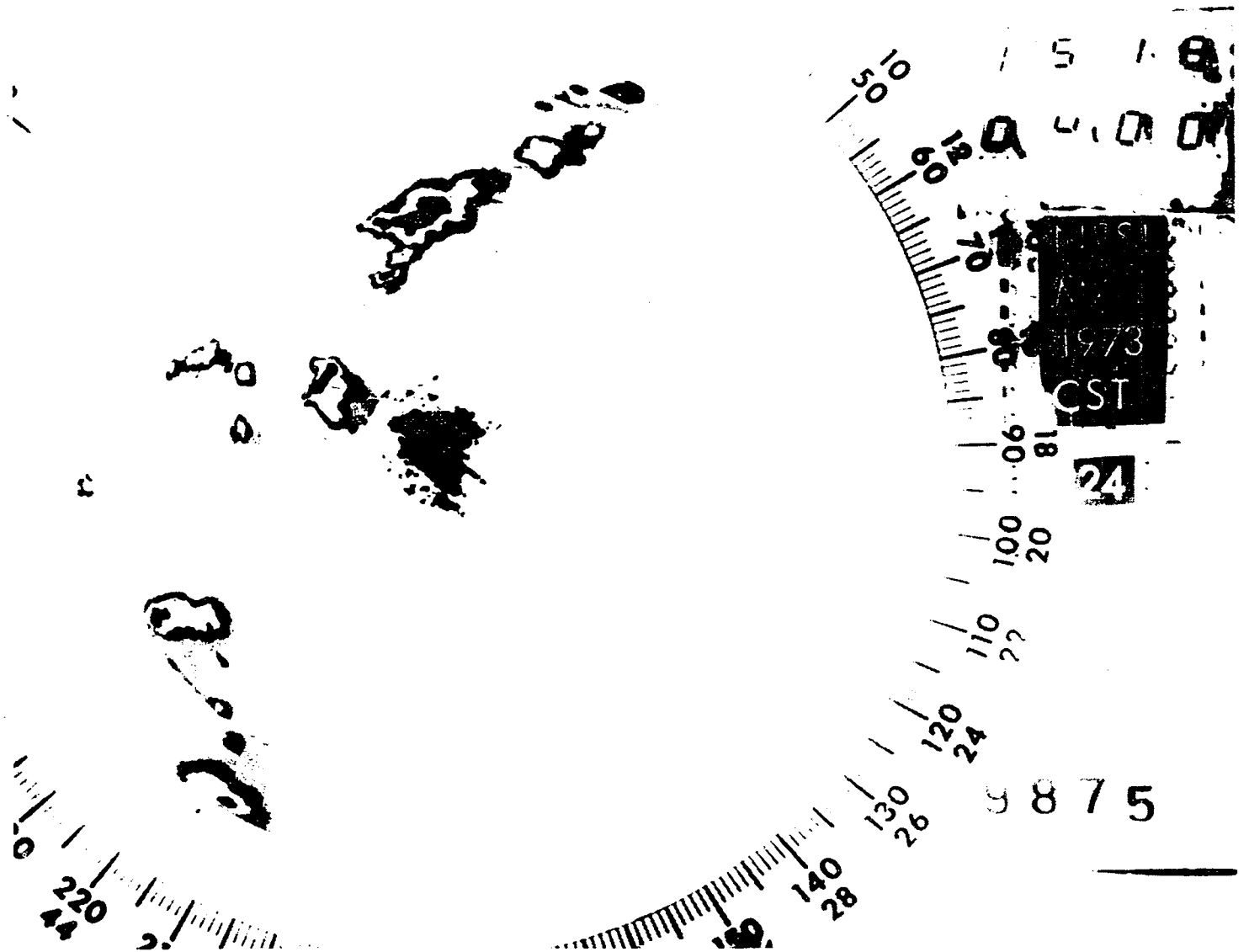


Figure B6. NSSL WSR-57 radar photograph at 1518 CST on May 24, 1973. Range marks at 40 km intervals.

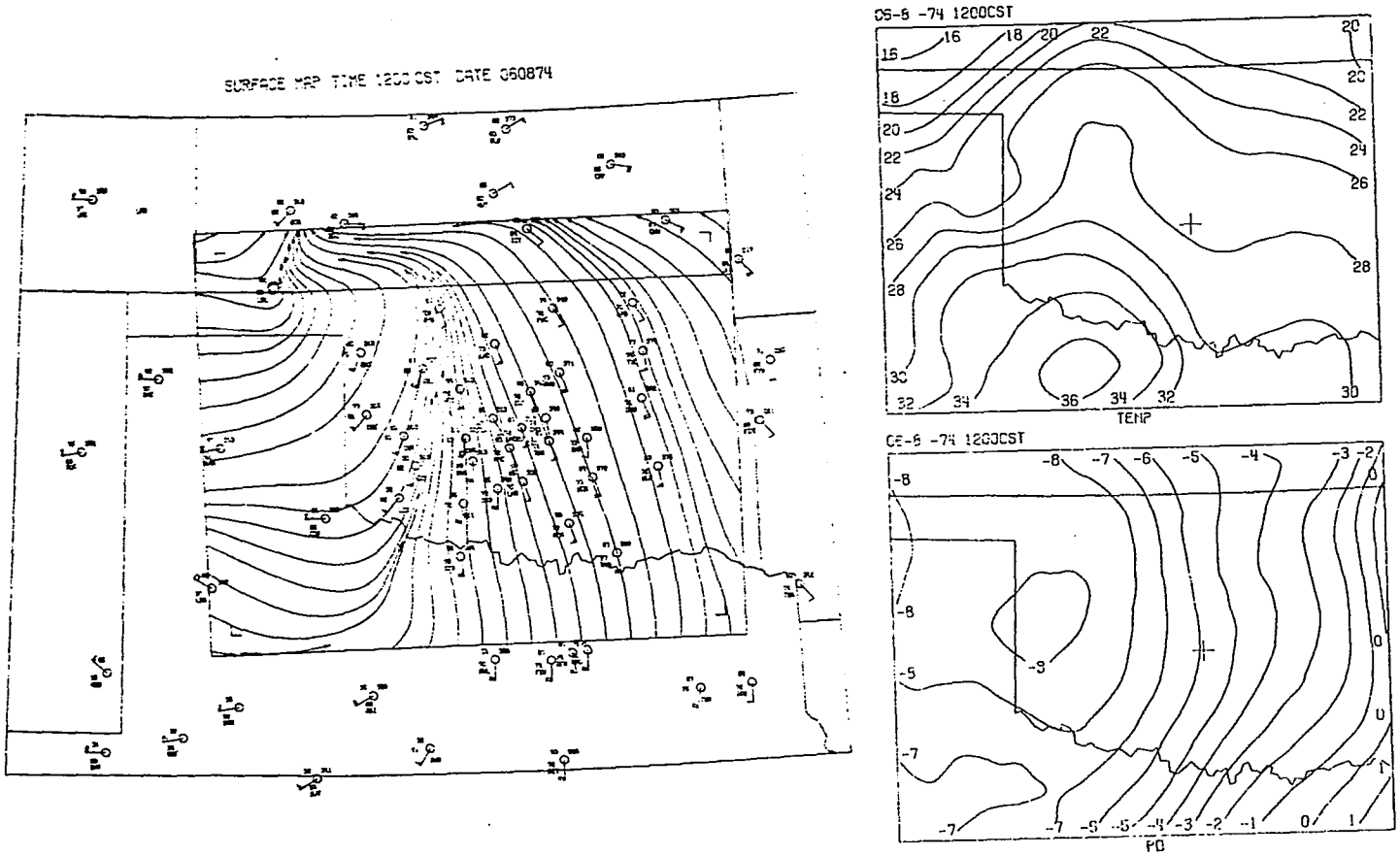


Figure C1(a). Analysis using NSSL package at 1200 CST on June 8, 1974. Temperature in deg C, "PO" denotes pressure anomaly (from 1000 mb), in mb.

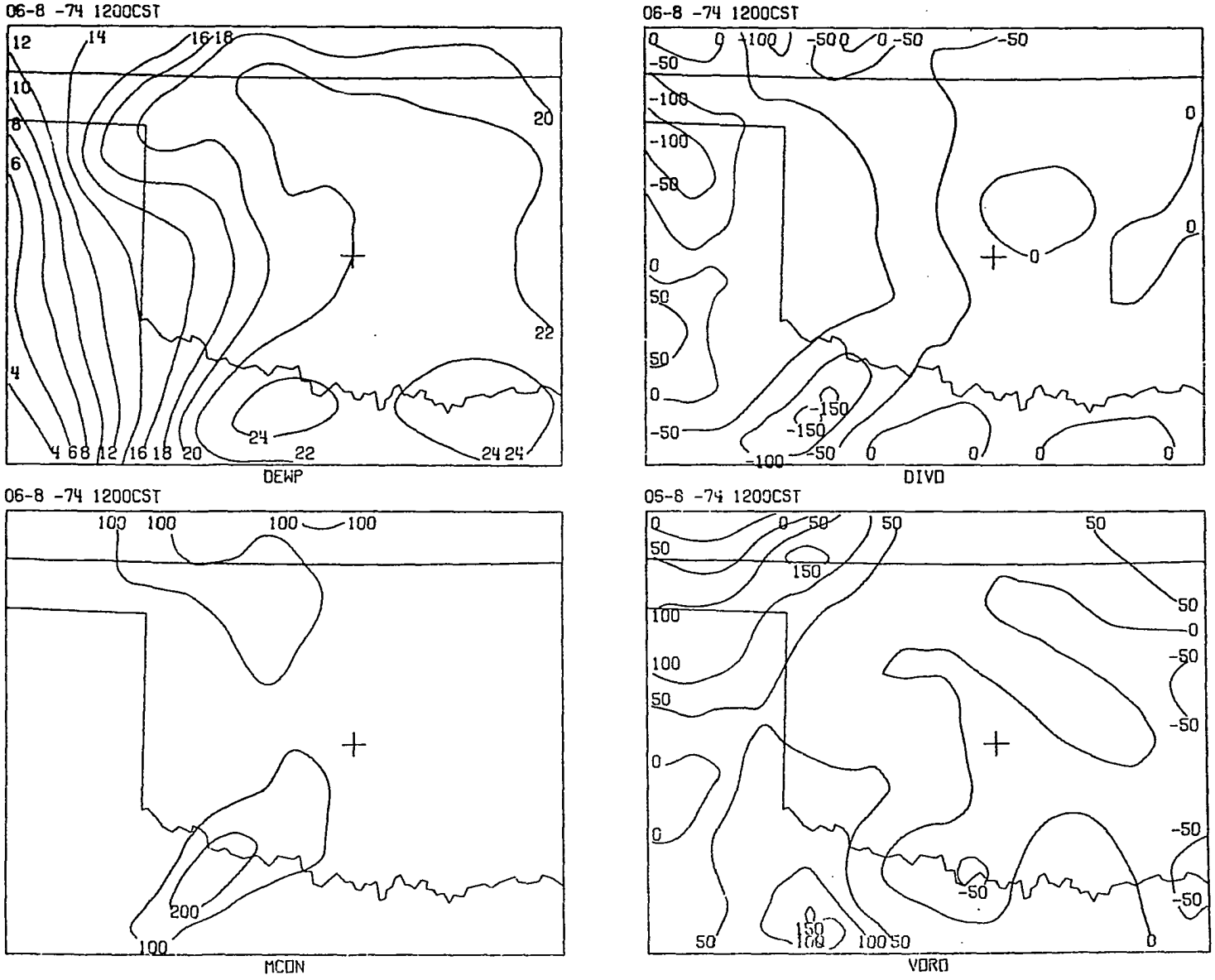


Figure C1(b). Dewpoint in deg C, divergence and vorticity times 10^6 with units of sec^{-1}, moisture divergence times 10^4 with units of g kg^{-1} sec^{-1}.

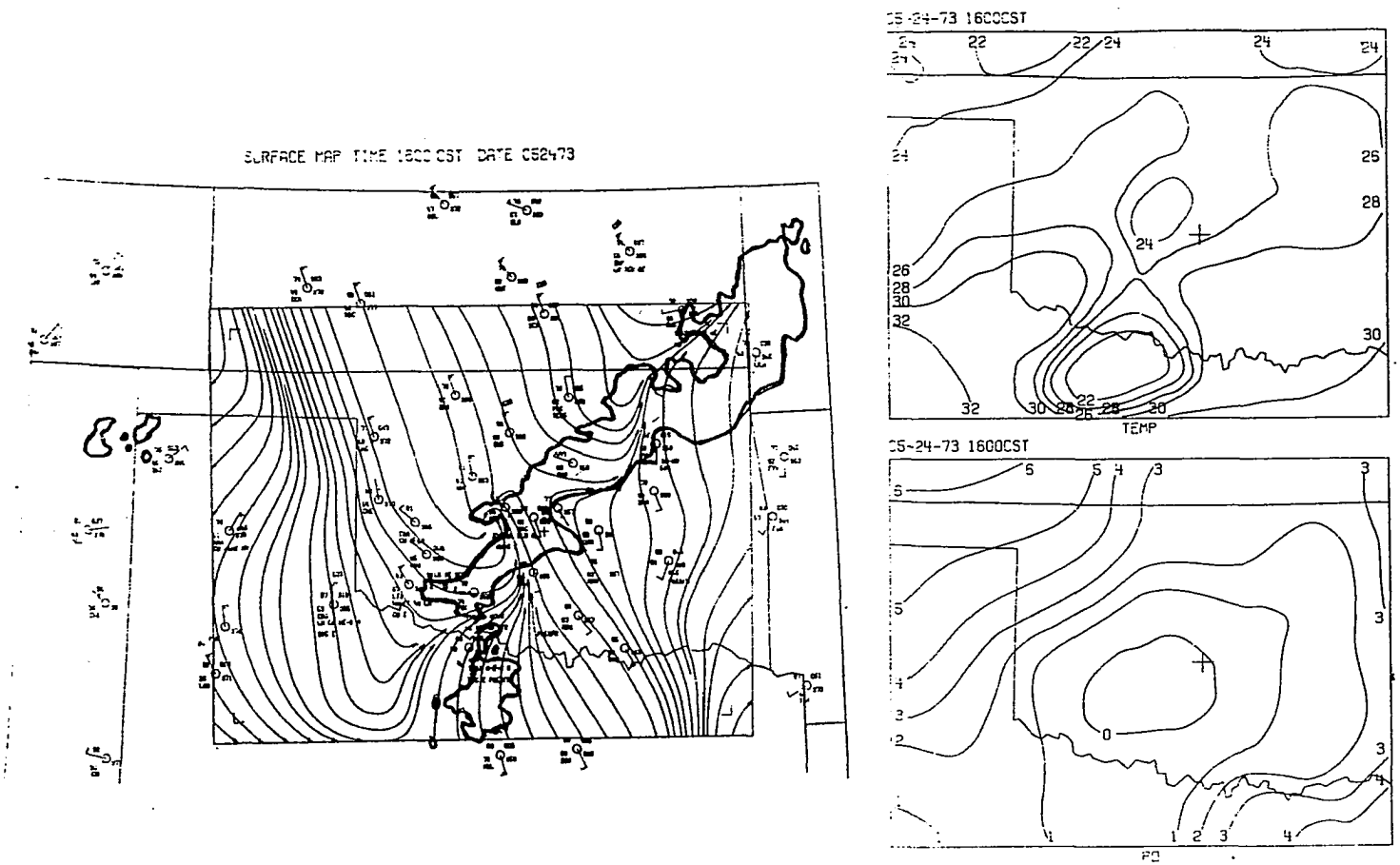


Figure C2(a). Same as Fig. C1(a), except for 1600 CST, May 24, 1973.

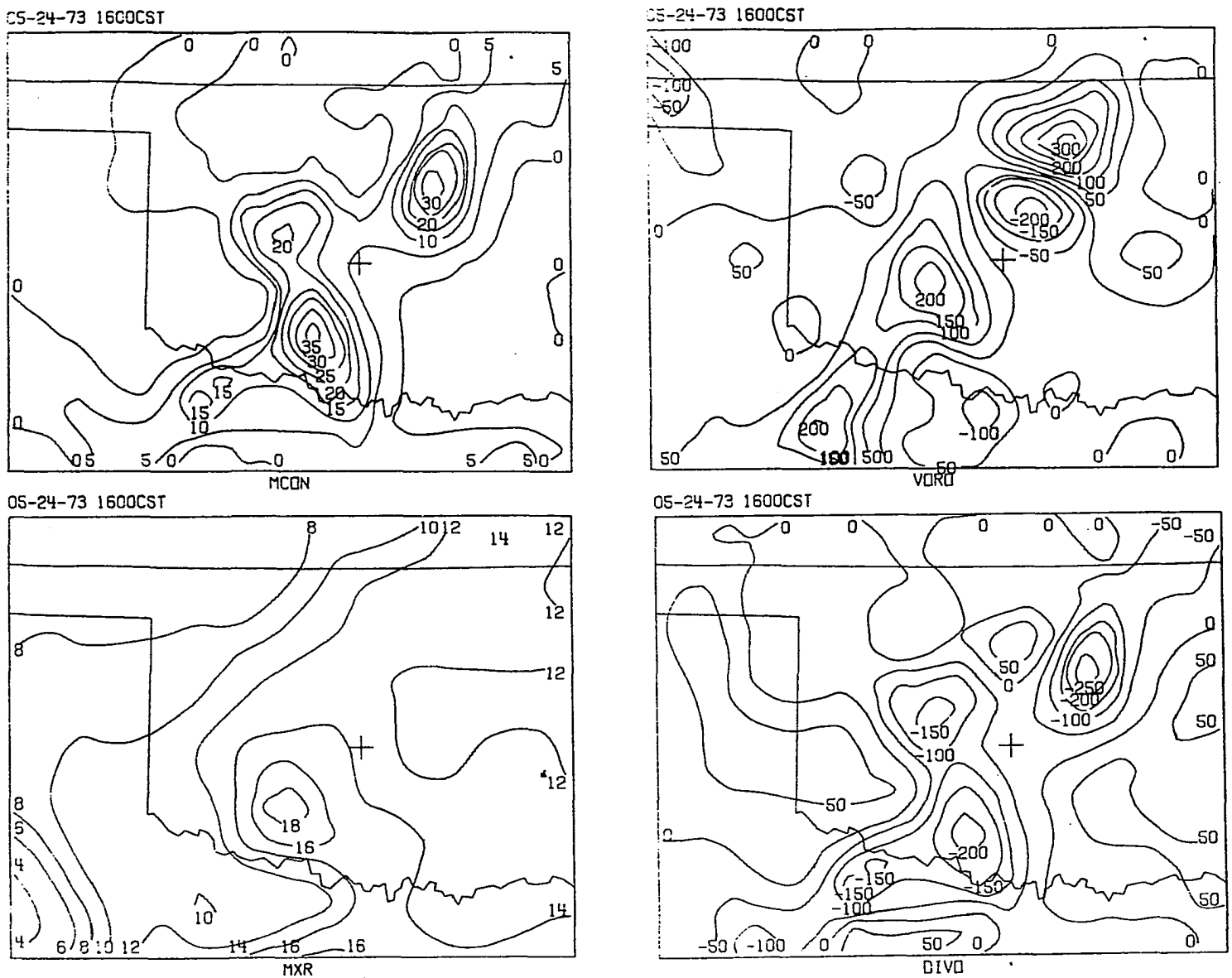


Figure C2(b). Same as Fig. C1(b), except for 1600 CST, May 24, 1973 and mixing ratio in g kg^{-1}.

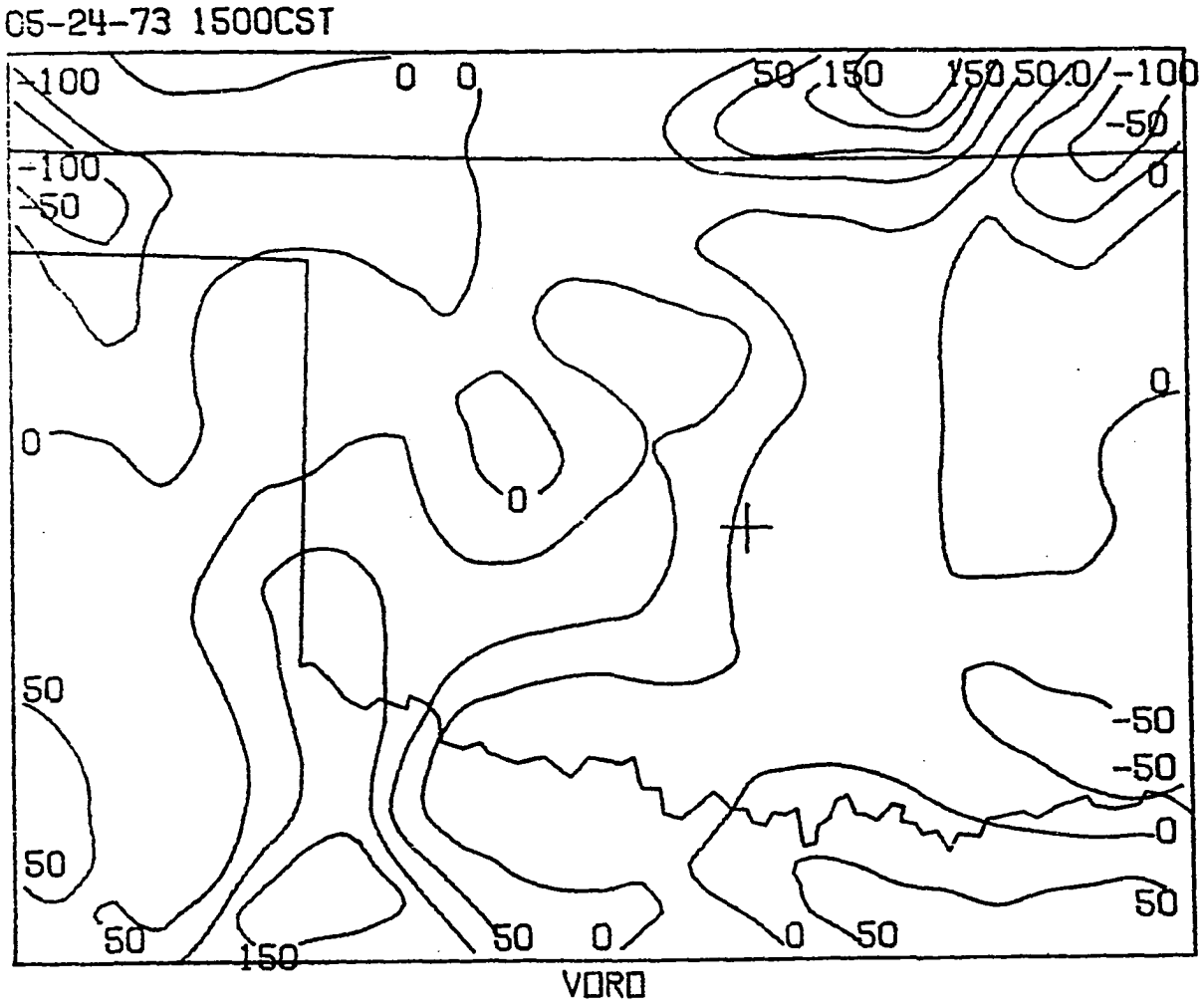


Figure C3. Vorticity times 10^6 (sec^{-1}) for 1500 CST, May 24, 1973.

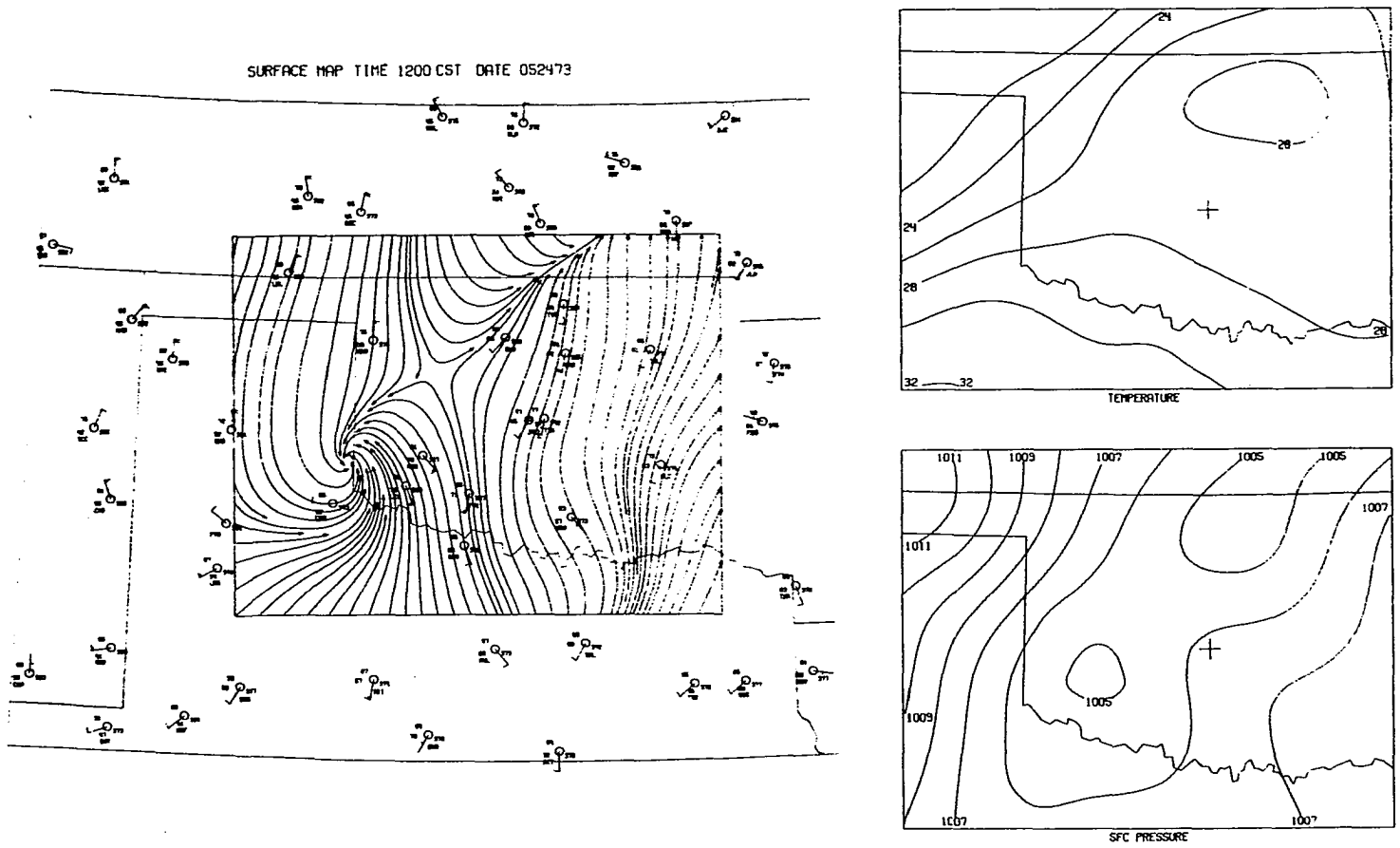


Figure C4(a). Successive corrections analysis (plus smoothing) for 1200 CST, May 24, 1973. Temperature in deg C; altimeter setting used for surface pressure, in mb.

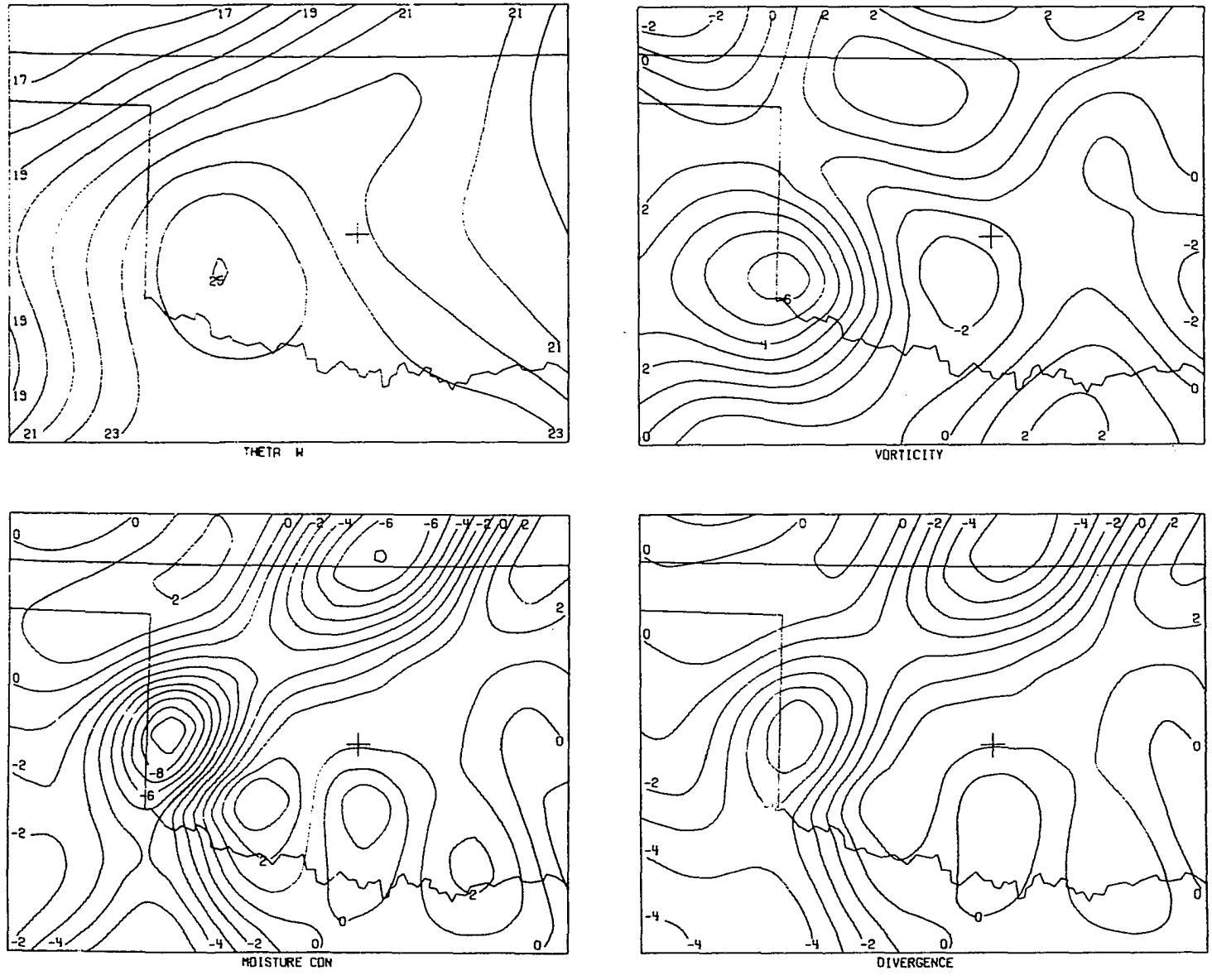


Figure C4(b). Potential wet-bulb temperature in deg C, vorticity and divergence times 10^5 (sec^{-1}), moisture divergence times 10^4 (g kg^{-1} sec^{-1}) -- note that moisture divergence is